NUREG/CR-7260

U.S.NRC
United States Nuclear Regulatory Commission
Protecting People and the Environment

CFD Validation of Vertical Dry Cask Storage System

Office of Nuclear Regulatory Research

AVAILABILITY OF REFERENCE MATERIALS IN NRC PUBLICATIONS

NRC Reference Material

As of November 1999, you may electronically access NUREG-series publications and other NRC records at NRC's Library at www.nrc.gov/reading-rm.html. Publicly released records include, to name a few, NUREG-series publications; *Federal Register* notices; applicant, licensee, and vendor documents and correspondence; NRC correspondence and internal memoranda; bulletins and information notices; inspection and investigative reports; licensee event reports; and Commission papers and their attachments.

NRC publications in the NUREG series, NRC regulations, and Title 10, "Energy," in the *Code of Federal Regulations* may also be purchased from one of these two sources.

1. **The Superintendent of Documents**
   U.S. Government Publishing Office
   Washington, DC 20402-0001
   Internet: bookstore.gpo.gov
   Telephone: (202) 512-1800
   Fax: (202) 512-2104

2. **The National Technical Information Service**
   5301 Shawnee Road
   Alexandria, VA 22312-0002
   www.ntis.gov
   1-800-553-6847 or, locally, (703) 605-6000

A single copy of each NRC draft report for comment is available free, to the extent of supply, upon written request as follows:

Address: **U.S. Nuclear Regulatory Commission**
Office of Administration
Multimedia, Graphics, and Storage & Distribution Branch
Washington, DC 20555-0001
E-mail: distribution.resource@nrc.gov
Facsimile: (301) 415-2289

Some publications in the NUREG series that are posted at NRC's Web site address www.nrc.gov/reading-rm/doc-collections/nuregs are updated periodically and may differ from the last printed version. Although references to material found on a Web site bear the date the material was accessed, the material available on the date cited may subsequently be removed from the site.

Non-NRC Reference Material

Documents available from public and special technical libraries include all open literature items, such as books, journal articles, transactions, *Federal Register* notices, Federal and State legislation, and congressional reports. Such documents as theses, dissertations, foreign reports and translations, and non-NRC conference proceedings may be purchased from their sponsoring organization.

Copies of industry codes and standards used in a substantive manner in the NRC regulatory process are maintained at—

The NRC Technical Library
Two White Flint North
11545 Rockville Pike
Rockville, MD 20852-2738

These standards are available in the library for reference use by the public. Codes and standards are usually copyrighted and may be purchased from the originating organization or, if they are American National Standards, from—

American National Standards Institute
11 West 42nd Street
New York, NY 10036-8002
www.ansi.org
(212) 642-4900

Legally binding regulatory requirements are stated only in laws; NRC regulations; licenses, including technical specifications; or orders, not in NUREG-series publications. The views expressed in contractor prepared publications in this series are not necessarily those of the NRC.

The NUREG series comprises (1) technical and administrative reports and books prepared by the staff (NUREG–XXXX) or agency contractors (NUREG/CR–XXXX), (2) proceedings of conferences (NUREG/CP–XXXX), (3) reports resulting from international agreements (NUREG/IA–XXXX),(4) brochures (NUREG/BR–XXXX), and (5) compilations of legal decisions and orders of the Commission and Atomic and Safety Licensing Boards and of Directors' decisions under Section 2.206 of NRC's regulations (NUREG–0750).

NUREG/CR-7260

U.S.NRC
United States Nuclear Regulatory Commission
Protecting People and the Environment

CFD Validation of Vertical Dry Cask Storage System

Manuscript Completed: April 2019
Date Published: May 2019

Prepared by:
K. Hall[1], G. Zigh[2], and J. Solis[2]

[1]Alden Research Laboratory, Inc.
Holden, MA 01541

[2]U.S. Nuclear Regulatory Commission

Don Algama, NRC Project Manager

Office of Nuclear Regulatory Research

ABSTRACT

Applicants submit spent nuclear fuel dry storage cask designs to the U.S. Nuclear Regulatory Commission (NRC) for certification under Title 10 of the *Code of Federal Regulations* (10 CFR) Part 72, "Licensing Requirements for the Independent Storage of Spent Nuclear Fuel, High-Level Radioactive Waste, and Reactor-Related Greater Than Class C Waste". The NRC staff performs its technical review of these designs in accordance with 10 CFR Part 72 and NUREG-1536, "Standard Review Plan for Spent Fuel Dry Storage Systems at a General License Facility," Revision 1, issued July 2010 [6]. To ensure that the cask and fuel material temperatures of the dry cask storage system remain within the allowable limits or criteria for normal, off-normal, and accident conditions, the NRC staff performs a thermal review as part of the technical review.

Recent applications have increasingly used thermal-hydraulic analyses using computational fluid dynamics (CFD) codes (e.g., ANSYS FLUENT) to demonstrate the adequacy of the thermal design. The applicants are also looking to license casks with decay heat close to 50 kW, resulting in peak cladding temperature (PCT) close to the ISG-11 suggested temperature of 400 C. These PCT predictions presented by the applicants usually are not supported by an uncertainty quantification calculation to assure the thermal reviewer that the calculated temperature margin is adequate. To remedy this, the NRC Office of Nuclear Material Safety and Safeguards asked the NRC Office of Nuclear Regulatory Research to be part of a validation study of the FLUENT CFD code to assist it in making regulatory decisions to ensure adequate protection for storage and transportation casks. The validation studies were based on data collected in a demonstration project at the North Anna Power Plant sponsored by Department of Energy (DOE). A TN-32B cask loaded with about 30.5 kW of high burn-up fuel was used for this validation. Extensive temperature measurements throughout the cask were performed, including temperature measurements throughout the height of several fuel assemblies and temperature measurements on the outer surface of the cask [2].

USNRC recognizes that CFD using finite volume is one of the best and most valuable method for the applicants to show compliance with the regulations concerning the dry cask storage systems (DCSS) thermal response. Additionally, when demonstrating compliance, it is valuable to quantify the uncertainty in the simulation result as a function of the computational mesh and simulation inputs. As a participant in this CFD validation, USNRC led the effort to include uncertainty quantification and follow the CFD best practice guidelines in this validation exercise [NUREG 2152].

This report discusses validation and uncertainty quantification of a CFD model using experimental data. Uncertainty quantification follows the procedures outlined in [1]. Sources of uncertainty that were examined in the analysis include iterative uncertainty, spatial discretization, and uncertainty due to approximately twenty input parameters. Input parameters investigated include environmental conditions, material properties, decay heat, and the spacing of the many small gaps in the installation. The uncertainty in gap size was found to be the principal source of uncertainty in this particular installation. The effect of the multiple fluid gap dependence and correlation on the uncertainty quantification was evaluated and discussed. As a result, the uncertainty quantification due to the fluid gaps was determined to be dependent due to the heat path dependence, and as such, a correlated error estimation was used.

Results of a “base case” using the conservative estimates outlined in the safety analysis report (SAR) are presented, as well as a “best estimate case” that uses more realistic values. These results are compared to experimentally measured values, which fall within the uncertainty band of the analysis. The model is then used to predict the peak cladding temperature (PCT) that would be expected when the cask is placed outside in an independent spent fuel storage installation (ISFSI). The method presented herein, showed that all the measured temperature values in all the seven lances inside the fuel region as well as the outside three columns of thermocouples measurements were predicted within the calculated uncertainty bands.

Experimental data to validate a CFD simulation of a dry cask storage system for both design and safety studies, suffers from a lack of local measurements, an insufficient number of measured flow variables, a lack of well-defined initial and boundary conditions, and a lack of information on experimental uncertainty. V&V 20-2009 and the work by the working group on CFD application to nuclear safety of the OECD-NEA-CSNI-WGAMA [10] established some requirements for CFD-grade experiments able to properly validate single phase CFD models. The work in this report highlights the quality of experiment used for the validation as a concern, especially due to the many lacking inputs that are of valuable interest to the modeler. The discussion on this topic establishes the criteria to judge whether an experiment can be considered of a CFD grade. CFD grade experiments should be able to validate CFD and the main concern is to minimize the validation uncertainty on some selected figure of merit (FoM). Usually, the Peak Cladding Temperature (PCT) is used as the figure of merit for dry cask applications. Other local temperature throughout or flow variable can also be a figure of merit.

Even though this validation was worth the time and the effort, the experiment cannot be classified as a CFD grade experiment due to lack of geometry specifications which resulted in large validation uncertainty. The lack of geometrical specification includes all the gaps that were part of the design specifications but not measured for the experiment performed in North Anna Power Plant.

A validation uncertainty of 63 K (113°F) was calculated for the current experiment to validate the model’s prediction of PCT. Therefore, this experiment cannot be classified as a CFD grade experiment because of the relatively large calculated validation uncertainty. Cask vendors have been submitting applications within margins close or less than 10-20 K (18-36°F) from ISG-11 specified temperature limit of 400°C (752°F). In order to be useful as a demonstration of the accuracy of the CFD modeling process or to improve the model’s capabilities, the validation uncertainty should be minimized to the desired margin of 10-20 K (18-36°F) or less. The primary simulation uncertainties consisted mainly of lack of knowledge of the size of fluid gaps that existed in the dry cask. The gap sizes are an important simulation input, and greatly influence the value of PCT predicted by the model.

TABLE OF CONTENTS

LIST OF FIGURES

LIST OF TABLES

EXECUTIVE SUMMARY

Computational fluid dynamics (CFD) technologies are rapidly expanding, with a large database of proven capabilities. The driving force for program development generally is not the nuclear community, as it was for the classical thermal-hydraulic system codes. Nevertheless, many applications overlap with those associated with the nuclear industry, and in particular, dry cask applications: flows in complex geometries, mixing in stratified fluids, flow separation and reattachment, turbulence, multiphase phenomena, chemical species interaction, and fire scenarios. Consequently, practitioners in areas related to dry cask applications can benefit from advancements in the technology taking place elsewhere. However, because of the complexity of modern commercial CFD packages, it is essential that care is taken with the inputs and equations used in order to avoid errors.

In 2017, DOE undertook an effort to perform an experiment for long-term cask storage with high burn-up fuel. Part of this effort was to measure temperature profiles in the fuel assemblies as well as the outer surface of the cask. This effort was an opportunity for USNRC to validate a CFD method for dry cask application using ANSYS-Fluent. The uncertainty quantification (UQ) and verification and validation (V&V) followed guidelines from V&V 20-2009 and best practice guideline NUREG 2152.

In USNRC, ASME V&V 20-2009 methods are used to evaluate uncertainties in CFD. Uncertainties Quantification (UQ) starts by clearly identifying the various sources of uncertainties. The deficiencies or inaccuracies of CFD simulations can be attributed to a wide number of errors and uncertainties. These errors and uncertainties consist of two main broad categories. The first category is related to modeling physics, while the second is concerned with numerical aspect of the solution. The first category includes simplification of physical complexity, boundary and initial conditions, and physical boundary conditions. The second category includes computer programming, round-off, spatial discretization, temporal discretization and iterative convergence. In the current validation, geometrical input was the main source of error including all the unknown fluid gaps that contributed immensely to the validation error. When performing validation simulations, it is mandatory to quantify and reduce the different errors and uncertainties originating from these sources. Despite all these errors and inaccuracies, CFD still remains a reliable method to simulate dry cask thermal response accurately with low margins when best practice guidelines are used. Best practice guidelines such as NUREG 2152 is an excellent source for the CFD user to avoid errors and quantify uncertainties.

The ASME V&V20-2009 standard for verification and validation in computational fluid dynamics and heat transfer clearly states that the scope of V&V is the quantification of the degree of accuracy of the simulation of a specified validation variable at a specified validation point for cases in which the conditions of the actual experiment are simulated. Practically, the standard V&V 20-2009 affirms that "The ultimate goal of V&V is to determine the degree to which a model is an accurate representation of the real world." This standard is strongly based on the use of experimental data for V&V and consequently for UQ. With this approach, the ASME standard puts a strong link between V&V and UQ.

The ASME standard methodology for uncertainty analysis underlines the role of verification and validation in the process of evaluating the confidence in CFD results. Uncertainties have to be

evaluated step by step, using clearly defined numerical aspects of the model such as time and space discretization (time step and mesh convergence) or physical models (turbulence models, physical assumptions) with associated evaluation of error.

The ASME Standard conforms to Nuclear Regulatory Commission (NRC) regulatory practices, procedures and methods for licensing dry cask systems as embodied in the United States Code of Federal Regulations and other pertinent documents such as Regulatory Guide 1.203, “Transient and Accident Analysis Methods” and NUREG-0800, “NRC Standard Review Plan” (U.S.NRC 2017).

Looking for validation experiment for CFD application to dry cask simulation for both design and safety studies, it appears that available data often suffer from a lack of local measurements, an insufficient number of measured flow variables, a lack of well-defined initial and boundary conditions, and a lack of information on experimental uncertainty. A working group on CFD application to nuclear safety of the OECD-NEA-CSNI-WGAMA established some requirements for CFD-grade experiments able to validate properly the single phase CFD tools [Bestion et al, 2019]. In this report, a look at the quality of experiment used for the validation was a concern due to the many lacking input parameters that were of valuable interest to the modeler. The discussion on this topic establishes if this experiment is of a CFD grade. CFD grade experiments should be able to validate a CFD model, and the main concern is to minimize the validation uncertainty on some selected figures of merit or target variable such as PCT.

Clear objectives should be first defined in an experimental program designed to validate a computational method. The success of the validation hinges in the constant collaboration between the experimentalist and the CFD specialist. This discussion should include the definition of the test section geometry, initial and boundary conditions, and the requirement on the measurement uncertainty. There needs to be agreement on what to measure, where it will be measured, and with which measurement technique. Acceptance criteria may be defined on the sensitivity of the measured parameters to the process of interest, and/or on the required accuracy of some selected physical quantity. Preliminary code simulations are necessary to define appropriate model boundaries and measurement locations, with sensitivity tests to determine uncertainty of initial and boundary conditions and of measured field parameters. Iterations may be necessary to optimize the design.

ABBREVIATIONS AND ACRONYMS

2D	Two Dimensional
3D	Three Dimensional
ASME	American Society of Mechanical Engineers
BIC	Boundary and Initial Conditions
CFD	Computational Fluid Dynamics
DCSS	Dry Cask Storage System
DO	Discrete Ordinates
DOE	Department of Energy
EPRI	Electric Power Research Institute
FoM	Figure of Merit
FSAR	Final Safety Analysis Report
HTC	Heat Transfer Coefficient
GCI	Grid Convergence Index
ISFSI	Independent Spent Fuel Storage Installation
NMSS	Nuclear Material Safety and Safeguards
NRC	Nuclear Regulatory Commission
PCT	Peak Cladding Temperature
PNNL	Pacific Northwest National Laboratory
PRA	Poison Rod Assembly
RE	Richardson Extrapolation
RMS	Root Mean Square
SER	Safety Evaluation Report
TN	Transnuclear
UFSAR	Updated Final Safety Analysis Report
UQ	Uncertainty Quantification
V&V	Verification and Validation
VVUQ	Verification, Validation and Uncertainty Quantification

1 INTRODUCTION

The US NRC has participated in a blind benchmark study sponsored by US DOE, aimed at assessing and improving the accuracy of CFD simulations for dry cask storage systems (DCSS). DOE and EPRI collected temperature data from a TN-32B dry storage cask at the North Anna Nuclear Generating Station, along with ambient temperature conditions.

USNRC took this unique opportunity to validate and verify a CFD method used in the dry cask application. This method used CFD best practice guidelines NUREG-2152 for dry cask applications [7]. Per these CFD guidelines, the solution was verified by calculating the Grid convergence index. In addition a thorough uncertainty quantification method was used to calculate the uncertainties of predicted PCT and other measured temperatures inside and outside the cask. Methods described in ASME V&V 20-2009 were used to quantify the uncertainty.

1.1 Objectives of a CFD-Grade Experiment

ASME V&V 20-2009, the standard for Verification and Validation (V&V) and Uncertainty Quantification (UQ) for computational Fluid Dynamics and Heat Transfer applications [1], established steps to assess the degree of accuracy of computational simulations. The accuracy of the method is obtained by the comparison between the experiment and the simulation of a local or global variable. From the validation process provided in the standard V&V 20-2009, criteria for CFD-grade experiment can be established as discussed also in (ASME 2009). A CFD grade experiment should be able to validate CFD with a minimization of the validation uncertainty on some selected figures of merit variable. As PCT is used in ISG-11 as a criterion to assess the safety of a dry cask, it is also used in this work as the figure of merit or the target variable to assess the validation uncertainty. In turn, the validation uncertainty will be used to qualify the experiment as CFD grade or not.

The validation comparison error E in any validation process is defined as the difference between the solution denoted by S, and the experimental data denoted by D:

$$\mathrm{E} = \mathrm{S} - \mathrm{D}$$

If T represents the true solution, then the error in the solution and experiment are:

$$\delta_{\mathrm{S}} = \mathrm{S} - \mathrm{T}$$

$$\delta_{\mathrm{D}} = \mathrm{D} - \mathrm{T}$$

Then E can be written as:

$$\mathrm{E} = (\mathrm{S} - \mathrm{T}) - (\mathrm{D} - \mathrm{T}) = \delta_{\mathrm{S}} - \delta_{\mathrm{D}}$$

The simulation error δ_S consists of three categories including the modeling error δ_{model} due to physical modeling input, including approximations and assumptions, the numerical solution error δ_{num} stemming out the numerical algorithm and the discrete mesh used to solve the partial differential equations, and the input data errors δ_{input} resulting from the simulation input parameters including initial conditions, boundary conditions, properties, etc. E is thus the overall result of all the errors coming from the experimental data and the simulation.

$$\mathrm{E} = \delta_{\mathrm{model}} + \delta_{\mathrm{input}} + \delta_{\mathrm{num}} - \delta_{\mathrm{D}}$$

The unknown error δ_{model} produced by the modelling is isolated:

$$\delta_{\mathrm{model}} = \mathrm{E} - (\,\delta_{\mathrm{input}} + \,\delta_{\mathrm{num}} - \delta_{\mathrm{D}})$$

The corresponding standard uncertainties for the input, numerical and experimental errors are $\mathrm{u}_{\mathrm{input}}$,$\mathrm{u}_{\mathrm{num}}$ and u_{D}.

The validation standard deviation of the combination error $\delta_{\mathrm{input}} + \,\delta_{\mathrm{num}} - \delta_{\mathrm{D}}$ is denoted as u_{val} and if the three errors are mutually independent then:

$$\mathrm{u}_{\mathrm{val}} = \sqrt{\mathrm{u}_{\mathrm{input}}^2 + \mathrm{u}_{\mathrm{num}}^2 + \mathrm{u}_{\mathrm{D}}^2}$$

$$\delta_{\mathrm{model}} = \mathrm{E} \pm \mathrm{u}_{\mathrm{val}}$$

If also δ_{model} is considered independent, then:

$$\mathrm{u}_{\mathrm{E}} = \sqrt{\mathrm{u}_{\mathrm{model}}^2 + \mathrm{u}_{\mathrm{input}}^2 + \mathrm{u}_{\mathrm{num}}^2 + \mathrm{u}_{\mathrm{D}}^2}$$

ASME standard gives solutions to evaluate every term of the comparison error (E) and the validation uncertainty ($\mathbf{u_{val}}$). The validation comparison error E sign and its magnitude are known once the validation comparison is made. The validation uncertainty can be estimated through the determination of the simulation uncertainty $\mathrm{u}_{\mathrm{simulation}}$ and the experimental uncertainty u_{D}. The simulation uncertainty consists of the numerical simulation uncertainty $\mathrm{u}_{\mathrm{num}}$ and the input uncertainty $\mathrm{u}_{\mathrm{input}}$. However there is no established method to estimate the physical modelling uncertainty $\mathrm{u}_{\mathrm{model}}$.

Propagation methods are mainly used to evaluate code result uncertainties coming from input parameters. Uncertainties of numerical solutions are given by the solution verification step or GCI method based on the Richardson extrapolation (RE) method. The standard indicates how to use the E and $\boldsymbol{u_{val}}$. These quantities give an accuracy of the model used through:

$$\mathrm{u}_{\mathrm{model}} = \sqrt{\mathrm{u}_{\mathrm{E}}^2 - \mathrm{u}_{\mathrm{val}}^2}$$

From these equations, the following criteria can be concluded:

- If $|\mathbf{E}| >> \mathbf{u_{val}}$, $\mathbf{u_{model}} \cong \mathbf{u_E}$. Then, $\mathbf{u_{val}}$ is relatively small and the modeling error is larger than the validation uncertainty. In this case, the comparison between the code predictions and the experimental data can provide a useful and precise information on the quality of the physical model. Consequently, the model has the possibility to be improved or calibrated using the data from the experiment in order to have less uncertainty on the result.

- If $|\mathbf{E}| < \mathbf{u_{val}}$, the larger validation uncertainty implies that the model accuracy cannot be improved if the combination δ_{input}, δ_{num} and δ_{D} cannot be reduced. In this case, the standard indicates that this is not a proof that the model has a good or bad quality but this kind of experiment will not be useful to make improvement to the model.

- If $|\mathbf{E}| = \mathbf{u_{val}}$, the modeling error is within the noise level imposed by the input, numerical and experimental uncertainties and the possibility of model improvement is a challenge.

- If model uncertainty $\mathbf{u_{model}}$ is known or expected, sensitivity analyses on sensitive modeling parameters can be performed to investigate the impact this model uncertainty can have on target variable such PCT and $\mathbf{u_{val}}$.

    - If $\mathbf{u_{model}} < \mathbf{u_{val}}$. The experiment is not very informative

    - **If** $\mathbf{u_{model}} > \mathbf{u_{val}}$. The experiment is capable of showing if the expected model uncertainty is reached

A CFD grade experiment is an experiment which can be used to validate the physical model, which means that it provides a relatively low uncertainty of validation $\mathbf{u_{val}}$ and allows a good determination of the model uncertainty $\mathbf{u_{model}}$. Therefore, an experiment which minimizes both $\boldsymbol{\delta_{input}}$ and $\boldsymbol{\delta_D}$ also minimizes $\mathbf{u_{val}}$ and provides more information on the accuracy of the model. A CFD-grade experiment should provide the lowest values of δ_{input} , and δ_{D} (i.e. low $\mathbf{u_{val}}$). In parallel, the CFD user or specialist should strive to minimize the numerical error $\mathbf{u_{num}}$ or at least follow well established methods to quantify it correctly.

However the capability for an experiment to provide information on the uncertainty of model parameters may not be the concern of a dry cask safety analysis. The final goal is often to compare a parameter of interest such as PCT to a safety criterion to assess if the dry cask is safe in the situation designed for. Very often, and due to the lack of geometrical details inside the cask as in the case of fluid gaps in the current validation as shown in in this report, it is much more difficult to know all necessary boundary and initial conditions (BIC) and flow field variables in the region of interest with a low uncertainty or high confidence. As a result, $\mathbf{u_{input}}$ may be large. Such experiments should at least provide sufficient information to quantify the accuracy of CFD code predictions for the relevant parameters of interest in the safety analysis such as some local temperatures or PCT. In turn, this accuracy prediction can be used to assess whether a reliable conclusion for the safety case can be made. The experiment should target a predetermined code uncertainty for the selected target variable such PCT or other variable. So, instead of providing data to allow quantifying the uncertainty on some specific model parameters, the goal is the prediction of the uncertainty on the target variable of interest. This uncertainty is the result of the propagation of various sources of uncertainty from $\boldsymbol{\delta_{input}}$, $\boldsymbol{\delta_{num}}$ and $\boldsymbol{\delta_D}$. As such, the minimization of these sources of errors remains the objective of the VVUQ process.

Another important requirement is the collaboration between the experiment designer and the code user from the start of the experimental project. The collaboration should target the models used in the dry cask application as shown in NUREG 2152 [7]. Code users and safety analysts can then expose the goal of the experiment, in terms of model validation. Among these modeling goals that can be targeted and investigated are type of turbulence model that govern the flow field, state laws for the fluid of interest, or porous media parameters if porous media model is used. A list of modeling challenges including boundary conditions for dry cask applications can be found in NUREG 2152 and NUREG 2208. In this important initial step, CFD code users can perform pre-calculations to help the definition of the mock-up in terms of geometrical design, range of flow variables, choice of boundary conditions, and scaling analyses. This collaboration can also be used to define the plan of the experiment. As such, a

CFD-grade experiment should first be characterized by an exchange between experimentalists and code users from the beginning of the design of the experiment to the end of the project.

The preliminary specification of fluid and solid volumes of interest and of inlet and outlet fluid surfaces is of prime importance to select where initial and boundary conditions have to be known. A CFD-grade experiment should specify the boundary conditions, initial conditions, and model domain in a way that they can be used as simulation input data with the required accuracy.

A general requirement may be to define a priori acceptance criteria before designing an experiment. If the only objective is to validate a CFD code on a specific flow configuration, the acceptance criterion may be to minimize the validation uncertainty (i.e. experimental, numerical, and input uncertainties) on a specific target variable. In dry cask applications, examples may be the following:

- If the objective is to validate a CFD code for PCT, the acceptance criterion may be that the validation uncertainty related to this PCT should not exceed a given value.

- If the objective is to predict the canister wall heat transfer in a ventilated cask, the acceptance criterion may be that the validation uncertainty related to a predetermined temperature difference ΔT between the air inlet and outlet should not exceed a given value.

- If the objective is to predict the air mass flow rate in a ventilated cask, the acceptance criterion may be that the validation uncertainty related to a measured mass flow rate in the air flow passage should not exceed a given value.

In the last few years, dry cask applicants applied for licenses for cask design close to 50 kW or higher. The analyses accompanying these applications presented CFD thermal analysis cases with PCT very close to the ISG-11 allowable limit of 400 C, with margins as small as 10 - 20°C (18 - 36°F). As such, in this validation, the calculated validation uncertainty $\mathbf{u_{val}}$ will be compared to these margins to make conclusions if the experiment used in this validation exercise can be classified as a CFD grade experiment.

1.2 Description of Validation Experiment

The cask used for the validation experiment was a TN-32B dry cask storage system. The TN-32B cask is cylindrical with a vertical orientation. It has an outer diameter of 8.5-ft (2.6 m) and a height of approximately 15-ft (4.6 m) with the protective cover and lid neutron shielding removed. A detailed description of the TN-32B demonstration project held in North Anna Power Plant can be found in [2]. According to the non-proprietary Safety Evaluation Report (SER) [3], the TN-32B cask consists of:

- A basket assembly which locates and supports the fuel assemblies
- An inner confinement vessel and lid, which comprises the primary confinement barrier;
- A carbon steel gamma shield structure surrounding the primary confinement vessel;
- Neutron shielding material (jacketed) exterior to the gamma shield;
- A protective cover which provides weather protection for the closure lid and seal components, the top neutron shield, and the overpressure system.

- An overpressure monitoring system which monitors pressure between the two seals of the cask lid. This system allows for early detection of cask seal leakage.
- Sets of upper and lower trunnions for lifting and support of the cask.

The cask is designed to handle 32 pressurized water reactor (PWR) fuel bundle assemblies, with a total maximum heat load of 32.7 kW, and an allowable peak cladding temperature (PCT) of 400°C.

The lid of the cask was modified to allow insertion of seven thermocouple lances in fuel assemblies 2, 6, 14, 19, 24, 28, and 31 (as shown in Figure 2-2). Each thermocouple lance contained nine thermocouples that were spaced throughout the height of the cask to provide a total of 63 temperature measurements spaced throughout the inner cask. The protective cover, top neutron shield, and standard overpressure system that are normally in place were removed for the experiment to provide access to the lid for the thermocouple lances.

In addition to the internal cask temperature measurements, fifteen surface temperature measurements were recorded to validate external heat transfer rates.

The cask was tested indoors in a test bay that provided access around the bottom of the cask, as well as a work platform that provided access to the top of the cask. Ambient temperature inside the building was recorded at several locations around the cask, which showed both spatial and temporal variations.

The test consisted of a “thermal soak”, where the cask was allowed to reach steady-state temperatures over a period of several days. Although the ambient temperatures inside the building were variable, the cask temperatures were found to be steady, owing to the larger thermal mass of the cask.

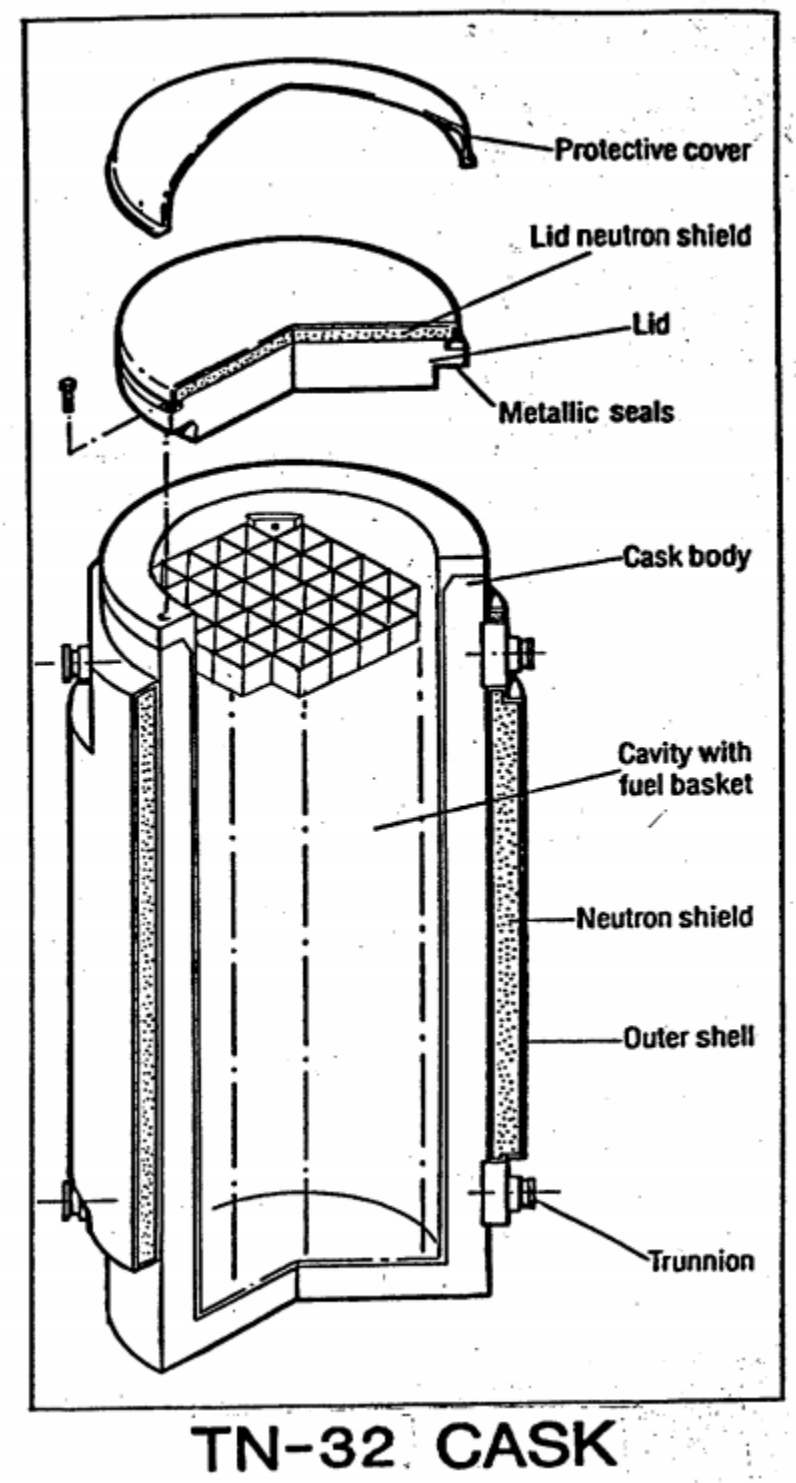

Figure 1-1 Layout of the TN-32 Cask from the Non-proprietary Safety Evaluation Report

2 COMPUTATIONAL MODEL DESCRIPTION

This chapter describes the settings and boundary conditions that were used to simulate the TN-32B dry cask storage system.

2.1 TN-32B Cask Model

The cask geometry was generated based on the drawings provided in the UFSAR [4].

2.1.1 Description of Mesh

The cask geometry was meshed using primarily hexahedral elements. A coarse model was initially created with 1 cell across many of the thin structural pieces to achieve a low cell count. This coarse mesh was refined to double the mesh resolution for the baseline mesh, and doubled again to achieve the fine mesh. This triplet of meshes was used to determine the grid convergence index (GCI) as described in Section 3.3.2 . A sample of the baseline mesh is shown in Figure 2-1.

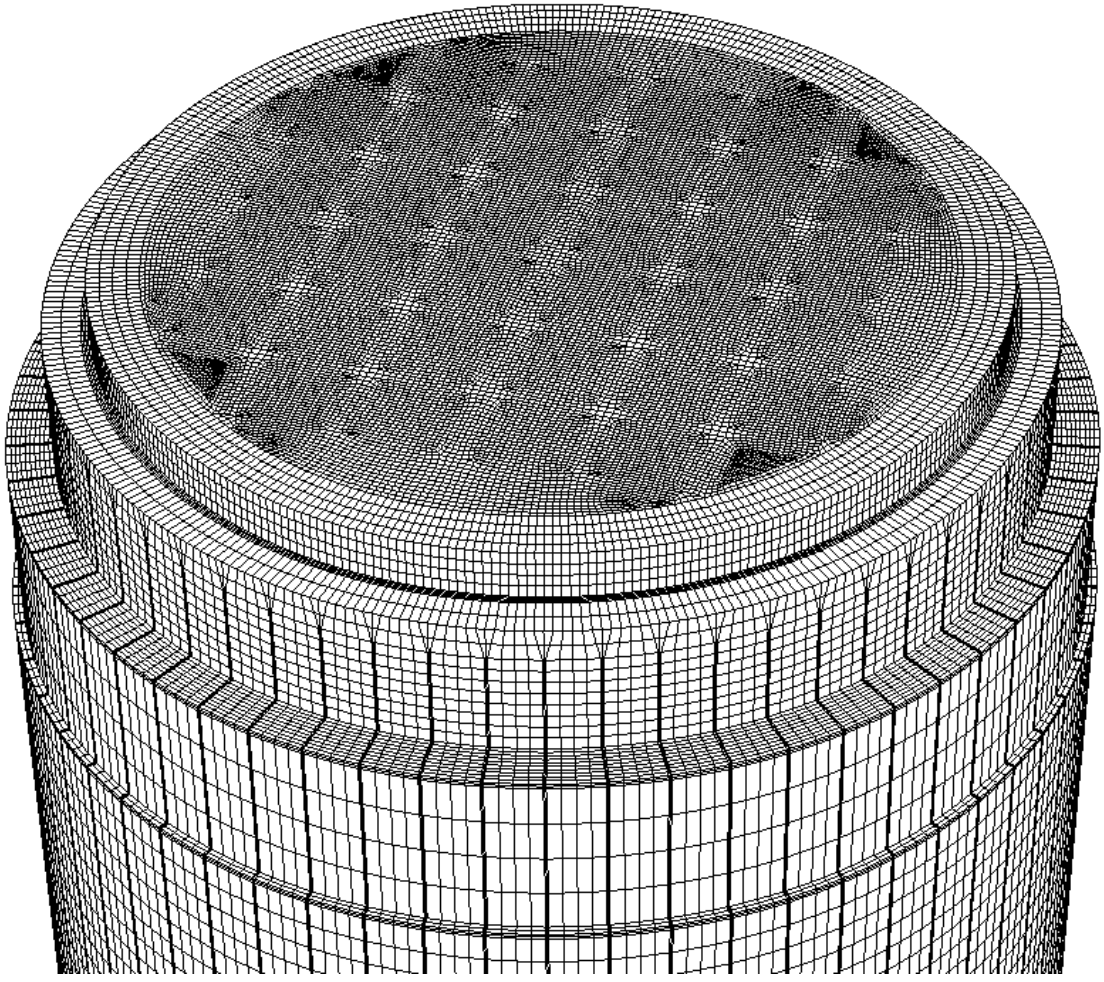

Figure 2-1 Cask External Surface Mesh

2.2 North Anna Thermal Round Robin Model Inputs

2.2.1 Material Properties

As much as possible, the CFD analysis used the material properties that were specified in the Thermal Evaluation (Chapter 4) of the UFSAR [4]. This includes thermal conductivities of helium, air, carbon steel, 6061 alloy aluminum, polyester resin used for neutron shielding, stainless steel, and 6063 alloy aluminum.

2.2.1.1 Fuel Properties

The fuel bundles are made up of many small components, which are too complex to simulate directly in the cask CFD model with current computational capabilities. Instead, the fuel bundles were simulated using porous media to provide the resistance to flow, and an effective thermal conductivity of the entire fuel bundle assembly in the axial and transverse directions.

The thermal conductivity and porosity calculations that were used in this analysis are based on the work presented in NUREG-2208 [8]. Thermal conductivities are based on a combination of conductive and radiative heat transfer, and are a function of temperature. The thermal conductivities used are in line with those presented for PWR fuel in the FSAR.

Six of the fuel bundles also contained poison rod assemblies (PRA). These fuel bundles were in positions 8, 13, 15, 18, 20, and 25. Effective thermal conductivities for these assemblies were caluclated using the same methods.

Uncertainty in fuel hydraulic resistance was assumed to be ±50%, which contributed very little to the uncertainty of the simulation result due to the very low circulation velocities in the fuel bundles.

Axial thermal conductivity for the baseline simulation was calculated assuming there was thermal conduction through the fuel cladding, as well as the helium, and the fuel pellets, which expand as the fuel is used so that they press against each other and create an effective heat path along the axis of the tube. When calculating the uncertainty in axial thermal conductivity, the uncertainty band was based on the difference between the baseline assumption, and allowing heat transfer only through the cladding, which is a conservative assumption made by other researchers. Uncertainty in the transverse thermal conducivity of the fuel bundles was assumed to be ±10%.

2.2.1.2 Internal Pressurization

The cask was filled with helium to a pressure of 2200 mbar (31.9 psia) [2]. It was assumed that all water had evaporated during the vacuum drying process, and that the gas was 100% pure helium. Intial analyses showed that the sensitivity of the simulation results to helium pressure were very low, so the influence of internal pressure is omitted from the UQ analysis.

2.2.2 Decay Heat

The decay heat for each of the 32 fuel bundle assemblies as of November 7, 2017 was provided as a modeling input, though loading did not occur until November 14, 2017 [2] and is presented in Figure 2-2. Thermal soak testing was conducted for roughly two weeks after loading. Total decay heat for the cask was reported to be 30.456 kW.

A normalized vertical decay heat profile (Figure 2-3) was provided for the validation exercise and applied to all 32 fuel bundles [2].

An uncertainty in decay heat of 2% was assumed for this analysis, which covers local variations in decay heat profile, as well as uncertainty in prediction of decay heat for each assembly on the date of testing.

2.2.3 Heat Dissipation to the Environment

Ambient temperatures were measured during testing as described in Thermal Modeling Round Robin input [2]. The temperatures varied over the several days it took to reach thermal equilibrium inside the cask, primarily from day/night cycles as the cask was placed next to an un-insulated roll-up door.

An average ambient temperature of 75°F (297K) was used for the analysis. This temperature was used to calculate external convection, as the heat sink for conduction through the ground support, and as the temperature that the surface of the cask was radiating to. Due to the variability in the temperature over time, as well as at different locations within the test area, an uncertainty in the ambient temperature of ±15°F (8.3K) was used in the UQ analysis.

A convection heat transfer coefficient (HTC) of 5.0 W/m^2-K was used for the vertical sidewalls of the cask. The convection coefficient was calculated based on the external skin temperature of the cask using several different turbulent natural convection Nusselt number correlations for vertical plates for the sides of the cask, which were in line with the method presented in the FSAR. HTC values for the vertical sidewalls of the cask fell between 4.0 and 6.0 W/m^2-K depending on the correlation used, and whether the minimum, maximum, or average surface temperature was used. This ±1.0 W/m^2-K variability in HTC was the basis for the uncertainty in the input value in the UQ analysis.

The uncertainty in HTC from the top of the cask was higher, owing to the lead blankets that were used as a temporary neutron shield. The thermal conductivity of the blankets was not provided with the experimental data, and they were randomly placed across the top of the cask, which increases the uncertainty of the effective HTC from the top of the cask. HTC values for the top of the cask without a blanket were estimated to be between 6 and 7 W/m^2-K, which is in line with the methods used in the FSAR, however the presence of the blankets would reduce this value somewhat. A value of 5.0 W/m^2-K was used for the top of the cask, with an uncertainty of ±2.0 W/m^2-K.

The cask was placed on a 1.5-inch thick steel leveling pad with several steel legs, which in turn rested on a stainless steel lined concrete floor. There was a 6” air gap between the leveling pad and the floor. Insufficient information was provided regarding the legs of the leveling pad to include them in the thermal analysis. This configuration includes several modes of heat transfer from the leveling pad, including:

- Conduction through the legs, and into the concrete floor.
- Convection from the leveling pad, legs, and floor to an unknown convection current or air running underneath the leveling pad.
- Radiation from the leveling pad to the floor.

The interplay in these heat transfer modes, and the inability to accurately calculate them from the information provided add to the uncertainty of the analysis. The HTC through the bottom of the cask from all of these modes was estimated at 10.0 ± 5.0 W/m^2-K.

Thermal radiation is another means of heat rejection from the cask to the environment. Emissivity values from the white painted external surfaces of the cask were taken to be 0.90 based on the FSAR [4]. An uncertainty of ±0.10 was used in the UQ analysis.

The North Anna thermal test was conducted indoors, so solar insolation was omitted from this analysis.

2.2.4 Thermal Gap Resistance

Due to the various materials used in the construction of the TN-32B cask, there are many small gaps throughout the design, which increase the resistance of heat transfer from the fuel assemblies to the environment. Many of these gap sizes are not – and cannot be – precisely known. Estimates of the largest size expected for each of these gaps were provided in the USFAR, and those values are used here in the baseline case. As such, they are considered to be maximum values, with the actual gap sizes expected to be smaller than what is used for the baseline case.

The gaps were treated as thin "shadow-walls" within the FLUENT solver, whereby they do not take up any physical space in the mesh, but an additional computational cell is added across the gap to allow the resistance due to thermal conduction and radiation across the gap. An effective thermal conductivity was calculated for each gap assuming both conduction through the gas and radiation across the gap. All gaps were small enough, with a small enough temperature gradient that natural convection was assumed to be negligible. The effective thermal conductivity is calculated from the thermal conductivity of the gas at the average gap temperature, the size of the gap, and the emissivity of the materials on either side of the gap assuming infinite plates in parallel.

$$k_{eff}(T) = k(T) + 4h\epsilon_{12}\sigma T^3$$

Where:

k_{eff} = effective thermal conductivity (W/m-K)

k = molecular thermal conductivity (W/m-K)

h = gap between walls (m)

ϵ_{12} = combined emissivity

σ = Stefan-Boltzmann constant (W/m^2-K^4)

T = Temperature (K)

The combined emissivity for two infinite parallel plates is a combination of the emissivity for each surface, ϵ_1 and ϵ_2:

$$\epsilon_{12} = \frac{1}{\frac{1}{\epsilon_1} + \frac{1}{\epsilon_2} - 1}$$

Due to gravity, construction methods, thermal expansion of dissimilar materials, and the fact that the center of the cask is hotter than the exterior, most of these gaps are expected to close (go towards zero) as the cask heats up. When addressing the uncertainty due to all of these gaps – which is considerable – the uncertainty is only on the negative side (i.e. - smaller gap, colder PCT). This introduces a significant bias error into the baseline solution, whereby the baseline simulation does not actually represent our best guess of what is occurring, but rather a much hotter result than exists in reality.

For this reason, a "best estimate" case is also included in the presentation of results, whereby all of the gaps except for one are set to zero. The only gap that is allowed to remain at the UFSAR specified size is the gap between the basket and the cask rails. This gap was expected to be 0.188 inches at thermal equilibrium within the cask [4]. This is one of the largest gaps within the system, and most of the heat in the cask passes across this gap. In the best estimate case, this basket-to-rails gap is maintained at 0.188 inches as stated in the UFSAR.

A list of all thermal gaps included in the model is provided in Table 2-1, including the nominal gap size and the corresponding uncertainty assumed. The locations of the gaps are shown in plan view in Figure 2-4, and elevation view in Figure 2-5.

The heat transfer across the inner cask / outer cask gap was listed as 375 Btu/hr-ft2-°F, with a conservative estimate of 200 Btu/hr-ft2-°F. These values were converted to a gap size for this analysis using the thermal conductivity of air at the average gap temperature.

Table 2-1 Summary of Helium Gaps

Helium Gap Location	Baseline Input (inches)	Input Uncertainty (inches)
Basket to rails	0.188	+0.000 / -0.188
Rails to cask	0.010	+0.000 / -0.010
SS sheet to Al plate	0.020	+0.000 / -0.020
Al basket plates	0.020	+0.000 / -0.020
Basket to bottom of cask	0.250	+0.000 / -0.250

Table 2-2 Summary of Air Gaps

	Baseline Input (inches)	Input Uncertainty (inches)
Cylindrical cask	0.00129	+0.000 / -0.00129
Cask bottom	0.125	+0.000 / -0.125
Resin boxes	0.010	+0.000 / -0.010
Lid seal	0.010	+0.000 / -0.010

	1 6T0 NAIF/P+Z Zirlo, 54.2 GWd 4.25%/3 cy/12.1 yr 912.2 W	2 (TC Lance) 3K7 AMBW M5, 53.4 GWd 4.55%/3 cy/8.7 yr 978.2 W	3 3T6 NAIF/P+Z Zirlo, 54.3 GWd 4.25%/3 cy/12.1 yr 914.4 W	4 6F2 NAIF/P+Z Zirlo, 51.9 GWd 4.25%/3 cy/13.5 yr 799.5 W	Drain Port
5 3F6 NAIF/P+Z Zirlo, 52.1 GWd 4.25%/3 cy/13.5 yr 800.9 W	6 (TC Lance) 30A AMBW M5, 52.0 GWd 4.55%/3 cy/7.2 yr 1008.6 W	7 22B AMBW M5, 51.2 GWd 4.55%/3 cy/5.7 yr 1142.4 W	8 (PRA) 20B AMBW M5, 50.5 GWd 4.55%/3 cy/5.7 yr 1121.2 W	9 5K6 AMBW M5, 53.3 GWd 4.55%/3 cy/8.7 yr 975.1 W	10 5D5 NAIF/P+Z Zirlo, 55.5 GWd 4.20%/3 cy/17.7 yr 814.5 W
11 (Vent Port) 5D9 NAIF/P+Z Zirlo, 54.6 GWd 4.20%/3 cy/17.7 yr 802.6 W	12 28B AMBW M5, 51.0 GWd 4.55%/3 cy/5.7 yr 1135.0 W	13 (PRA) F40 LOPAR Zry-4, 50.6 GWd 3.59%/3 cy/30.6 yr 573.8 W	14 (TC Lance) 57A AMBW M5, 52.2GWd 4.55%/3 cy/7.2 yr 1037.0 W	15 (PRA) 30B AMBW M5, 50.6 GWd 4.55%/3 cy/5.7 yr 1124.8 W	16 3K4 AMBW M5, 51.8 GWd 4.55%/3 cy/8.7 yr 941.3 W
17 5K7 AMBW M5, 53.3 GWd 4.55%/3 cy/8.7 yr 961.7 W	18 (PRA) 50B AMBW M5, 50.9 GWd 4.55%/3 cy/5.7 yr 1131.1 W	19 (TC Lance) 3U9 NAIF/P+Z Zirlo, 53.1 GWd 4.45%/3 cy/10.6 yr 920.2 W	20 (PRA) 0A4 NAIF Low-Sn Zry-4, 50.0 GWd 4.00%/2 cy/23.2 yr 646.2 W	21 15B AMBW M5, 51.0 GWd 4.55%/3 cy/5.7 yr 1135.8 W	22 6K4 AMBW M5, 51.9 GWd 4.55%/3 cy/8.7 yr 941.2 W
23 3T2 NAIF/P+Z Zirlo, 55.1 GWd 4.25%/3 cy/12.1 yr 934.7 W	24 (TC Lance) 3U4 NAIF/P+Z Zirlo, 52.9 GWd 4.45%/3 cy/10.6 yr 914.2 W	25 (PRA) 56B AMBW M5, 51.0 GWd 4.55%/3 cy/5.7 yr 1133.7 W	26 54B AMBW M5, 51.3 GWd 4.55%/3 cy/5.7 yr 1136.3 W	27 6V0 AMBW M5, 53.5 GWd 4.40%/3 cy/8.7 yr 988.2 W	28 (TC Lance) 3U6 NAIF/P+Z Zirlo, 53.0 GWd 4.45%/3 cy/10.6 yr 916.9 W
	29 4V4 AMBW M5, 51.2 GWd 4.40%/3 cy/9.1 yr 914.2 W	30 5K1 AMBW M5, 53.0 GWd 4.55%/3 cy/8.7 yr 968.0 W	31 (TC Lance) 5T9 NAIF/P+Z Zirlo, 54.9 GWd 4.25%/3 cy/12.1 yr 927.7 W	32 4F1 NAIF/P+Z Zirlo, 52.3 GWd 4.25%/3 cy/13.5 yr 804.3 W	

Figure 2-2 System Loading Map

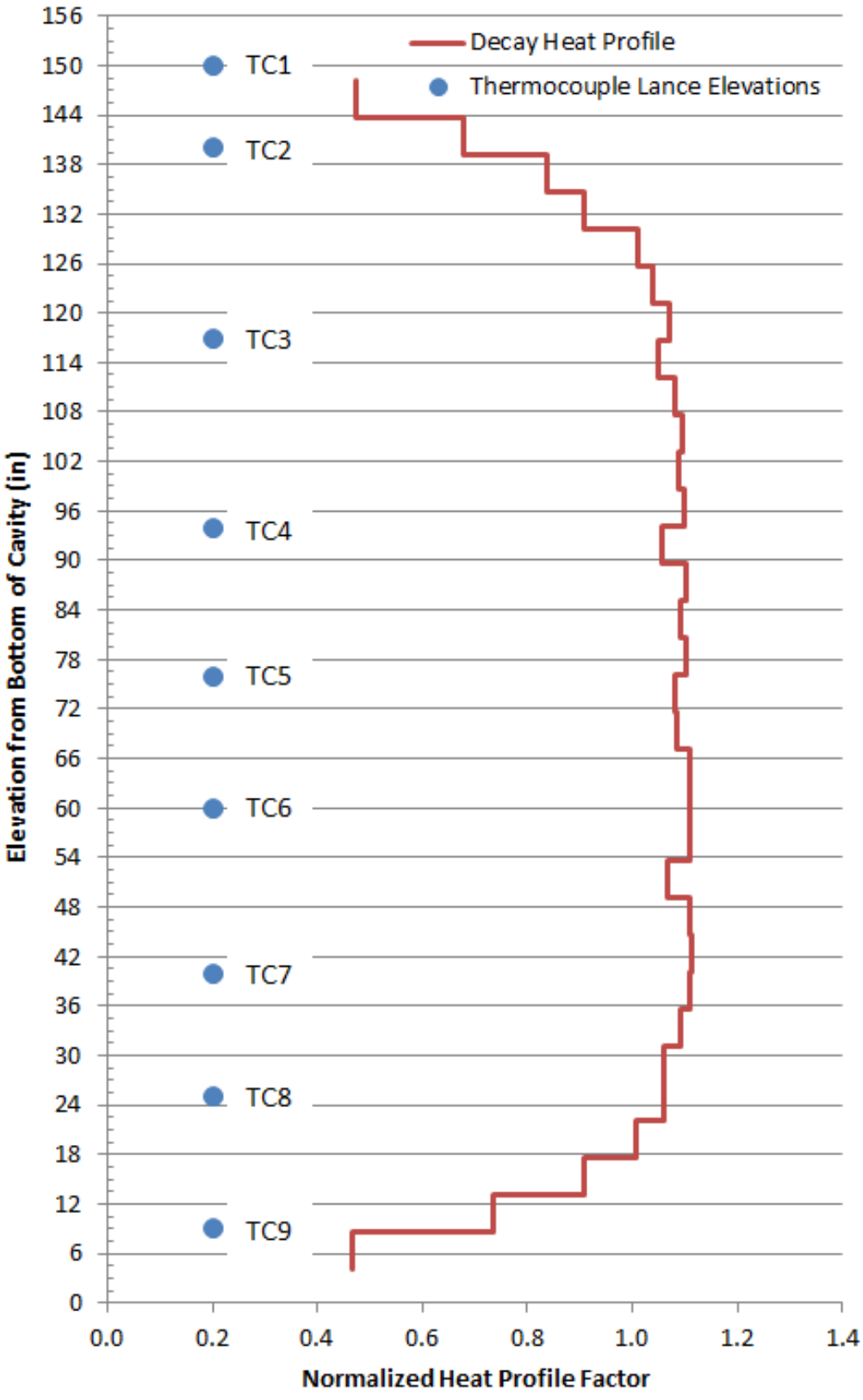

Figure 2-3 Normalized Fuel Decay Heat Profile and Thermocouple Elevations

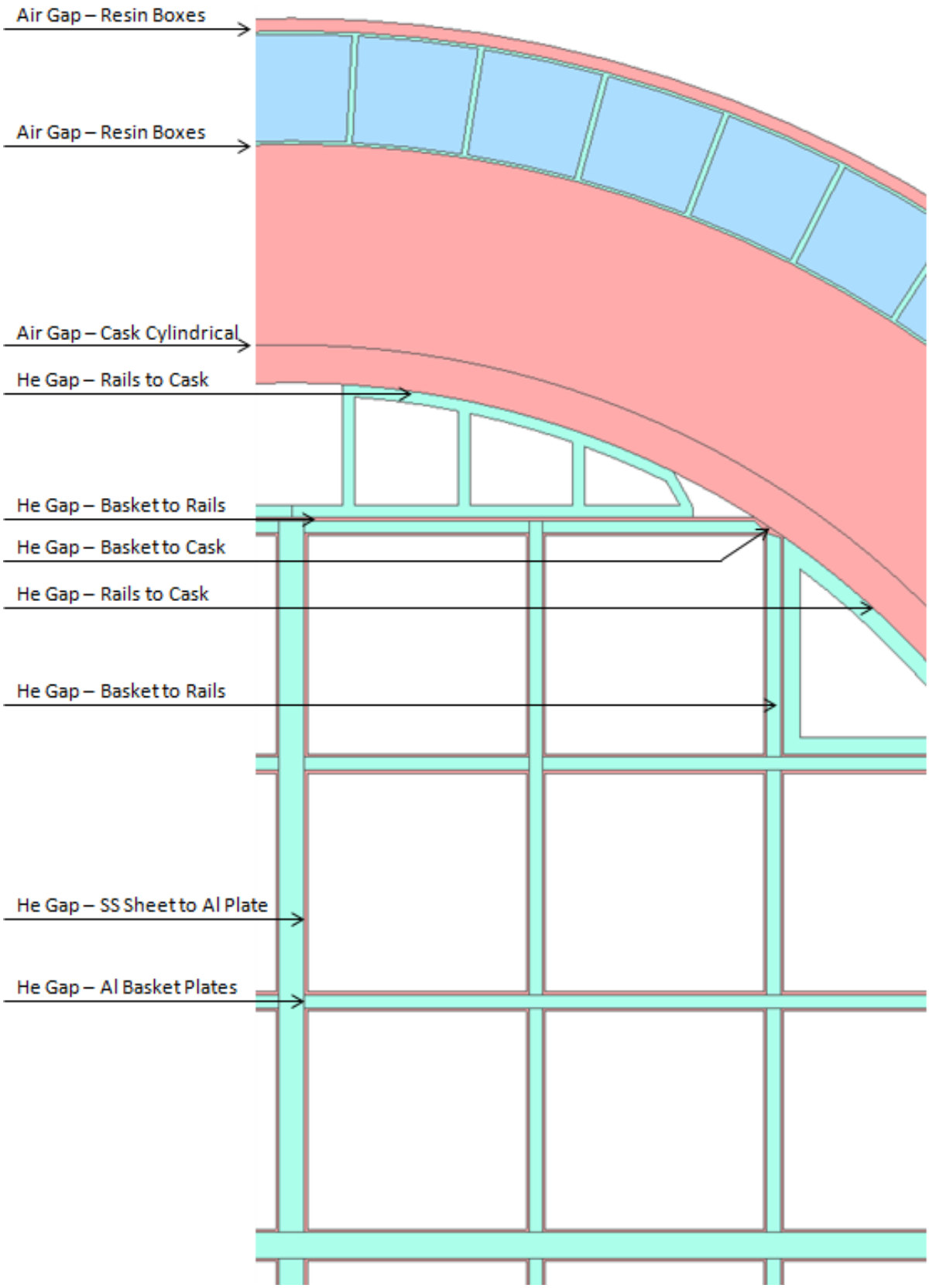

Figure 2-4 Thermal Gap Summary for Validation Case – Plan View

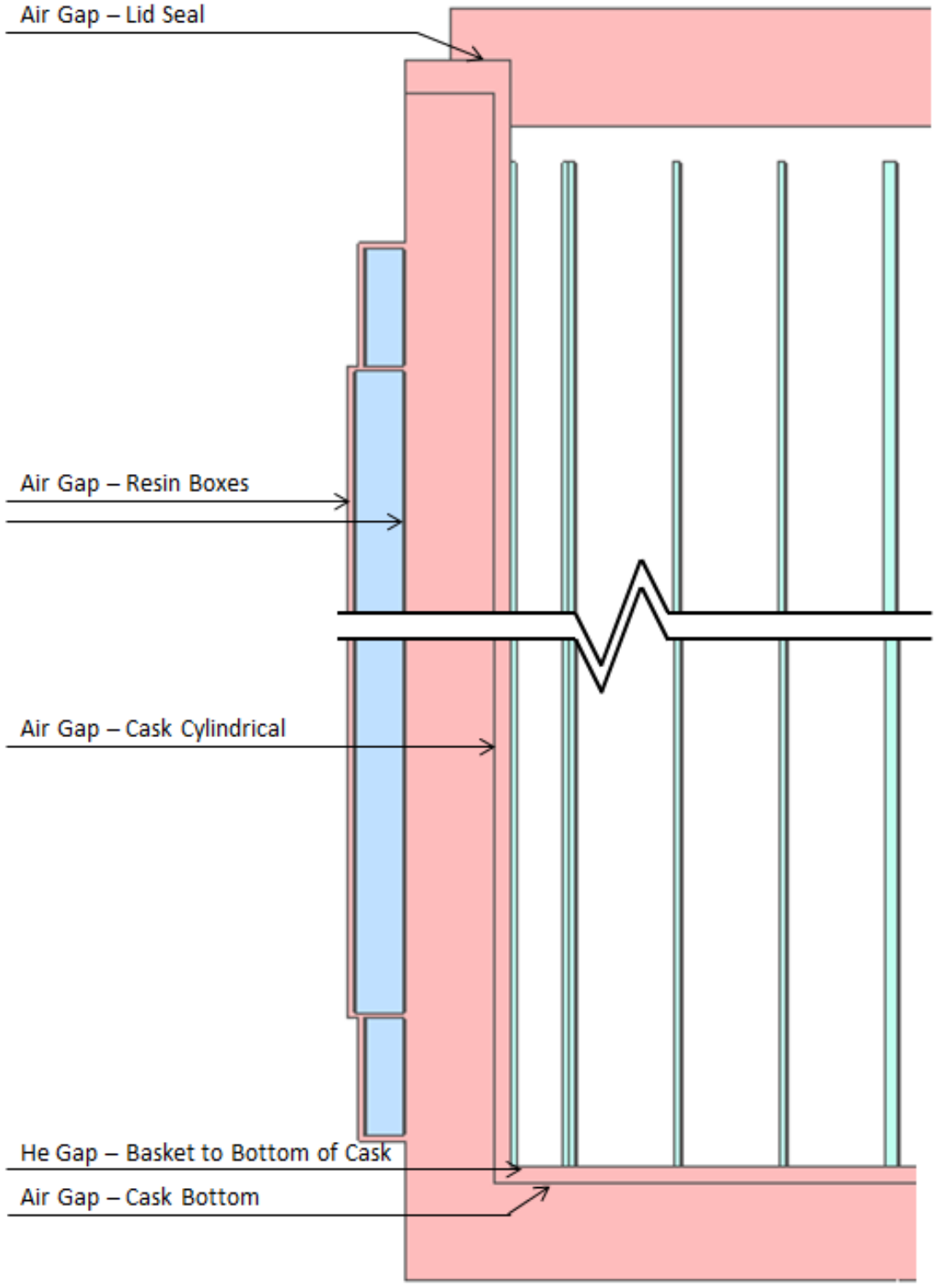

Figure 2-5 Thermal Gap Summary for Validation Case – Elevation View

2.3 Solver Settings

ANSYS-Fluent v.19.0 was used as the solver. The solver settings are presented in Table 2-3.

Table 2-3 CFD Solver Settings

CFD Solver Settings:	Input Value:
Solver Code	ANSYS-Fluent v19.0
Solver Type	Pressure-Based
Viscous	Laminar
Radiation	Discrete Ordinates, Gray Model
Pressure-Velocity Coupling Scheme	SIMPLE
Time Discretization	Steady-State
Spatial Discretization:	
Gradient	Green-Gauss Node Based
Pressure	Second Order Upwind
Momentum	Second Order Upwind
Energy	Second Order Upwind
Discrete Ordinates	Second Order Upwind

Rayleigh Number calculations for helium inside the inner cask confirm that the flow is laminar.

The settings for the radiation model are presented in Table 2-4. Testing has indicated that the sensitivity to these parameters is less than the iterative convergence uncertainty (discussed later in this report), so sensitivity to these values is not included in the input uncertainty analysis.

Table 2-4 Radiation Model Settings

Discrete Ordinates, Gray Model Inputs:	Input Value:
Theta Divisions	4
Phi Divisions	4
Theta Pixels	4
Phi Pixels	4
Energy Iterations per Radiation Iteration	10

3 VALIDATION RESULTS

The uncertainty quantification will be conducted according to ASME V&V 20-2009 [1]. The main sources of uncertainty that will be investigated include: numerical uncertainty, which includes iterative uncertainty and grid uncertainty; and input uncertainty. These are addressed below. Another source of uncertainty – experimental uncertainty in the data provided for validation – was provided by the personnel conducting the experiment.

3.1 Baseline Simulation Results

Decay heat is generated in each assembly, and makes its way out to the environment through many parallel paths of conduction, convection, and radiation. The assemblies in the center of the cask have the longest path for heat to escape, and consequently have the highest temperatures. The highest temperature in the cask was found in assembly 14, one of the four assemblies in the very center of the cask (Figure 2-2). The PCT in the baseline simulation was found to be 535 K (503°F). Contours of temperature through a horizontal and vertical slice are shown in Figure 3-2 and Figure 3-3 respectively.

Although radiation and convective heat transfer are included in the analysis, neither mode of heat transfer appreciably contributes to heat fluxes inside the cask. In areas with large open volumes where convection or radiation may play a significant role, there are aluminum rails, which are very effective at conducting heat. This effective heat conduction results in small temperature gradients that minimize the heat flux via radiation and natural convection. In the case of natural convection, this is confirmed by the observed predicted low velocities throughout the cask. The highest predicted velocity anywhere inside the cask is below 1 m/s (3.28 ft/s), with most rail cavities having velocities below 0.25 m/s (0.82 ft/s). , The highest velocity inside a fuel bundle was considerably lower at 0.02 m/s (0.07 ft/s) due to the increased hydraulic resistance.

The thermal resistances across the gaps are a dominant feature in determining the temperature distribution throughout the cask. Significant dislocations in temperature gradient can be seen across gaps between different cask components (Figure 3-2 and Figure 3-3). Whereas there is very little temperature gradient across monolithic structures such as the steel inner and outer casks, the aluminum rails, and the aluminum resin boxes around the perimeter of the cask.

Since these thermal gaps are such a dominant component of the thermal resistance between the decay heat source and ambient heat sink, and since there is a great deal of uncertainty in how large these gaps actually are, it follows that the thermal resistance due to these gaps are a great source of uncertainty when predicting the temperatures of the spent fuel inside the cask. This will be demonstrated in the sections that follow.

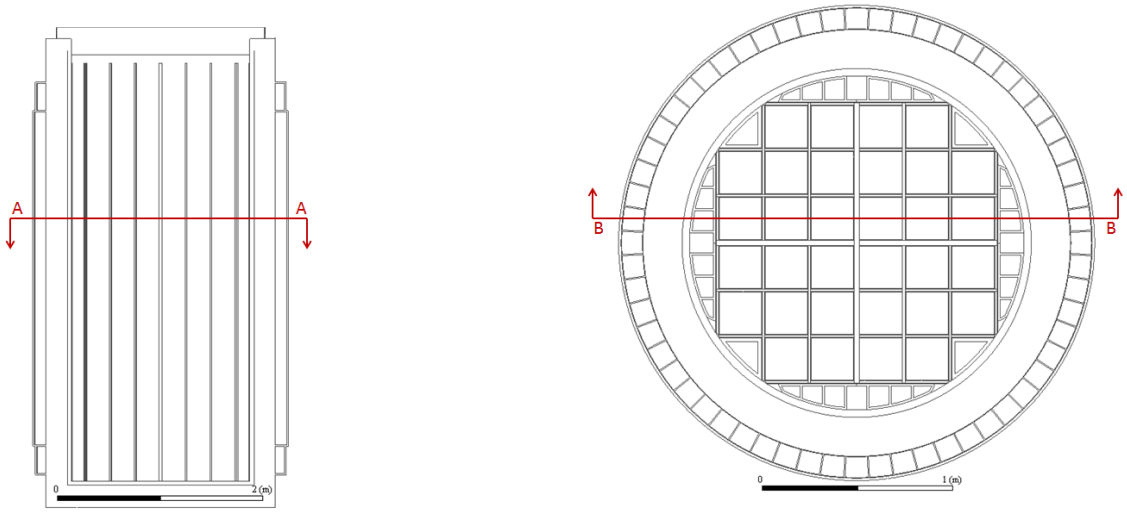

Figure 3-1 Section A-A at Elevation 2000mm, Section B-B 5" Off of Cask Centerline

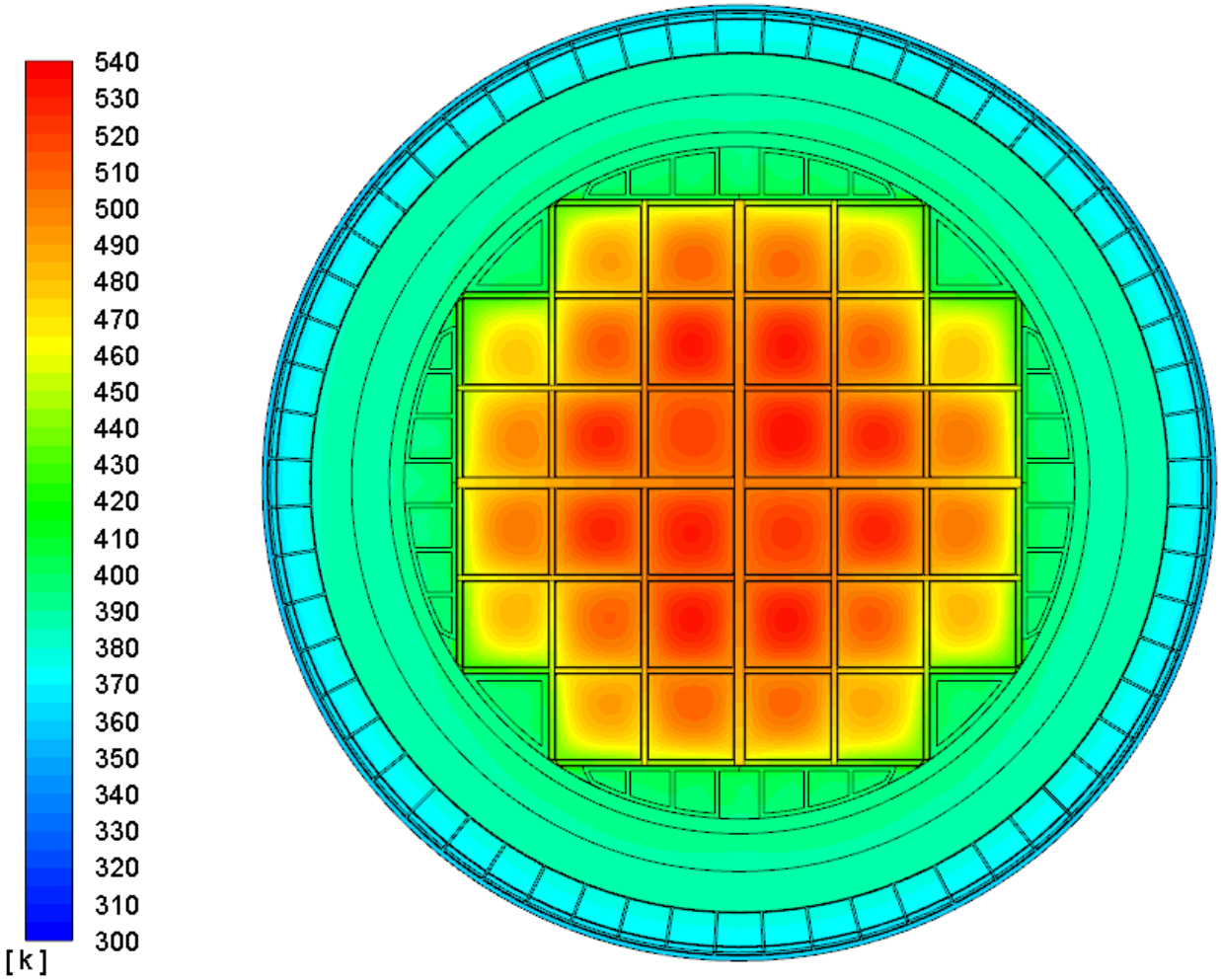

Figure 3-2 Temperature at Section A-A, Validation Baseline Case (K)

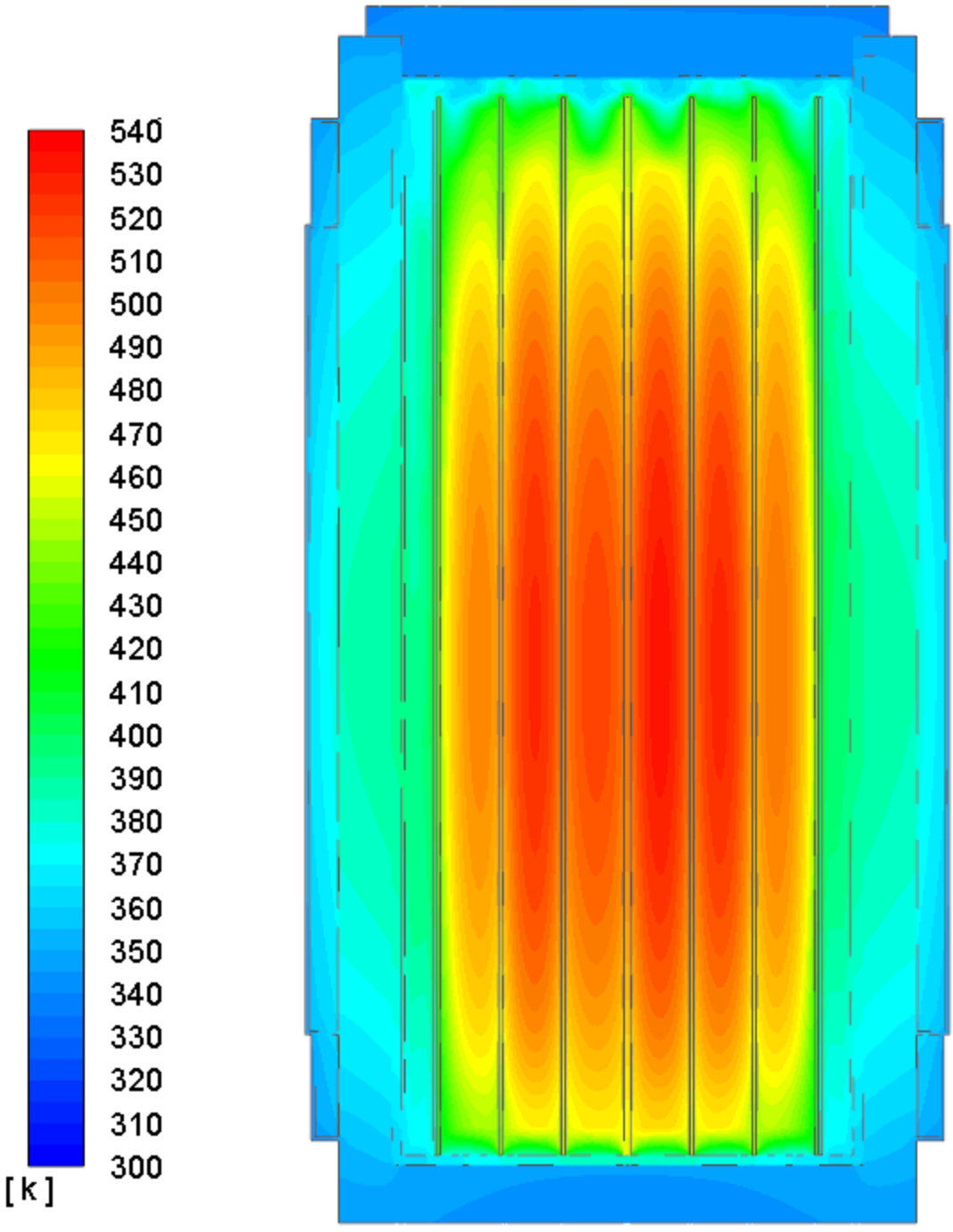

Figure 3-3 Temperature at Section B-B, Validation Baseline Case (K)

3.2 Consistency Check

The first step in validating the simulation and quantifying the uncertainty is to ensure that the simulation is internally consistent. Two consistency checks that are easy to demonstrate are

mass conservation and energy conservation across the boundaries of the model. In this case, there are no inlet or outlet flow boundaries, so mass conservation is inherently met at the model boundaries.

The fuel decay heat for the model should be 30.456 kW per the input values presented in Figure 2-2. Due to discretization of the decay heat profile over the height of the fuel bundle (steps in decay heat profile provided in Figure 2-3 do not exactly align with computational element spacing in the CFD model), the actual model heat input for the baseline model was 30.409 kW (0.15% error). The reported heat flux from all external surfaces of the model was 30.441 kW (0.11% error based on model input value). These errors are quite small compared to other sources of error and uncertainty in this simulation, and demonstrate consistency of the simulation with respect to conservation of energy.

3.3 Numerical Uncertainty

Numerical uncertainty is made up of three major sources: computer round-off error, iterative convergence uncertainty, and discretization uncertainty. Discretization uncertainty can be spatial or temporal; however this simulation is steady-state so temporal uncertainty is not of concern. Tables A-1 through A-12 contain the individual components that went into the uncertainty quantification for the PCT and each outer surface and internal fuel temperature measurement in the cask.

Computer round-off error is extremely small compared to other sources, and so is not considered here.

3.3.1 Iterative Uncertainty

It is generally known among CFD engineers that the models need to run until they are "converged." This is supposed to mean that the solution no longer varies with additional iterations. In reality however, some solutions are better behaved than others. Some solutions converge very nicely, and the solution changes very little with each additional iteration; but some solutions are much "noisier," and their solution can vary significantly within a range of values. This variation can be due to numerical instability in the solution, or due to physically based unsteady flow patterns in a steady-state solution.

Once the solution reaches something resembling convergence, the output in question should be recorded for a large number of iterations to determine the range of values over which the output wanders. This range represents the iterative convergence uncertainty of a solution.

The PCT was recorded each iteration for 3000 iterations for the baseline solution (Figure 3-4). The average PCT value was found to be 535.37 ± 0.09 K (504.00 ± 0.16°F) within a 95% confidence level, or within two standard deviations of the average value.

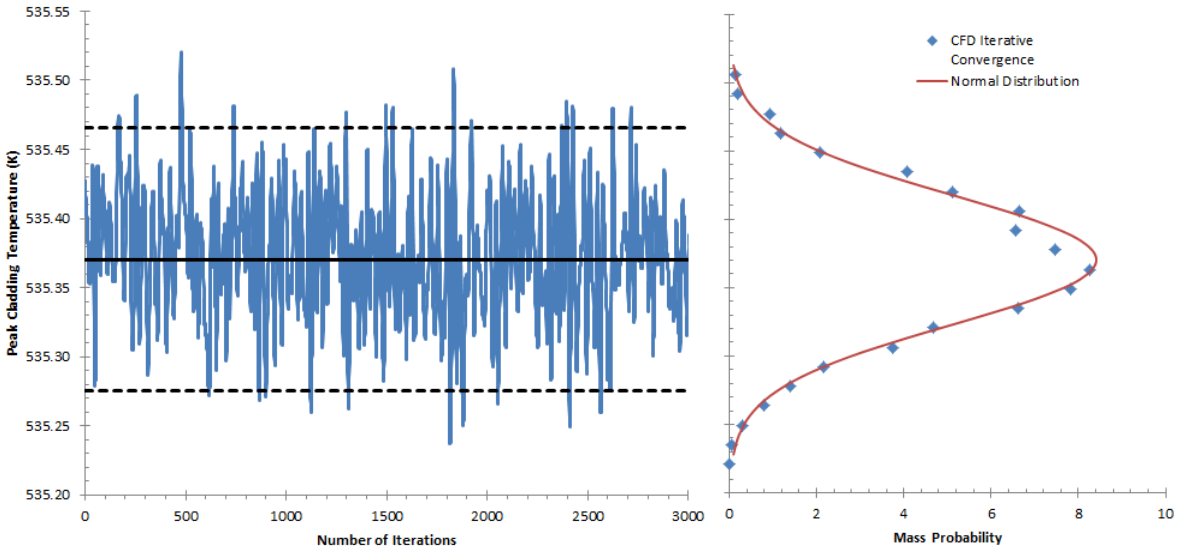

Figure 3-4 Iterative Convergence of PCT for the Baseline Case

The distribution of values gathered during the iterative convergence testing were plotted against a normal distribution to determine if two standard deviations can safely be used as the 95% confidence level for the iterative convergence uncertainty. The data closely follows a normal distribution, so this is a valid assumption.

The iterative uncertainty of ±0.09K (±0.16°F) is very small compared to the temperature range of interest as well as other sources of error in this analysis.

3.3.2 Discretization Uncertainty

The grid convergence index (GCI) as outlined in ASME V&V 20-2009 [1] recommends that at least three grids should be used to determine the uncertainty of a solution with respect to the mesh. In this case, a coarse, medium and a fine mesh are used, where each level of refinement is accomplished by doubling the mesh resolution (Table 3-1).

Table 3-1 Grid Convergence Index Mesh Sizes

GCI Mesh Size:	3D Cells:	2D Cells	Total Cells
Coarse	274,752	87,704	362,456
Medium	2,198,016	350,816	2,548,832
Fine	17,584,128	1,403,264	18,987,392

Due to the use of shell conduction zones to simulate the thin gaps between adjacent pieces of structure, there are 2D elements that accompany the typical 3D cells in the mesh. These cells remain only 1 cell thick during mesh refinement, so when the mesh resolution is doubled the number of 2D cells is 4 times greater. With 3D cells, doubling the mesh resolution results in 8 times as many 3D cells.

The GCI, which is the 95% confidence level uncertainty in the solution as a result of the mesh, can be calculated for the finest of 3 meshes as follows:

$$GCI_{fine} = \frac{F_s * |\varphi_2 - \varphi_1|}{r^p - 1}$$

Where ϕ is the solution result, and 1, 2, and 3 represent the fine, medium and coarse meshes respectively. F_s is an empirically derived factor of safety, which is 1.25 for an asymptotically converging set of 3 or more meshes. For a constant grid refinement ratio, r the order of convergence, p can be calculated as follows:

$$p = \frac{\ln\left(\frac{\varphi_3 - \varphi_2}{\varphi_2 - \varphi_1}\right)}{\ln(r)}$$

The medium mesh is used for all evaluations outside of the grid refinement study, so it is useful to be able to calculate the GCI of the medium mesh as well, which is calculated as follows:

$$GCI_{medium} = GCI_{fine} * r^p$$

Calculating the GCI using this Richardson Extrapolation (RE) method only works when the successive refinement results in a solution that asymptotically converges towards a fixed value at a cell size of zero.

In order to achieve a meaningful GCI, ASME V&V 20-2009 highly recommends using a constant grid refinement ratio, geometrically similar cells in each refinement level, and structured cells where possible. For many problems this is a challenge, but was possible here. It is allowable to use a grid refinement ratio of less than 2 (but preferably greater than 1.3), however in this case there were several thin solids sections that were meshed only 1 cell across in the coarse mesh. This mesh topology dictated that a doubling of the mesh was the smallest grid refinement ratio that could be used.

When the discretization uncertainty of the PCT is calculated on the three meshes for the baseline case, they are indeed asymptotically converging with an order of convergence of 2.12 as shown in Table 3-2. The uncertainty in PCT on the baseline (medium) mesh due to spatial discretization error is 1.3K, which is small compared to many other sources of error in this analysis.

It should be noted that the GCI computed with PCT is not representative of the discretization uncertainty everywhere in the mesh. The GCI was calculated at every location where an experimental temperature measurement recorded, and many of those locations did not demonstrate asymptotic convergence with the three meshes used, particularly in areas of strong temperature gradients. ASME V&V 20-2009 suggests that 4 or more mesh resolutions should

be used to convincingly demonstrate asymptotic response in difficult problems, however the computational resources necessary to perform another doubling of mesh resolution were prohibitive.

At measurement locations that did not obey asymptotic convergence, the GCI was calculated from just two mesh resolutions: the medium mesh and the coarse mesh. In this situation, ASME V&V 20-2009 suggests using a factor of safety of 3.0 to account for the greater uncertainty associated with using only two mesh refinement levels, and an order of convergence p of 1. This allows the GCI to be calculated everywhere in the mesh so that the discretization uncertainty can be included in the overall uncertainty when comparing simulation results to experimental measurements at all the temperature measurement locations.

When calculating the PCT GCI using the two mesh method, the discretization uncertainty is 10.2 K (18.4°F) significantly higher than when using the 3 mesh method (Table 3-2), but there are still several sources of uncertainty in the analysis that are greater than this.

For the PCT and temperature measurement locations that obey asymptotic convergence, the 3 mesh method was used to determine the discretization uncertainty. At locations where grid refinement did not obey asymptotic convergence, the 2 mesh method was used.

Table 3-2 GCI Values for PCT

GCI for Peak Cladding Temperature (PCT):	3 Mesh GCI	2 Mesh GCI
Refinement Ratio, r	2	2
Factor of Safety, Fs	1.25	3
Coarse Mesh	538.8 K (510.2°F)	538.8 K (510.2°F)
Medium Mesh	535.4 K (504.1°F)	535.4 K (504.1°F)
Fine Mesh	534.4 K (502.3°F)	
Order of Convergence, p	2.12	1
GCI, fine mesh	0.3 K (0.5°F)	
GCI, medium mesh	1.3 K (2.3°F)	10.2 K (18.4°F)

3.3.3 Overall Numerical Uncertainty on PCT

The overall numerical uncertainty from all sources is presented in Table 3-6. When computing the total numerical uncertainty, it is not sufficient to use RMS addition of iterative convergence error and discretization error, because the two errors are correlated (ASME 2009). Instead they must be combined using simple addition. Detailed calculations are shown in Table A-1.

Table 3-3 Overall Numerical Uncertainty for PCT

Numerical Uncertainty	Cold Side
Computer Round-off	**± 0.0 K (± 0.0°F)**
Iterative Convergence	**± 0.1 K (± 0.2°F)**
Spatial Discretization	**± 1.3 K (± 2.3°F)**
Total Numerical Uncertainty	**± 1.4 K (± 2.5°F)**

3.4 Input Uncertainty

3.4.1 Input Uncertainty Method

The input uncertainty method used was the finite difference method (also variously called: sensitivity coefficient method, perturbation method, mean value method, and possibly others). This is a local approach to determining the input uncertainty, whereby an independent input variable (e.g. total decay heat) is changed by a small amount, and the effect that this variable has on the solution is recorded. If the uncertainty of the input is known, then the resulting uncertainty on the solution due to the uncertainty of the input can be calculated using the following equation:

$$u_{input}{}^2 = \sum_{i=1}^{n} \left(\frac{\partial S}{\partial X_i} u_{X_i} \right)^2$$

Where:

u_{input} = Total input uncertainty
S = Simulation result
u_{X_i} = Corresponding standard uncertainty in input parameter X_i
X_i = Input parameter
n = Number of inputs in the sensitivity study
$\partial S/\partial X_i$ = Sensitivity Coefficient

Each input variable was perturbed both up and down by its uncertainty value, so two separate cases were run for each input variable in addition to the baseline case. Thermal gap sizes were already at their maximum size in the baseline simulation, so for that case only one sensitivity case needed to be run with the smaller gap sizes.

This method only works in the local neighborhood around the baseline solution, and only as long as the solution is fairly linear with respect to the inputs in that neighborhood. There are more complex global methods of determining uncertainty (Monte Carlo, Latin Hypercube, etc.), but they typically require more knowledge of the probability distribution of the input variables than are generally available, and with a large number of input variables require hundreds or perhaps thousands of cases to achieve statistical significance.

3.4.2 Correlated vs. Uncorrelated Input Variables

Many of the input variables in this analysis cannot be considered to be entirely independent from each other, as there are several heat paths acting in parallel. By increasing or decreasing the heat flow through one path, it necessarily impacts the heat flow through all other paths. Since it is impractical to run the hundreds or thousands of simulations required by the global input uncertainty methods to fully account for the interdependency of all the input variables, another approach is required.

In order to address the multiple heat paths in parallel problem, perturbations of similar variables were considered in a single simulation run. For example, external heat transfer coefficients through the top, sides, and bottom of the cask were all increased to their maximum perturbed value in one run (colder PCT), and all decreased to their minimum value in another run (hotter PCT). Similarly, the gaps were all reduced to their minimum size in one simulation run (colder PCT). The baseline case has all gaps at their maximum size, so the uncertainty in gap size does not contribute to the hot side uncertainty in PCT.

One example of the inter-dependence of inputs on results is located in the bottom of the cask, where there were assumed to be two relatively large gaps – one between the basket and the floor of the inner cask, and the other between the inner cask and the outer cask. Heat travelling through the bottom of the cask must pass across both of these gaps to reach the leveling pad. When the first gap was closed and the second allowed to remain open, it was found that the PCT was reduced by 4.0°C. When the second gap was closed with the first gap open, the PCT was reduced by 0.9°C. If the uncertainty in PCT due to the uncertainty in gap size for these two gaps was independent of one another, the expected reduction in PCT from closing both gaps would be 4.1°C (RMS summing). If the uncertainty was dependent and additive, the expected reduction in PCT from closing both gaps would be 4.9°C, however neither of these was found to be the case. By closing both gaps, the effect was more than additive; the reduction in PCT was 7.5°C. The insulating effect of each gap alone was large enough to drive most of the heat radially outward through the side of the cask. By closing both gaps, the total thermal resistance through the bottom of the cask was substantially reduced. This allowed a significant amount of heat that was passing though the side or top of the cask to pass through the bottom of the cask instead, causing a large reduction in PCT.

Similarly, the uncertainty quantification was also evaluated by considering the closing of the gaps individually and all together and the same time as shown in Table 4. When the gaps were considered independent from each other, the input uncertainty on the PCT was calculated as 36.9°C. When gaps uncertainty were considered dependent and additive, an uncertainty of 72.1°C on PCT was calculated. When all gaps were closed an uncertainty of 62.9°C on PCT was determined. These uncertainty were also calculated for all the measured point in the experiment using different ways when the errors where combined. In this case, considering dependent additive uncertainty quantification over-estimated the effect of the gap uncertainty as compared when all the gaps were considered closed all the same time. This is a clear demonstration that the gaps dependency is not a straight linear relationship. As such, the gaps effect were modeled all open and all closed to evaluate the uncertainty quantification on the PCT as well as other monitored temperature values.

Table 3-4 Thermal Gap Input Uncertainties for PCT

Thermal Gap:	PCT Uncertainty
He Gap – Basket to Rails	-29.8 K (-53.6°F)
He Gap – Rails to Cask	-1.7 K (-3.0°F)
He Gap – SS Sheet to Al Plate	-11.1 K (-20.0°F)
He Gap – Al Basket Plates	-16.7 K (-30.1°F)
He Gap – Basket to Bottom of Cask	-4.0 K (-7.2°F)
Air Gap – Cask Bottom	-0.9 K (-1.7°F)
Air Gap – Cask Cylindrical	-0.5 K (-1.0°F)
Air Gap – Resin Boxes	-7.1 K (-12.8°F)
Air Gap – Lid Seal	-0.2 K (-0.4°F)
Total Gap Uncertainty (Uncorrelated)	**-36.9 K (-66.4°F)**
Total Gap Uncertainty (Correlated)	**-72.1 K (-130°F)**
Both Bottom Gaps Closed	-7.5 K (-13.5°F)
Gap Uncertainty When All Gaps Closed at Once	**-62.9 K (-113°F)**

In another case, the external heat transfer coefficients are a weak function of the external temperature. The external HTC is driven by natural convection, which is a function of the temperature difference between the cask surface and the ambient temperature. Technically, anything that changes this temperature difference will be correlated with the external HTC. However, the uncertainty in external HTC as a result of the uncertainty in the other variables is small, so this is considered to be included in the HTC uncertainty, and the external HTC is considered to be an independent input variable.

3.4.3 Input Uncertainty Results

There were 9 input variables that were assessed in the input uncertainty analysis. There are a large number of inputs to this simulation, so there were several other variables that could also have been evaluated, but the uncertainty in these input values were deemed to be of minor importance to the overall simulation uncertainty. The input variables that were evaluated are listed in Table 3-5, along with their associated contribution to the uncertainty on PCT.

Perturbations that caused the PCT to rise were put in the hot side column in Table 3-5. Conversely, perturbations that caused the PCT to fall were put in the cold side column. The input variables used were assumed to be uncorrelated, so uncertainties for the hot side and cold side were taken as the root mean square (RMS) of all the individual input uncertainties in each column. Descriptions of each input variable, its baseline value, and its associated uncertainty is presented in Section 2.2.

Table 3-5 Input Uncertainty Variables for PCT

Input Variable:	Cold Side	Hot Side
External HTC (top, side, and bottom)	-3.7 K (-6.7°F)	+4.5 K (+8.1°F)
Ambient Temperature	-4.8 K (-8.6°F)	+5.0 K (+9.0°F)
External Emissivity	-2.2 K (-4.0°F)	+2.5 K (+4.5°F)
Carbon Steel Emissivity	-0.1 K (-0.2°F)	+0.5 K (+0.9°F)
Aluminum Emissivity	-0.2 K (-0.4°F)	+0.1 K (+0.2°F)
Fuel Hydraulic Resistance (axial and transverse)	-0.6 K (-1.1°F)	+0.1 K (+0.2°F)
Total Decay Heat	-4.0 K (-7.2°F)	+3.9 K (+7.0°F)
Fuel Thermal Conductivity (axial and transverse)	-3.0 K (-5.4°F)	+3.6 K (+6.5°F)
Thermal Gaps (all)	-62.9 K (-113.2°F)	+0.0 K (+0.0°F)
Total Input Uncertainty	**-63.5 K (-114.3°F)**	**+8.9 K (+16.0°F)**

The uncertainty in the size of the thermal gaps introduces a much greater uncertainty in PCT than any of the other input variables. As discussed previously, the thermal conductivity of gas is much lower than metal, so even a very small gas-filled gap results in a large temperature gradient across that gap. Radiation across the gap is included in the analysis as well as conduction, but radiative heat transfer does not become significant until the gap size and temperature difference is already quite large.

The nature of the cask construction makes it difficult to know precisely how large any of these gaps are, particularly after the cask is brought up to temperature by the decay heat from the fuel assemblies.

3.5 Experimental Uncertainty

The uncertainty in temperature readings for internal thermocouples was reported to be 1.4°C (2.5°F), plus 0.3% of the measured value in °C, valid over the range of temperatures measured with a 95% confidence and a normal distribution [2].

Experimental uncertainty for the temperature readings on the system's surface was a fixed value of 1.1°C (2.0°F) [2].

The PCT in the experiment was not measured directly. However, a thermocouple was located in the hottest assembly in the chamber very close to the location of the PCT (assembly 14, elevation 4), and the simulation result showed that this measured value was very nearly the same temperature as the PCT. The experimental uncertainty associated with an internal thermocouple measurement at the highest recorded internal temperature of 229°C (502 K) (444°F) is ± 2.1 K (3.8°F).

3.6 Simulation Uncertainty Quantification

The total simulation uncertainty is a combination of the numerical uncertainty and the input uncertainty, presented in Table 3-6. These calculations of simulation uncertainty were repeated for all locations corresponding to the 63 internal temperature measurements, and 15 external temperature measurements in the experiment, as well as the PCT. These simulation uncertainties are the basis for the error bars on the baseline simulation result discussed in the following section, which are compared to experimental results with associated experimental uncertainties.

Table 3-6 Total Simulation Uncertainty for PCT

Total Simulation Uncertainty	Cold Side	Hot Side
Total Numerical Uncertainty	-1.4 K (-2.5°F)	+1.4 K (+2.5°F)
Total Input Uncertainty	-63.5 K (-114.3°F)	+8.9 K (+16.0°F)
Total Simulation Uncertainty	**-63.5 K (-114.3°F)**	**+9.0 K (+16.2°F)**

The total simulation uncertainty is dominated by the input uncertainty, and particularly the uncertainty due to the gaps. This is true of the PCT as demonstrated in Table 3-6, as well as all other internal temperature measurements.

Surface temperature uncertainties are significantly lower with an average of ± 8.3 K (±14.9°F), and are driven more by the uncertainty in ambient temperature, external emissivity, and external heat transfer coefficients. The uncertainty in gap sizes plays only a minor role in the uncertainty in surface temperature prediction.

3.7 Validation Uncertainty Quantification

The total validation uncertainty is a combination of the numerical uncertainty, the input uncertainty and the experimental uncertainty, presented in Table 3-7. There was no experimental measurement at the exact location of the PCT, so instead the highest temperature measurement in the experiment is used, which was at elevation 4 in assembly 14, with a measured temperature of 502.4 K (444.7°F). These calculations of overall validation uncertainty were repeated for all locations corresponding to the 63 internal temperature measurements, and 15 external temperature measurements in the experiment.

Table 3-7 Total Validation Uncertainty for Cell 14, Elevation 4 (i.e. PCT)

Total Simulation Uncertainty	Cold Side	Hot Side
Total Numerical Uncertainty	-1.4 K (-2.5°F)	+1.4 K (+2.5°F)
Total Input Uncertainty	-63.5 K (-114.3°F)	+8.9 K (+16.0°F)
Total Experimental Uncertainty	-2.1 K (-3.8°F)	+2.1 K (+3.8°F)
Total Simulation Uncertainty	**-63.5 K (-114.3°F)**	**+9.3 K (+16.7°F)**

The validation uncertainty band is similar to the simulation uncertainty band, owing to the large contribution of the input uncertainty (specifically due to the gaps), and the small contribution of the experimental uncertainty.

3.8 Comparison with Experimental Data

3.8.1 Surface Temperature Results

Cask surface temperatures were measured in 15 locations in order to provide validation information regarding the heat transfer rate to the environment (Figure 3-5). The experimental data compares very well to the simulation results with associated uncertainty (Figure 3-6). The average comparison error between baseline results and experimental data is 2.4°C (4.3°F), whereas the experimental uncertainty is 1.1°C (2.0°F), and the average simulation uncertainty for all surface temperatures is ±8.3°C (14.9°F). Furthermore, the simulation uncertainty encompasses the experimental uncertainty for all temperature measurement locations. These results demonstrate that the external boundary conditions used in the simulation accurately predict the external heat flux to within the uncertainty of the simulation and experimental data.

Reduction in the spatial and temporal variability in ambient temperature during the test, and more information regarding the heat transfer coefficients from the top, bottom and sides of the cask would have helped to reduce the input uncertainty for the surface temperature predictions.

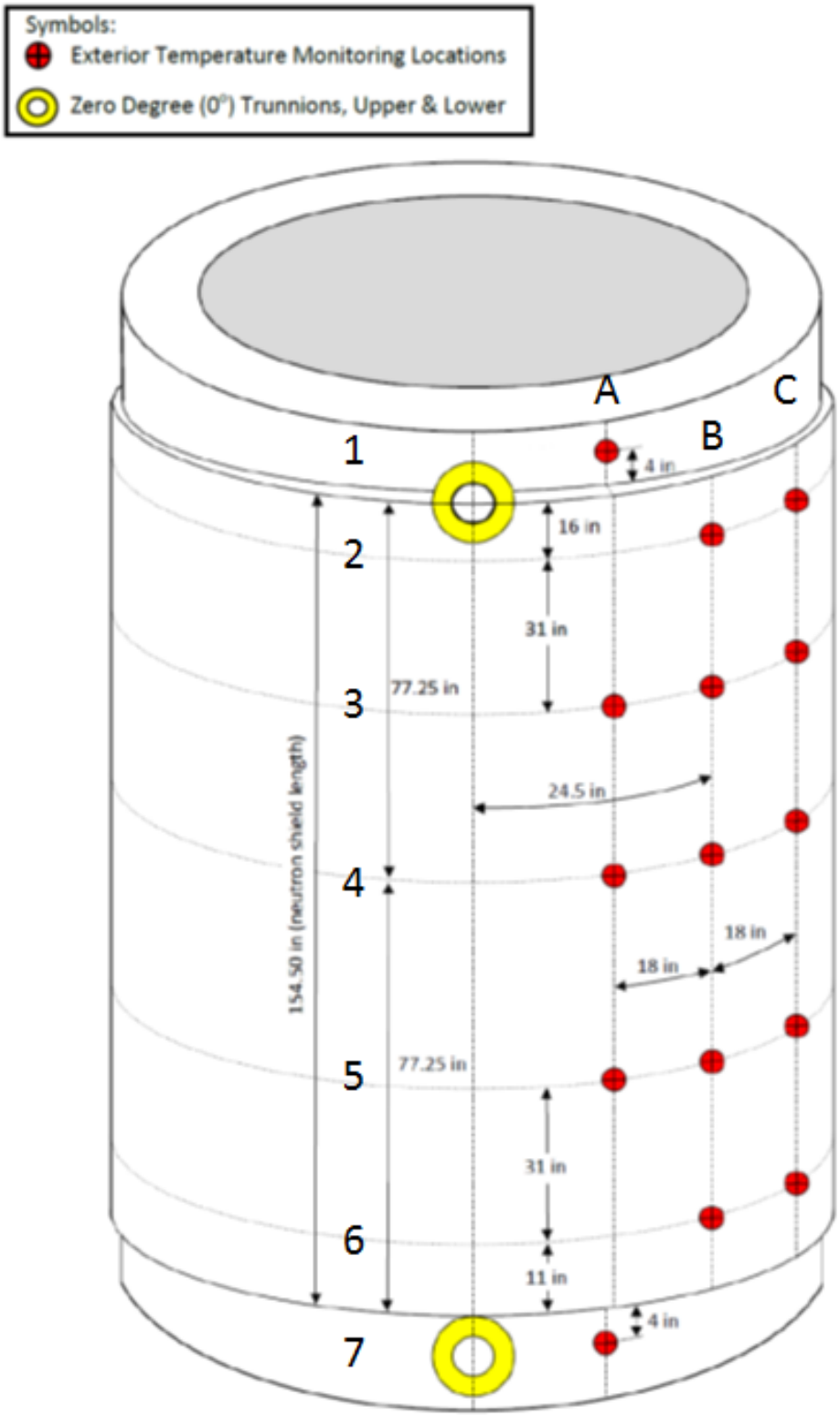

Figure 3-5 Surface Temperature Locations

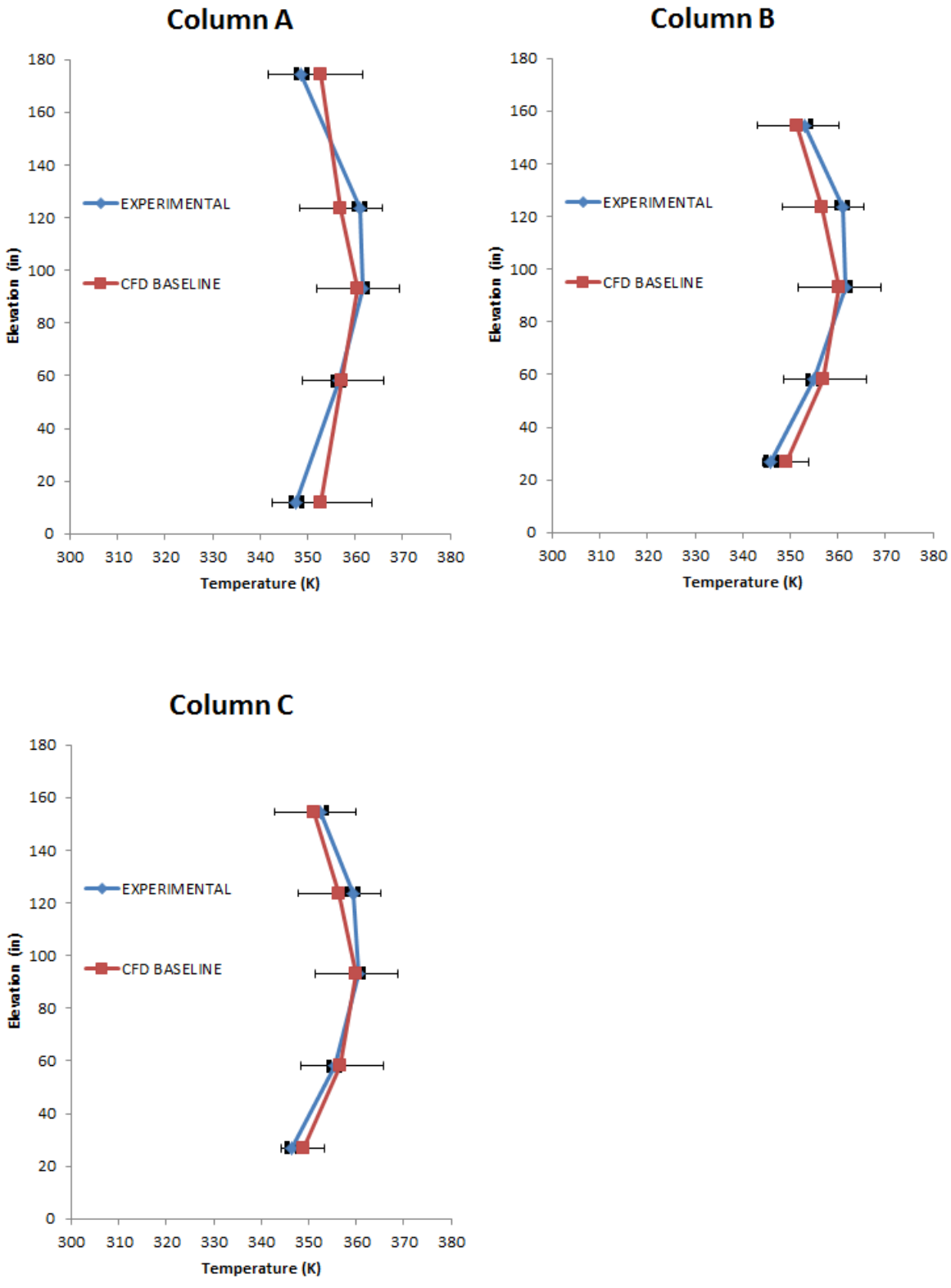

Figure 3-6 Surface Temperature and Uncertainty for Experiment and Baseline Simulation

3.8.2 Fuel Assembly Temperature Results

The temperature profiles in each of the seven instrumented fuel bundles for cells 2, 6, 14, 19, 24, 28 and 31 are plotted in Figure 3-7 and Figure 3-8 for the following data sets:

1. Experimentally measured values in blue, with bold error bars indicating experimental uncertainty.

2. Baseline CFD results in red, with fine error bars indicating the total simulation uncertainty. Note that uncertainty on the hot side is not the same as the cold side. Most factors analyzed contribute to uncertainty on both the hot side and the cold side of the simulation result. However, the conservatively large gaps, which are the dominant source of uncertainty in the simulation, contribute to uncertainty only on the cold side of the simulation result.

In each case, the baseline simulation predicts higher temperatures than recorded in the experiment, and in some cases the simulation result is more than 60°C (110°F) larger than the experimentally measured value. However, owing to the large uncertainty band, all experimental results are within the uncertainty of the simulation.

The temperature error at the bottom of the cask is much greater than at the top of the cask. This is primarily due to two large gaps at the bottom of the cask that are likely not there in reality. The 3.2mm (0.125”) air gap between the inner and outer cask bottom and the 6.4mm (0.250”) helium gap between the basket assembly and the bottom of the inner cask each constitute a large thermal resistance, and explain a large part of the observed temperature error in the bottom of the cask.

Besides the thermal gaps, all other uncertainty sources are on the order of 10°C (18°F) or less, which can be seen in relatively smaller error bars on the hot side of the baseline simulation result, which does not include any uncertainty due to thermal gaps.

Since the comparison error E falls within the validation uncertainty band, the simulation can be considered to be validated. However, the large validation uncertainty does not allow meaningful conclusions to be drawn about the modeling uncertainty of the simulation. To reduce the validation uncertainty, the gap sizes would need to be known with more precision, which is not a practical measurement to make with this particular cask design. As such, this is clear evidence that this experiment cannot be qualified as a CFD grade experiment.

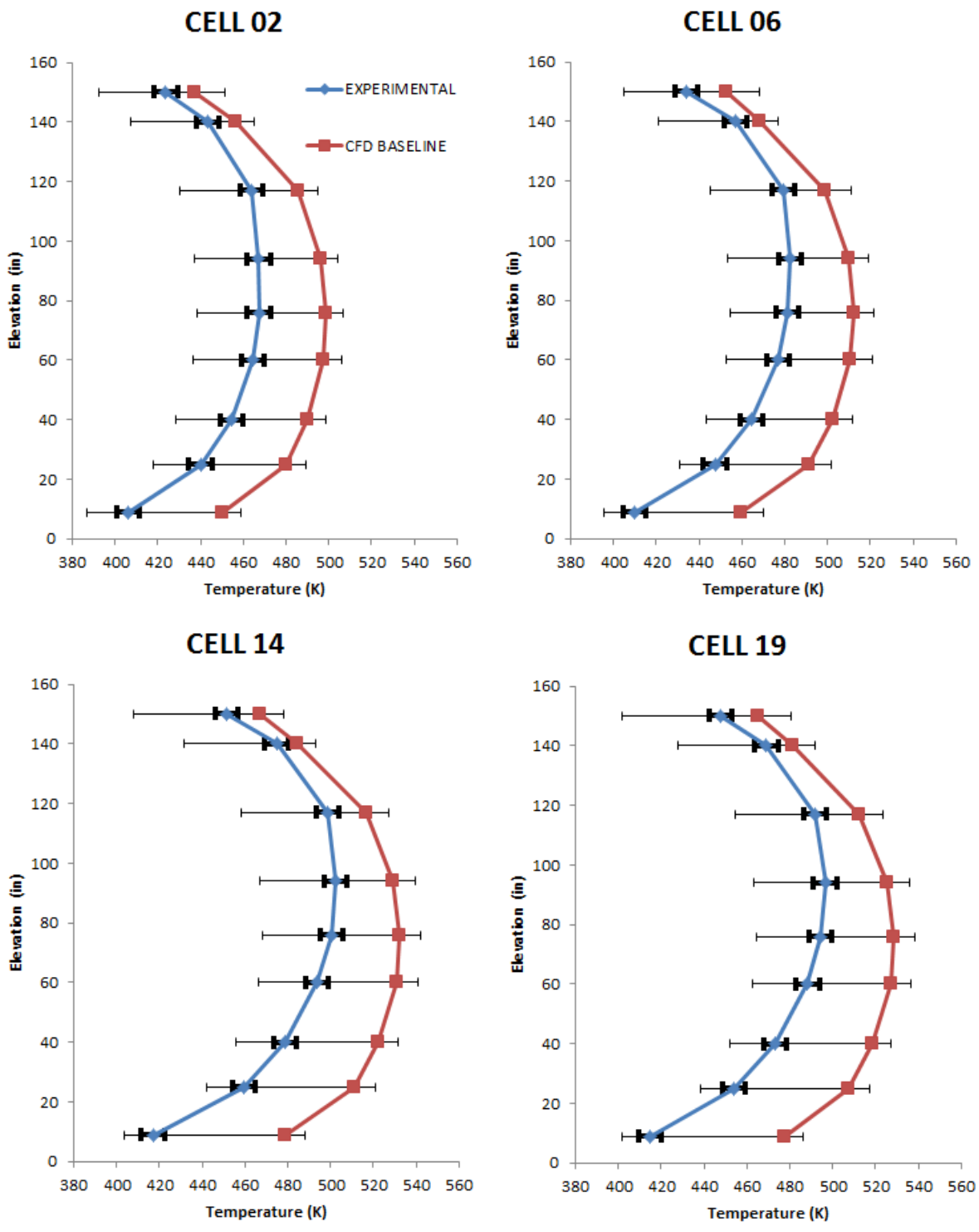

Figure 3-7 Temperature Validation for Cells 2, 6, 14, and 19

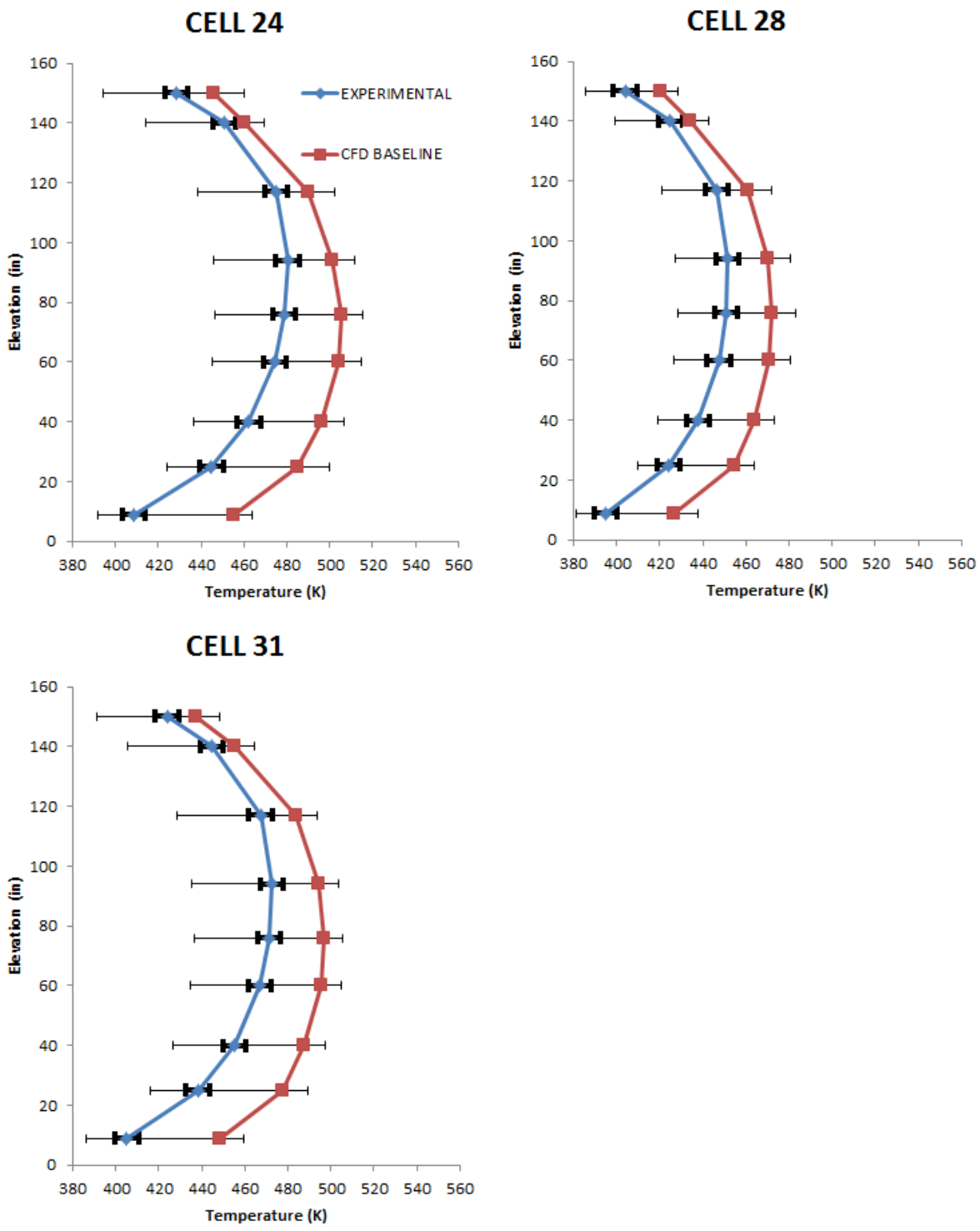

Figure 3-8 Temperature Validation for Cells 24, 28, and 31

To further illustrate the point that was brought up in Section 3.4.2 regarding the effect of assuming input variables as correlated or uncorrelated, the temperature profiles are re-plotted for cell 14 (Figure 3-9). In the left plot under the heading “correlated gaps”, the uncertainty bands are presented as in Figure 3-7, where the uncertainty due to thermal gaps was calculated by running a single case with all gaps closed. In this case, the simulation uncertainty encompasses the experimental data everywhere along the height of the fuel assembly.

In the right plot under the heading “uncorrelated gaps”, the experimental results (blue) and baseline simulation results (red) are the same as before, but the error bars were calculated with the assumption that the uncertainty due to each thermal gap was independent of the uncertainty in the other gap sizes. This required running a separate simulation for each gap, as outlined in Table 3-4. The resulting simulation uncertainty based on the uncorrelated gap assumption is plotted in the right figure.

In the uncorrelated gap assumption, the uncertainty in the baseline simulation covers the experimentally measured values at the top of the cask, but not at the bottom of the cask. The effect of closing both bottom gaps, which increases heat transfer through the bottom of the cask is evident here, and the assumption that the uncertainty in these gap sizes are independent of each other is clearly not valid.

As mentioned previously, the size of the gaps have little effect on the uncertainty in surface temperature predictions. The effect of using correlated or uncorrelated gap uncertainties on the surface temperature profile is presented in Figure 3-10, where the difference in the uncertainty bars between the two plots is not noticeable.

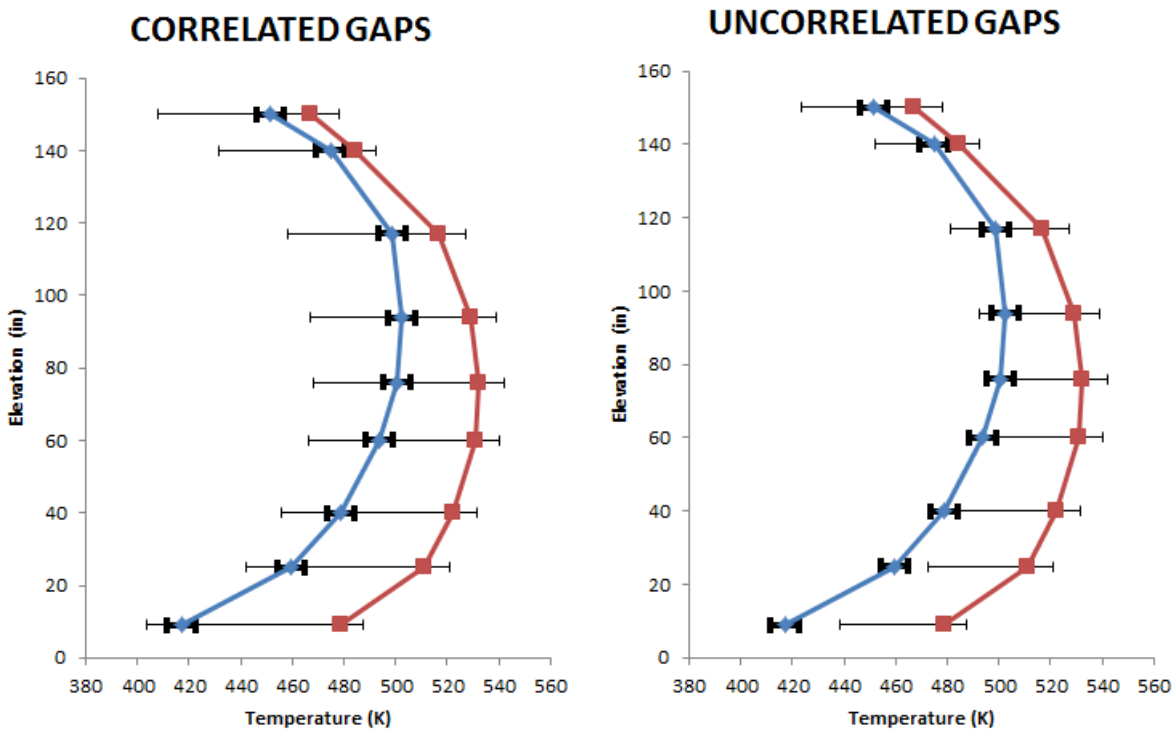

Figure 3-9 Temperature Profile in Cell 14 Using Uncertainty Bands Calculated with Thermal Gaps Assumed to be Correlated (left) and Uncorrelated (right)

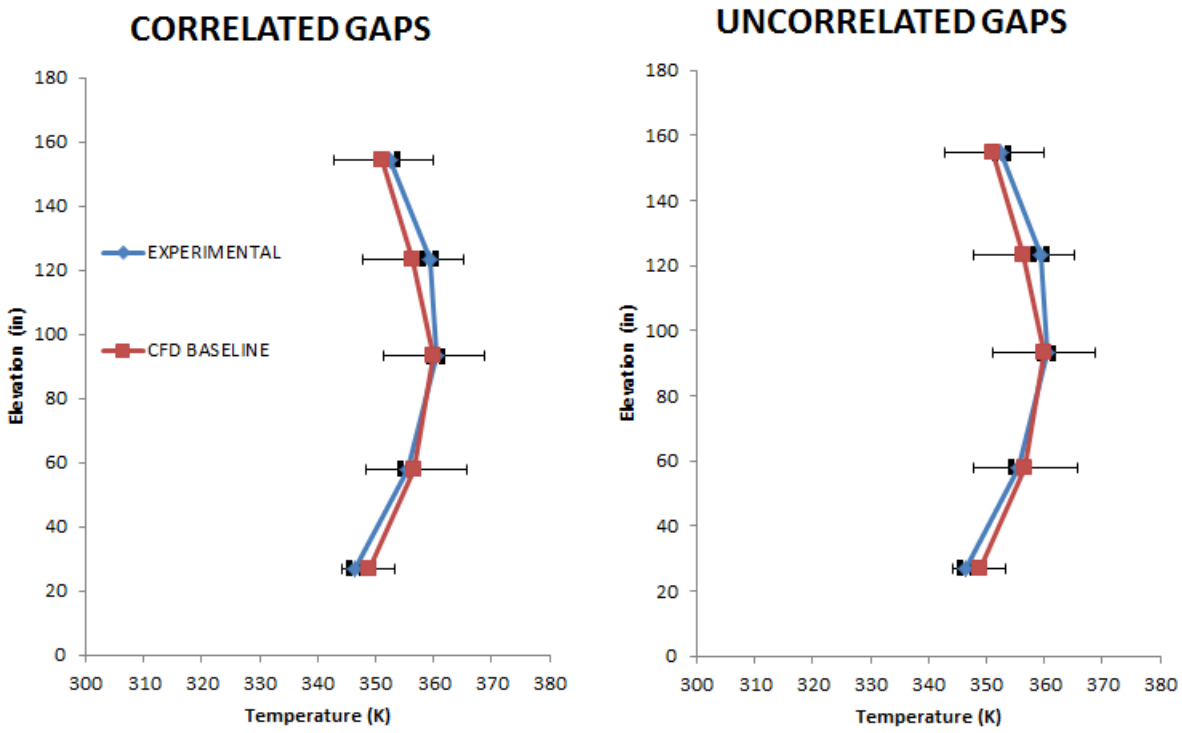

Figure 3-10 Surface Temperatures on Column A using Uncertainty Bands Calculated with Thermal Gaps Assumed to be Correlated (left) and Uncorrelated (right)

3.8.3 Best Estimate Results

Since the gap sizes throughout the cask taken from the UFSAR were conservative estimates, a "best estimate" case was also run. In this case, all gap sizes with the exception of the basket-to-rails gap were closed. Gravity, bolting force, and thermal expansion act to close all of these gaps when the cask is in service.

The basket-to-rails gap is one of the largest gaps in the design, and is necessary to insert the basket assembly into the cask. The language describing the basket to rails gap in the FSAR described the 0.188 inch gap as the "nominal gap [size] … at thermal equilibrium between the periphery of the basket and the rails." So this was assumed to be a somewhat reasonable value. Besides the gap sizes, all other boundary conditions that were used for the baseline case were also used for the best estimate case.

The gap sizes slightly changed the amount of heat rejected through each path, so small changes in surface temperature are observed (Figure 3-11). However, since the gaps are all internal to the cask, and the same amount of heat needs to be removed no matter the gap size, the surface temperatures predicted by the best estimate case are similar to those of the baseline case.

The PCT for the best estimate results was 500 K (440°F), or 35 K (63°F) below the baseline simulation PCT.

The internal temperature profiles including the best estimate predictions (shown in green) are presented in Figure 3-12 and Figure 3-13. The uncertainty quantification analysis was not propagated from the best estimate case, so no error bars are presented with this result.

The results from the best estimate simulation are much closer to the experimental results than the baseline case, particularly in the bottom of the cask where the best estimate simulation result falls within the experimental uncertainty band for many of the experimentally measured test points. Further, since the best estimate case inputs are bounded by the various sensitivity cases that were conducted on the baseline case, the best estimate results lie within the uncertainty bars of the baseline case.

There could be several reasons for the colder temperature predictions at the top of the cask compared to experimental measurements. A few potential candidates might be that the gap sizes are likely not uniform everywhere, or that the axial decay heat profile used in the simulation is not the same for every fuel bundle. Although the best estimate case is very close to the experimental results, the large uncertainty due to the simulation inputs – particularly gap sizes – prevents a more detailed investigation into what may be the source of the modeling errors in the simulation.

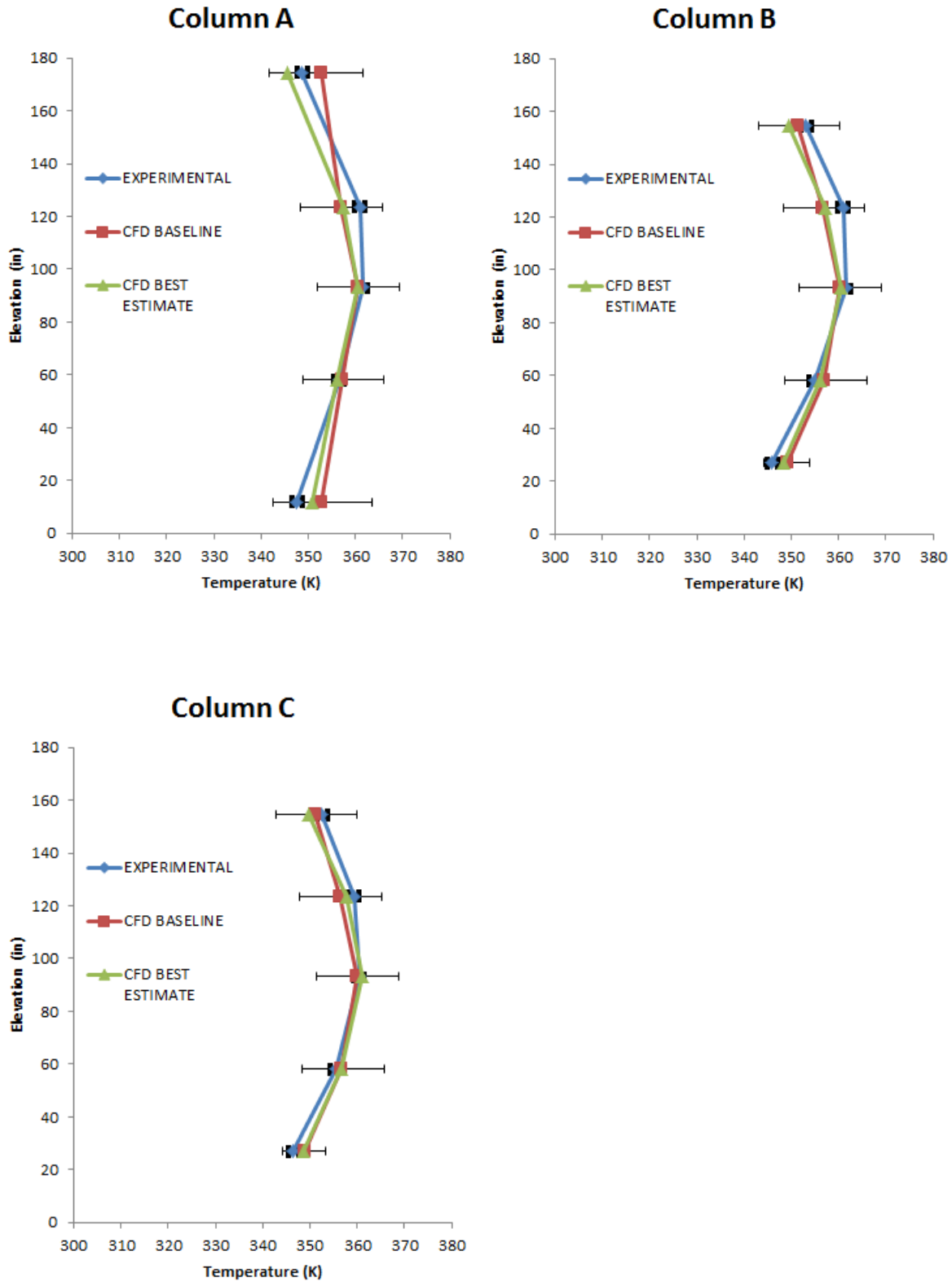

Figure 3-11 Surface Temperature Profiles Including Best Estimate Results

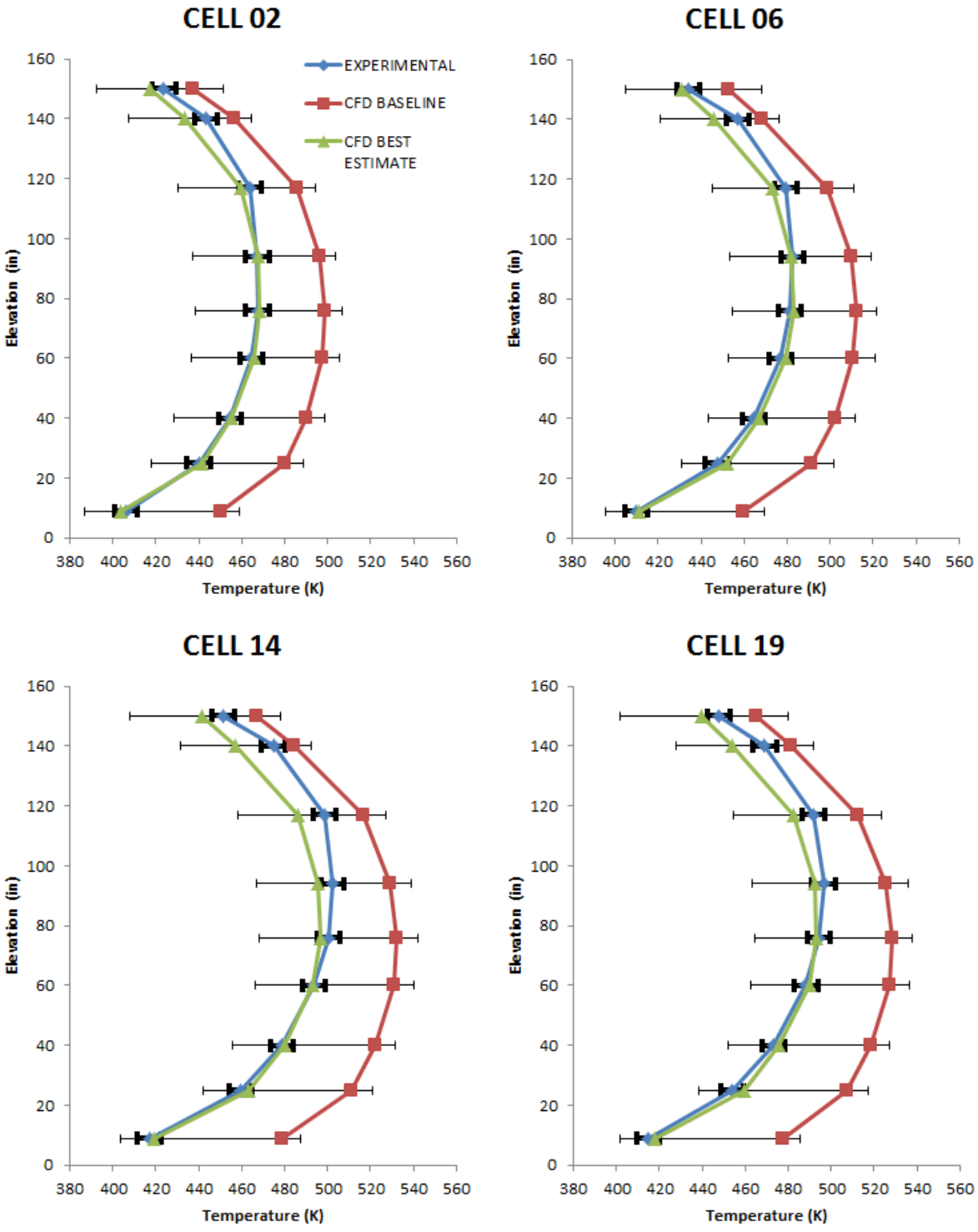

Figure 3-12 Temperature Profiles in Cells 2, 6, 14, and 19 Including Best Estimate Results

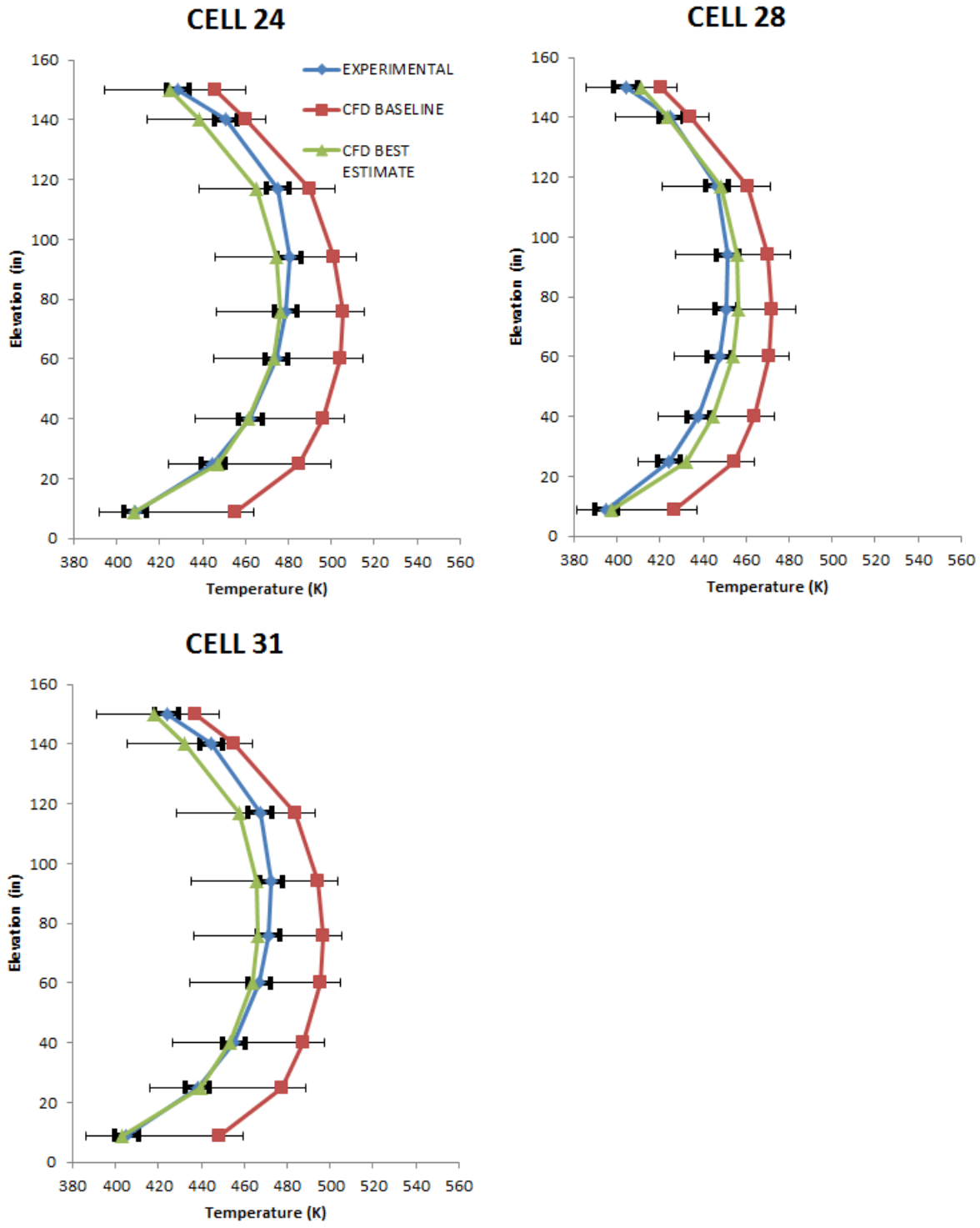

Figure 3-13 Temperature Profiles in Cells 24, 28, and 31 Including Best Estimate Results

4 ISFSI RESULTS

4.1 ISFSI Simulation Inputs

4.1.1 Baseline Simulation

The simulation inputs for the ISFSI simulation are mostly the same as for the baseline validation case. The difference in simulation inputs pertain to the fact that the cask is located outside on a concrete pad, and is analyzed for extreme hot day conditions.

The ambient air temperature for the ISFSI case is taken as a 24 hour average temperature of 38°C (100°F) (EPRI 2018). This is intended to cover hotter peak temperatures, but since the thermal mass of the cask is large, a short duration peak has less impact than a longer duration event. The same external heat transfer coefficient is used for the top and sides of the cask as was used for the experimental validation.

The bottom thermal boundary condition was based on intimate thermal contact with a concrete pad 0.91 m (36”) thick, extending 0.91 m (36”) around the base of the cask. The cask is in perfect thermal contact with the concrete, and the concrete is in contact with soil at 21°C (70°F). This condition is equivalent to a heat transfer coefficient from the bottom of the cask of 0.233 W/m2-K (0.041 Btu/h-ft^2-°F).

When the cask is located outdoors, it will be exposed to insolation. The total insolation for a 12-hour period is 1475 Btu/ft^2 for curved surfaces and 2950 Btu/ft^2 for flat surfaces per 10CFR (Transnuclear, Inc. 2014). Since all cask surfaces exposed to sunlight are curved, the curved surface value was used. This 12-hour heat flux was averaged over a 24 hour period. Additionally, the solar absorptivity of the painted surfaces of the cask was reported to be 0.3 [4]. This results in an average solar heat flux on all exposed external surfaces of 58.16 W/m^2 (18.44 Btu/h-ft^2).

In the ISFSI configuration, the lid neutron shield and the protective cover will be in place, so these are included in the simulation. Gaps between these components as specified by the UFSAR were included in the simulation (Figure 4-1, Figure 4-2).

4.1.2 Best Estimate Simulation

A best estimate simulation was also run, similar to the validation case. All gaps, with the exception of the basket-to-rails gap were closed, otherwise the model inputs were the same as for the baseline ISFSI simulation.

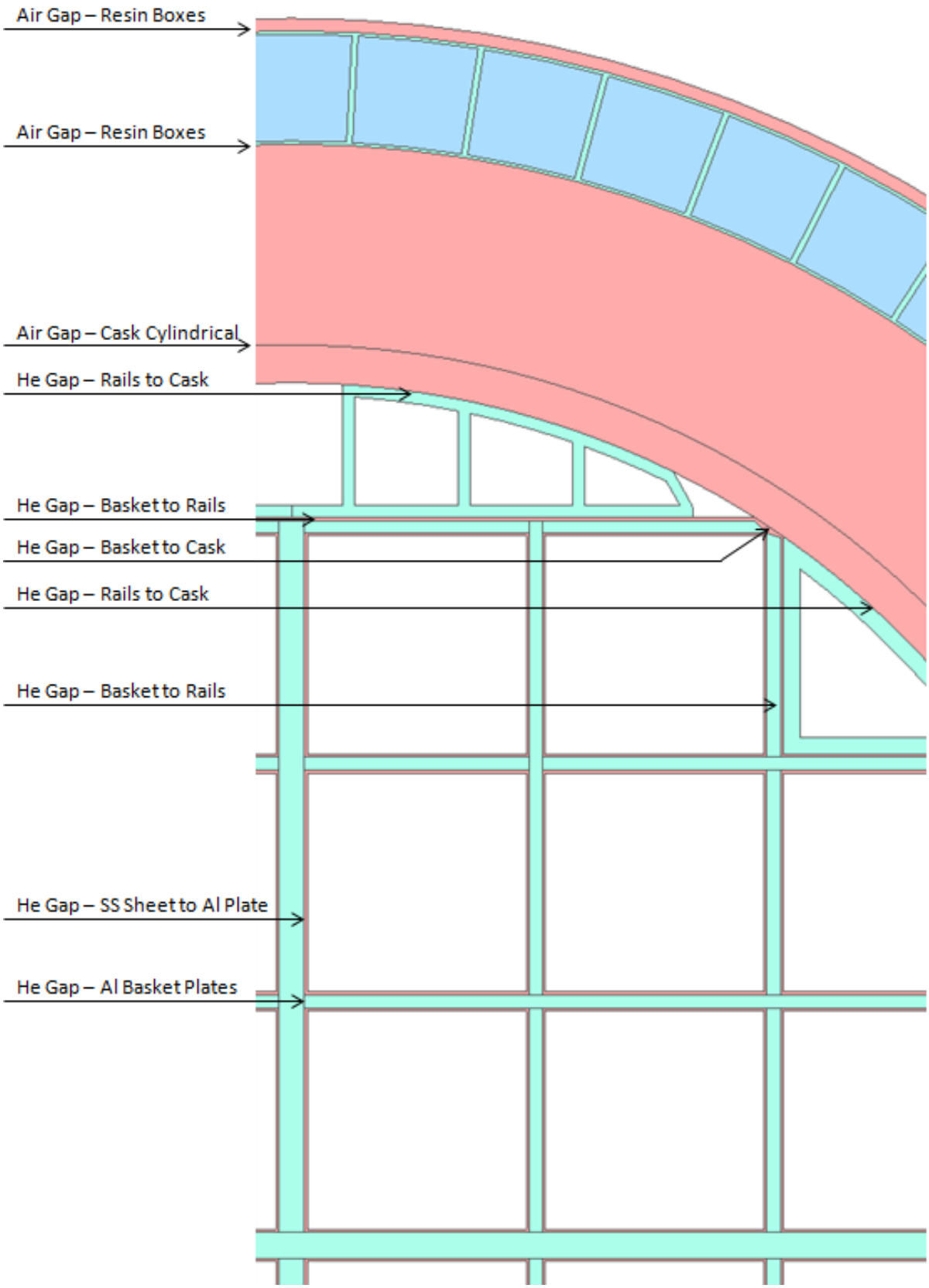

Figure 4-1 Thermal Gap Summary for ISFSI Case – Plan View

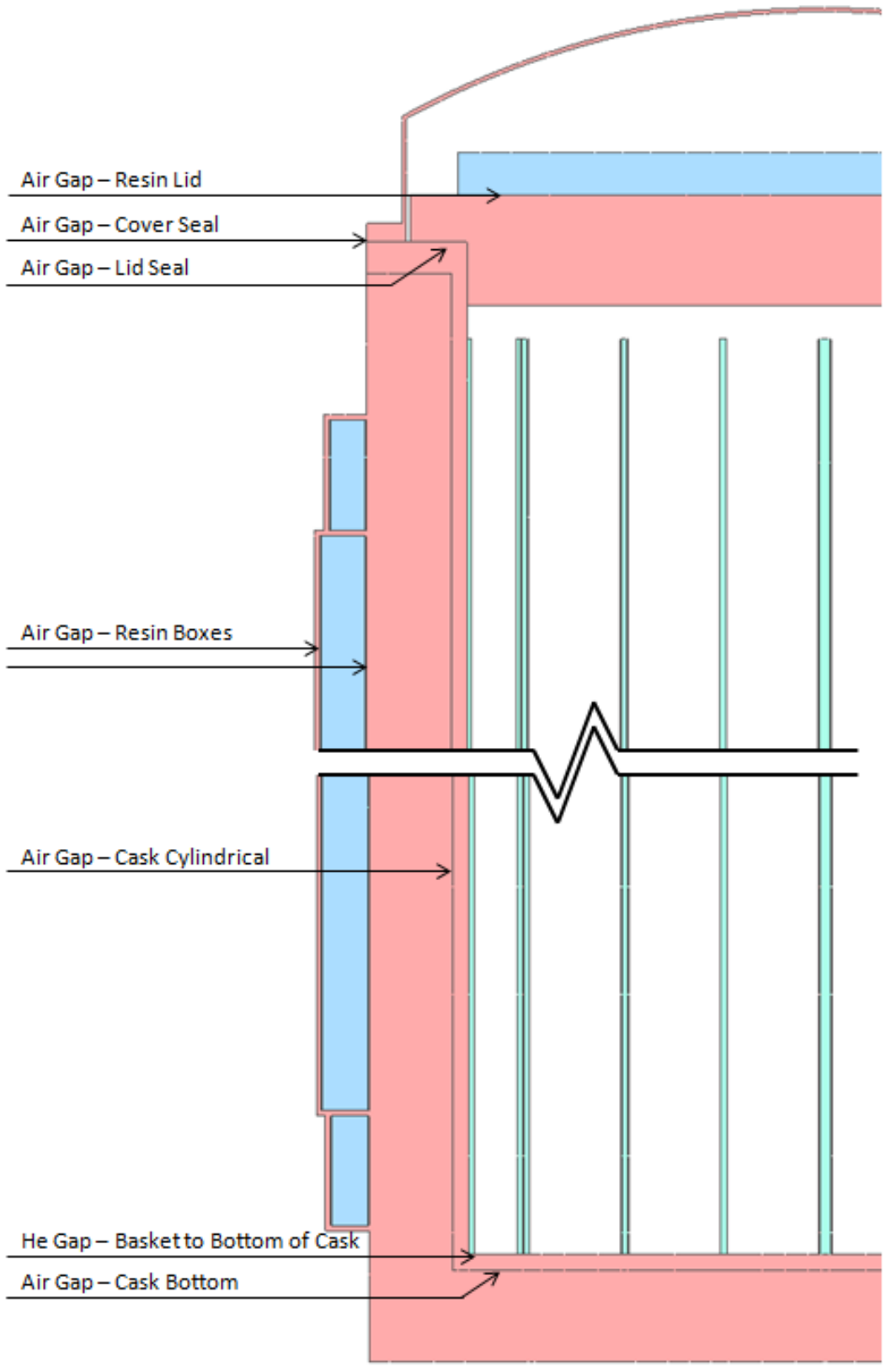

Figure 4-2 Thermal Gap Summary for ISFSI Case – Elevation View

4.2 ISFSI Simulation Results

Surface temperatures for the baseline and best estimate ISFSI case are presented in Figure 4-3. Fuel bundle temperatures for the baseline and best estimate ISFSI cases are presented in Figure 4-4 and Figure 4-5.

The peak cladding temperature for the baseline ISFSI case was found to be 552 K (534°F)

The peak cladding temperature for the best estimate ISFSI case was found to be 518 K (473°F), which is 34°C (61°F) below the baseline result – a similar difference as in the validation case.

Both of these temperatures are below the PCT limit of 400°C (673 K) (752°F). No uncertainty analysis was conducted for the ISFSI case, but if a UQ analysis was to be conducted, it would be done in a similar manner to what was presented in section 3. If the total hot side PCT uncertainty of 9°C (16°F) was applied to the calculated PCT for the baseline ISFSI case, the resulting temperature of 561 K (550°F) would still be far below the cask PCT limit.

Many of the environmental input variables that were measured in the validation case are specified as design inputs for the ISFSI case. As a result, there is no simulation uncertainty as a result of ambient temperature, ground temperature for the ISFSI case. These are all specified as part of the design, and represent the reasonable worst case scenario expected for the cask.

The uncertainty due to gap size would remain the largest uncertainty in the analysis, but due to the bias error in selecting the largest likely gap size for all gaps, the large uncertainty is to the cold side of the simulation result.

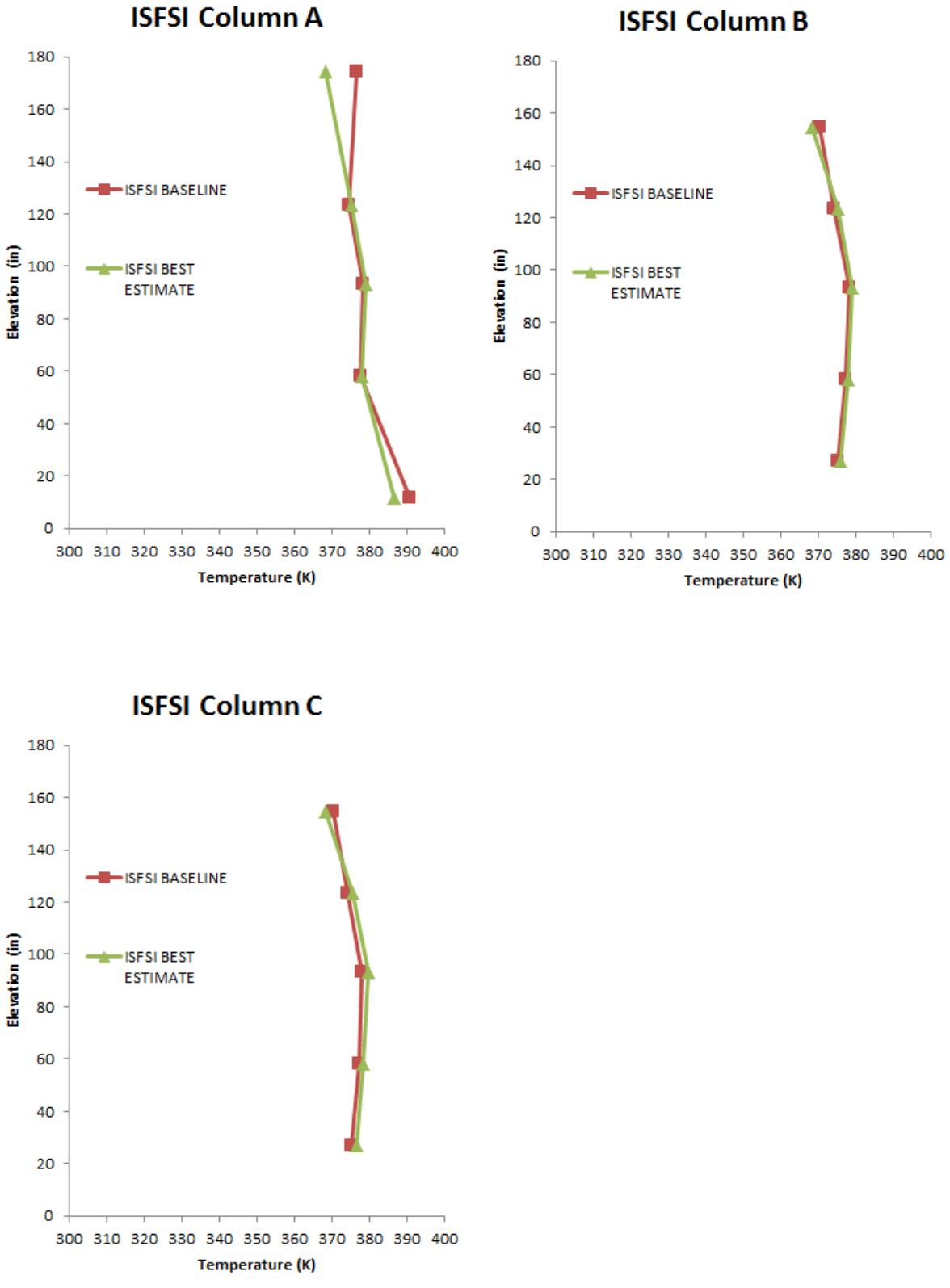

Figure 4-3 Surface Temperature Profiles for ISFSI Case

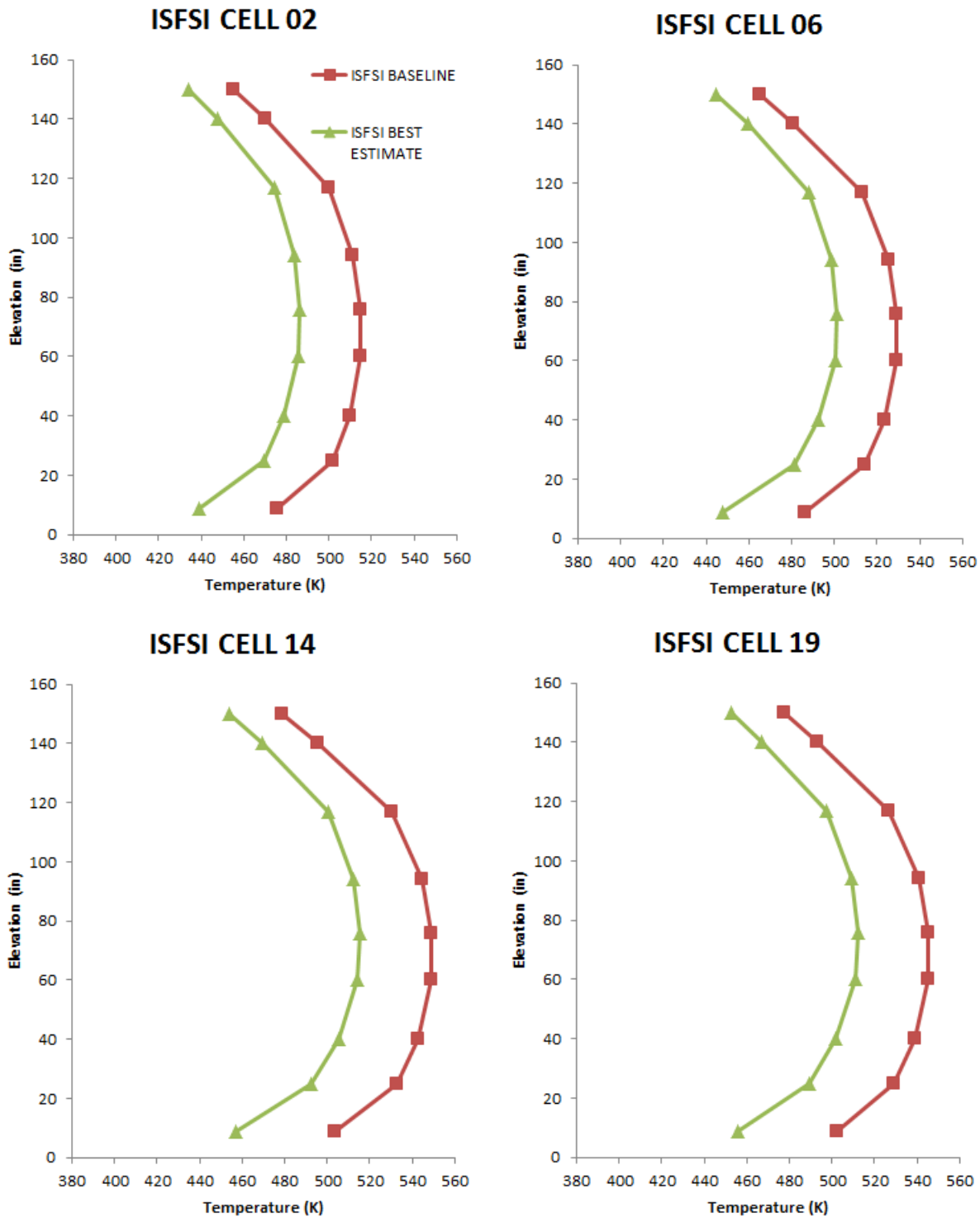

Figure 4-4 ISFSI Temperature Profiles for ISFSI Case in Cells 2, 6, 14, and 19

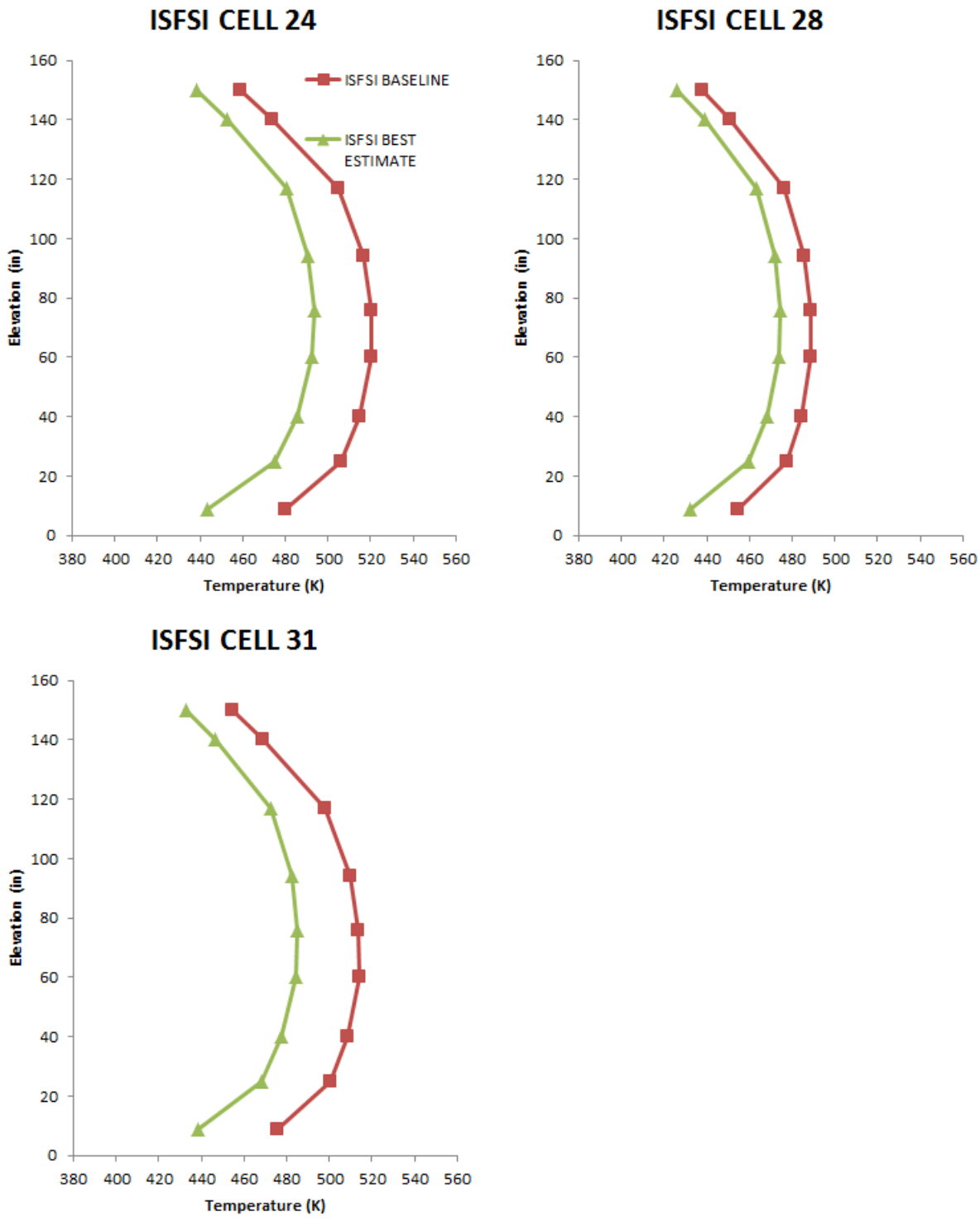

Figure 4-5 ISFSI Temperature Profiles for ISFSI Case in Cells 24, 28, and 31

5 CONCLUSIONS

This report has demonstrated that the CFD simulation results of the TN-32B cask are within the validation uncertainty of the experimental values that were measured by EPRI at the North Anna Nuclear Plant in November 2017. Moreover, the process outlined here demonstrates the process by which simulation uncertainty can be quantified as outlined in ASME V&V20-2009 for a complex, real-world application.

Of the many sources of uncertainty evaluated, by far the largest source of uncertainty in the simulation of this particular cask design is the thermal resistance across the many gaps between adjacent pieces of structure. The thermal conductivity of gas is many times lower than through metal, so very small gaps result in large differences in temperature across the gaps.

The typical certification process requires that the applicant demonstrate compliance under the worst case scenarios. In the case of dry cask storage, the PCT must remain below the safe operating limits of the materials under the hottest ambient conditions that are expected to occur at a particular site. Using the same line of thinking, the gap sizes that would be used for this analysis are not the most likely gap size, but the largest possible gap sizes, which would result in the highest PCT. The same goes for other simulation inputs such as emissivity, external heat transfer coefficients, etc. which would all be chosen as conservatively bounding values that would be sure to yield a PCT value from the simulation that is equal to or greater than the actual PCT value. This type of approach helps to ensure safe operation.

When using the conservative inputs for the TN-32B cask that were provided in the UFSAR for a validation test, this conservative bias was evident in the fact that the simulation results over-predicted the experimental measurements everywhere, and by more than 60°C (110°F) in some locations.

There is no such bias when considering numerical uncertainty. The discretization of the mesh, although small compared to the input uncertainty in this case, is still an important contribution to the overall uncertainty of the simulation. Spatial discretization was found here to be an important factor, especially in areas that did not obey asymptotic convergence criteria. In those areas a large penalty was taken, resulting in uncertainties as high as 12.5°C (22.5°F). Iterative uncertainties in this case were very small, but for simulations with separated or unsteady flow patterns, iterative uncertainty can be quite large. These uncertainties need to be considered when presenting results for certification, particularly when the simulation result is close to the allowable limit.

Whereas the certification process is concerned with producing a safe result, validation of CFD models is concerned more with producing the most accurate result with the smallest uncertainty band possible. The conservative bias in input variables that were provided in the UFSAR are intended to produce a safe result, but are perhaps not the best values for CFD model validation. Although the experimental results fell within the uncertainty band of the CFD model simulation, the many uncertainties in the experimental setup resulted in a very large simulation uncertainty band. This large uncertainty band makes it difficult to assess how accurate the simulation could be if all the inputs were known with great precision, and what factors contribute to the differences between the simulation and the experimentally measured values.

A validation uncertainty of 63 Kelvin was calculated for the current experiment to validate the model's prediction of PCT. As such, this experiment cannot be classified as a CFD grade experiment. Cask vendors have been submitting applications within margins in the range of about 10-20°C from the ISG-11 temperature limit of 400°C. In order to be useful as a demonstration of the accuracy of the CFD modeling process or to improve the model's capabilities, the validation uncertainty should be less than this 10-20°C margin. The primary simulation uncertainties consisted mainly of lack of knowledge of the size of fluid gaps that existed in the dry cask. The gap sizes are an important simulation input for this cask design, and greatly influence the value of PCT predicted by the model. This issue is central to the validation of CFD models. Designs that are complex enough to benefit from CFD modeling generally have a great many inputs that influence the simulation result. CFD grade experiments are those that precisely measure each and every one of these inputs so that the input uncertainty of the simulation can be minimized. This is a difficult and complicated task to design and conduct such an experiment even for relatively simple configurations, which is why so few are conducted. However, in order to gain confidence in the application of CFD as a tool in the certification process, especially with more complex physics, validation exercises such as this are necessary.

As expected and shown in the uncertainty quantification section, the resulting uncertainty on PCT and other temperature values in other locations depended on how the individual error are related to each other. The effect of the multiple fluid gap dependence on the uncertainty quantification was evaluated and discussed. As a result, the uncertainty quantification due to the fluid gaps was determined using correlated error estimation. This method was chosen as the different gaps are dependent on each other.

The method presented herein, showed that all the measured temperature values in all the seven lances inside the fuel region as well as the outside three columns of thermocouple measurements as shown in the results section were predicted within the calculated uncertainty bands. As such, the CFD models and inputs that were used in the TN-32B cask modeling approach as suggested in CFD best practice guidelines [NUREG-2152] were successfully validated using the data obtained in the DOE cask demonstration project.

Often, the cask applicant uses the worst case scenario to perform dry cask thermal analyses especially when there is enough margin from the allowable PCT limit. However, when the cask is designed for higher decay heat and the PCT values are getting close to the limit, and the obtained margin is questionable, the method presented in this report to evaluate the uncertainty quantification should be used as a guide to show compliance with the PCT limit. The method presented herein when used properly will inform the applicant about the right margin to have for any cask design.

6 REFERENCES

[1] ASME. ASME V&V 20-2009*,* Standard for Verification and Validation in Computational Fluid Dynamics and Heat Transfer*.* ASME, 2009.

[2] EPRI. High-Burnup Used Fuel Dry Storage System Thermal Benchmark Modeling Results, Round Robin Results, Draft . 2019.

[3] Transnuclear, Inc. TN-32 Dry Storage Cask System Safety Evaluation Report. 2000.

[4] Transnuclear, Inc. TN-32 Updated Final Safety Analysis Report, Revision 6. 2014.

[5] U.S.NRC. NUREG-0800 Standard Review Plan for the Review of Safety Analysis Reports for Nuclear Power Plants: LWR Edition*.* 2017.

[6] U.S.NRC. NUREG-1536 Standard Review Plan for Spent Fuel Dry Storage Systems at a General License Facility. 2010.

[7] U.S.NRC. NUREG-2152 Computational Fluid Dynamics Best Practice Guidelines for Dry Cask Applications. 2013.

[8] U.S.NRC. NUREG-2208, Validation of Computational Fluid Dynamics Methods Using Prototypic Light Water Reactor Spent Fuel Assembly Thermal-Hydraulic Data*.* Office of Nuclear Regulatory Research, 2017.

[9] W.L. Oberkampf, C.J. Roy. Verification and Validation in Scientific Computing. Cambridge University Press, 2010.

[10] D. Bestion et al, Requirement For CFD-Grade Experiments For Nuclear Reactor Thermal-Hydraulics, OECD-NEA-CSNI-WGAMA-CFD group, to be pubslished in 2019.

APPENDIX A
VALIDATION UNCERTAINTY SCOREBOARD

The following tables contain the individual components that went into the uncertainty calculations for the PCT and each surface and internal temperature measurement in the cask. These values were used to create the error bars on the validation baseline simulation plots.

The tables are called “scorecards” because they help to demonstrate what the largest uncertainty sources are. Each individual component is also highlighted according to how much uncertainty it contributes – positive uncertainty is highlighted red, and negative uncertainty is highlighted blue. All temperatures are reported in Kelvin.

Table A-1 Uncertainty Quantification Scorecard for PCT

Validation Uncertainty Scorecard: PCT (K)
(95% Confidence Level)

Numerical Uncertainty:	PCT:
Computer Roundoff	0.0
Iterative Convergence	0.1
Grid Convergence:	1.3
Total Numerical Uncertainty:	**1.4**

Experimental Uncertainty:	PCT:
Total Experimental Uncertainty:	2.1

Input Uncertainty (COLD):	PCT:
External Heat Transfer Coefficients	-3.7
Ambient Temperature	-4.8
External Emissivity	-2.2
Carbon Steel Emissivity	-0.1
Aluminum Emissivity	-0.2
Fuel Hydraulic Resistance	-0.6
Total Decay Heat (u = 2%)	-4.0
Fuel Thermal Conductivity	-3.0
Thermal Gaps - Correlated	-62.9
Thermal Gaps - Uncorrelated	-36.9
Input Uncertainty (COLD SIDE) - Gaps Correlated	**-63.5**
Input Uncertainty (COLD SIDE) - Gaps Uncorrelated	**-37.8**

Input Uncertainty (HOT):	PCT:
External Heat Transfer Coefficients	4.5
Ambient Temperature	5.0
External Emissivity	2.5
Carbon Steel Emissivity	0.5
Aluminum Emissivity	0.1
Fuel Hydraulic Resistance	0.1
Total Decay Heat (u = 2%)	3.9
Fuel Thermal Conductivity	3.6
Thermal Gaps - Correlated	0.0
Input Uncertainty (HOT SIDE):	**8.9**

Compiled Results	PCT (K):
Simulation Results:	
Experimental	-
Baseline CFD	535.4
Best Estimate	500.1
Comparison Error:	
Baseline - Experimental	-
Best Estimate - Experimental	-
Simulation Uncertainty:	
Negative (Gaps Correlated)	-63.5
Negative (Gaps Uncorrelated)	-37.8
Positive	9.0
Validation Uncertainty:	
Negative	-63.5
Positive	9.3
ISFSI Results:	
Baseline CFD	552.5
Best Estimate	518.3

Table A-2 Uncertainty Quantification Scorecard for Surface Temperatures, Column A

Validation Uncertainty Scorecard: Surface Temperatures, Column A (K)
(95% Confidence Level)

Numerical Uncertainty:	surf.a1	surf.a3	surf.a4	surf.a5	surf.a7
Computer Roundoff	0.0	0.0	0.0	0.0	0.0
Iterative Convergence	0.3	0.2	0.1	0.1	0.1
Grid Convergence:	0.2	0.2	0.4	0.0	0.7
Total Numerical Uncertainty:	0.5	0.4	0.5	0.1	0.8

Experimental Uncertainty:	surf.a1	surf.a3	surf.a4	surf.a5	surf.a7
Total Experimental Uncertainty:	1.1	1.1	1.1	1.1	1.1

Input Uncertainty (COLD):	surf.a1	surf.a3	surf.a4	surf.a5	surf.a7
External Heat Transfer Coefficients	-4.2	-4.2	-4.4	-4.5	-6.1
Ambient Temperature	-6.3	-6.1	-6.0	-6.1	-6.3
External Emissivity	-2.8	-3.1	-3.0	-2.9	-2.1
Carbon Steel Emissivity	0.5	0.1	0.0	-0.2	-0.6
Aluminum Emissivity	0.2	0.1	-0.1	-0.1	-0.1
Fuel Hydraulic Resistance	0.4	-0.1	-0.2	-0.3	-0.4
Total Decay Heat (u = 2%)	-1.0	-1.0	-1.0	-1.0	-1.0
Fuel Thermal Conductivity	-0.1	-0.1	0.0	0.0	0.0
Thermal Gaps - Correlated	-7.5	2.0	2.0	0.7	-4.4
Thermal Gaps - Uncorrelated	-5.0	-2.7	-3.1	-3.2	-5.0
Input Uncertainty (COLD SIDE) - Gaps Correlated	-11.1	-8.4	-8.4	-8.2	-10.1
Input Uncertainty (COLD SIDE) - Gaps Uncorrelated	-9.5	-8.5	-8.7	-8.8	-10.4

Input Uncertainty (HOT):	surf.a1	surf.a3	surf.a4	surf.a5	surf.a7
External Heat Transfer Coefficients	4.9	5.0	5.2	5.5	8.1
Ambient Temperature	6.7	6.4	6.2	6.2	6.4
External Emissivity	2.9	3.3	3.4	3.3	2.3
Carbon Steel Emissivity	0.4	0.4	0.4	0.4	0.8
Aluminum Emissivity	0.0	0.1	0.1	0.1	0.0
Fuel Hydraulic Resistance	-0.4	-0.2	-0.1	0.1	0.1
Total Decay Heat (u = 2%)	0.8	0.8	1.0	1.0	0.9
Fuel Thermal Conductivity	0.2	0.0	0.1	0.0	-0.1
Thermal Gaps - Correlated	0.0	0.0	0.0	0.0	0.0
Input Uncertainty (HOT SIDE):	8.8	8.8	8.9	9.0	10.6

Compiled Results	surf.a1	surf.a3	surf.a4	surf.a5	surf.a7
Simulation Results:					
Experimental	348.7	360.9	361.5	356.5	347.6
Baseline CFD	352.7	356.8	360.4	357.1	352.8
Best Estimate	345.5	357.3	360.5	356.2	350.7
Comparison Error:					
Baseline - Experimental	4.0	-4.1	-1.1	0.6	5.2
Best Estimate - Experimental	-3.2	-3.6	-1.0	-0.3	3.1
Simulation Uncertainty:					
Negative (Gaps Correlated)	-11.1	-8.4	-8.4	-8.2	-10.2
Negative (Gaps Uncorrelated)	-9.6	-8.5	-8.7	-8.8	-10.5
Positive	8.8	8.8	8.9	9.0	10.6
Validation Uncertainty:					
Negative	-11.1	-8.4	-8.4	-8.3	-10.2
Positive	8.9	8.8	9.0	9.0	10.7
ISFSI Results:					
Baseline CFD	376.8	374.5	378.5	377.6	390.8
Best Estimate	368.3	375.2	379.2	378.1	386.6

Table A-3 Uncertainty Quantification Scorecard for Surface Temperatures, Column B

Validation Uncertainty Scorecard: Surface Temperatures, Column B (K)
(95% Confidence Level)

Numerical Uncertainty:	surf.b2	surf.b3	surf.b4	surf.b5	surf.b6
Computer Roundoff	0.0	0.0	0.0	0.0	0.0
Iterative Convergence	0.2	0.2	0.1	0.1	0.1
Grid Convergence:	0.7	0.3	0.9	0.4	4.6
Total Numerical Uncertainty:	0.9	0.4	1.1	0.5	4.7

Experimental Uncertainty:	surf.b2	surf.b3	surf.b4	surf.b5	surf.b6
Total Experimental Uncertainty:	1.1	1.1	1.1	1.1	1.1

Input Uncertainty (COLD):	surf.b2	surf.b3	surf.b4	surf.b5	surf.b6
External Heat Transfer Coefficients	-4.0	-4.2	-4.4	-4.5	-4.3
Ambient Temperature	-6.3	-6.2	-6.1	-6.1	-6.3
External Emissivity	-2.9	-3.1	-3.1	-2.9	-2.9
Carbon Steel Emissivity	0.2	0.1	0.0	-0.2	-0.1
Aluminum Emissivity	0.1	0.0	-0.1	-0.1	-0.1
Fuel Hydraulic Resistance	-0.1	-0.2	-0.2	-0.3	-0.2
Total Decay Heat (u = 2%)	-0.9	-1.0	-1.1	-1.0	-0.9
Fuel Thermal Conductivity	-0.1	-0.1	-0.1	0.0	0.0
Thermal Gaps - Correlated	-1.7	1.8	1.8	0.6	-1.1
Thermal Gaps - Uncorrelated	-1.3	-2.3	-2.7	-2.9	-1.6
Input Uncertainty (COLD SIDE) - Gaps Correlated	-8.3	-8.3	-8.4	-8.2	-8.2
Input Uncertainty (COLD SIDE) - Gaps Uncorrelated	-8.2	-8.5	-8.6	-8.7	-8.3

Input Uncertainty (HOT):	surf.b2	surf.b3	surf.b4	surf.b5	surf.b6
External Heat Transfer Coefficients	4.7	4.9	5.2	5.5	5.1
Ambient Temperature	6.5	6.4	6.2	6.2	6.3
External Emissivity	3.0	3.3	3.4	3.3	3.1
Carbon Steel Emissivity	0.3	0.4	0.4	0.4	0.4
Aluminum Emissivity	0.1	0.1	0.1	0.1	0.1
Fuel Hydraulic Resistance	-0.2	-0.2	-0.1	0.1	-0.1
Total Decay Heat (u = 2%)	0.7	0.8	0.9	0.9	0.8
Fuel Thermal Conductivity	0.1	0.0	0.0	0.0	-0.1
Thermal Gaps - Correlated	0.0	0.0	0.0	0.0	1.0
Input Uncertainty (HOT SIDE):	8.7	8.7	8.8	9.0	8.8

Compiled Results	surf.b2	surf.b3	surf.b4	surf.b5	surf.b6
Simulation Results:					
Experimental	353.2	360.9	361.5	354.8	345.9
Baseline CFD	351.4	356.6	360.2	356.9	349.1
Best Estimate	349.4	357.3	360.4	356.0	348.3
Comparison Error:					
Baseline - Experimental	-1.7	-4.3	-1.3	2.1	3.2
Best Estimate - Experimental	-3.7	-3.7	-1.1	1.2	2.3
Simulation Uncertainty:					
Negative (Gaps Correlated)	-8.3	-8.3	-8.4	-8.3	-9.5
Negative (Gaps Uncorrelated)	-8.2	-8.5	-8.7	-8.7	-9.5
Positive	8.7	8.7	8.9	9.0	10.0
Validation Uncertainty:					
Negative	-8.4	-8.4	-8.5	-8.3	-9.5
Positive	8.8	8.8	8.9	9.0	10.0
ISFSI Results:					
Baseline CFD	370.5	374.3	378.3	377.4	375.4
Best Estimate	368.2	375.1	379.1	378.0	376.0

Table A-4 Uncertainty Quantification Scorecard for Surface Temperatures, Column C

Validation Uncertainty Scorecard: Surface Temperatures, Column C (K)
(95% Confidence Level)

Numerical Uncertainty:	surf.c2	surf.c3	surf.c4	surf.c5	surf.c6
Computer Roundoff	0.0	0.0	0.0	0.0	0.0
Iterative Convergence	0.3	0.2	0.1	0.1	0.1
Grid Convergence:	0.8	0.1	0.7	0.2	4.4
Total Numerical Uncertainty:	1.1	0.4	0.9	0.3	4.5

Experimental Uncertainty:	surf.c2	surf.c3	surf.c4	surf.c5	surf.c6
Total Experimental Uncertainty:	1.1	1.1	1.1	1.1	1.1

Input Uncertainty (COLD):	surf.c2	surf.c3	surf.c4	surf.c5	surf.c6
External Heat Transfer Coefficients	-4.0	-4.2	-4.4	-4.5	-4.4
Ambient Temperature	-6.4	-6.3	-6.1	-6.1	-6.2
External Emissivity	-2.9	-3.1	-3.1	-3.0	-2.9
Carbon Steel Emissivity	0.0	0.0	0.0	-0.1	-0.1
Aluminum Emissivity	-0.1	-0.1	-0.1	-0.1	-0.1
Fuel Hydraulic Resistance	-0.2	-0.2	-0.2	-0.2	-0.2
Total Decay Heat (u = 2%)	-0.8	-0.9	-1.0	-1.0	-0.9
Fuel Thermal Conductivity	0.0	0.0	0.0	-0.1	0.0
Thermal Gaps - Correlated	-1.2	2.5	2.4	1.2	-0.6
Thermal Gaps - Uncorrelated	-1.3	-2.6	-3.0	-3.1	-2.3
Input Uncertainty (COLD SIDE) - Gaps Correlated	-8.2	-8.5	-8.5	-8.3	-8.2
Input Uncertainty (COLD SIDE) - Gaps Uncorrelated	-8.2	-8.6	-8.7	-8.8	-8.5

Input Uncertainty (HOT):	surf.c2	surf.c3	surf.c4	surf.c5	surf.c6
External Heat Transfer Coefficients	4.8	4.9	5.2	5.5	5.3
Ambient Temperature	6.5	6.3	6.2	6.2	6.3
External Emissivity	3.0	3.3	3.4	3.3	3.2
Carbon Steel Emissivity	0.3	0.4	0.4	0.4	0.4
Aluminum Emissivity	0.1	0.1	0.1	0.1	0.1
Fuel Hydraulic Resistance	-0.2	-0.2	-0.1	0.0	0.0
Total Decay Heat (u = 2%)	0.7	0.7	0.9	0.9	0.9
Fuel Thermal Conductivity	-0.1	-0.1	0.0	0.0	0.0
Thermal Gaps - Correlated	0.0	0.0	0.0	0.0	1.0
Input Uncertainty (HOT SIDE):	8.6	8.7	8.9	9.0	8.9

Compiled Results	surf.c2	surf.c3	surf.c4	surf.c5	surf.c6
Simulation Results:					
Experimental	352.6	359.3	360.4	355.4	346.5
Baseline CFD	351.2	356.4	359.9	356.6	348.8
Best Estimate	349.6	357.8	360.9	356.5	348.6
Comparison Error:					
Baseline - Experimental	-1.4	-2.9	-0.4	1.3	2.4
Best Estimate - Experimental	-2.9	-1.5	0.5	1.1	2.1
Simulation Uncertainty:					
Negative (Gaps Correlated)	-8.3	-8.5	-8.6	-8.3	-9.4
Negative (Gaps Uncorrelated)	-8.3	-8.6	-8.8	-8.8	-9.4
Positive	8.7	8.7	8.9	9.0	10.0
Validation Uncertainty:					
Negative	-8.4	-8.6	-8.6	-8.4	-9.4
Positive	8.7	8.8	9.0	9.1	10.1
ISFSI Results:					
Baseline CFD	370.3	374.1	378.1	377.2	375.2
Best Estimate	368.3	375.6	379.7	378.5	376.5

Table A-5 Uncertainty Quantification Scorecard for Cell 2 Internal Temperatures

Validation Uncertainty Scorecard: Internal Temperatures, Cell 2 (K)

(95% Confidence Level)

Numerical Uncertainty:	tc02.1	tc02.2	tc02.3	tc02.4	tc02.5	tc02.6	tc02.7	tc02.8	tc02.9
Computer Roundoff	0.0	0.0	0.0	0.0	0.0	0.0	0.0	0.0	0.0
Iterative Convergence	2.9	0.5	0.2	0.1	0.1	0.1	0.1	0.1	0.1
Grid Convergence:	7.4	3.0	4.5	0.8	0.7	1.7	1.9	4.5	3.2
Total Numerical Uncertainty:	10.3	3.5	4.6	1.0	0.8	1.8	2.0	4.6	3.3

Experimental Uncertainty:	tc02.1	tc02.2	tc02.3	tc02.4	tc02.5	tc02.6	tc02.7	tc02.8	tc02.9
Total Experimental Uncertainty:	1.9	1.9	2.0	2.0	2.0	2.0	1.9	1.9	1.8

Input Uncertainty (COLD):	tc02.1	tc02.2	tc02.3	tc02.4	tc02.5	tc02.6	tc02.7	tc02.8	tc02.9
External Heat Transfer Coefficients	-3.4	-3.6	-3.6	-3.6	-3.7	-3.8	-4.0	-4.2	-4.6
Ambient Temperature	-7.2	-5.5	-5.0	-4.9	-4.9	-4.9	-5.0	-5.1	-5.3
External Emissivity	-3.7	-3.0	-2.8	-2.8	-2.7	-2.7	-2.2	-2.6	-2.7
Carbon Steel Emissivity	-2.1	-0.8	-0.4	-0.5	-0.6	-0.2	-0.3	-0.3	-0.4
Aluminum Emissivity	0.0	-0.7	-0.5	-0.6	-0.6	-0.2	-0.2	-0.2	-0.2
Fuel Hydraulic Resistance	-4.0	-1.7	-0.8	-1.0	-1.1	-0.9	-1.4	-2.0	-2.7
Total Decay Heat (u = 2%)	-0.2	-3.0	-3.5	-3.7	-3.8	-3.7	-3.2	-3.4	-3.1
Fuel Thermal Conductivity	-1.1	-3.2	-4.0	-3.9	-3.9	-3.9	-3.4	-3.5	-0.7
Thermal Gaps - Correlated	-42.7	-48.6	-54.7	-58.5	-60.1	-60.5	-60.8	-61.2	-62.2
Thermal Gaps - Uncorrelated	-26.9	-31.0	-34.0	-36.0	-36.7	-36.8	-36.6	-36.7	-38.4
Input Uncertainty (COLD SIDE) - Gaps Corr.	-43.8	-49.4	-55.4	-59.1	-60.7	-61.1	-61.3	-61.8	-62.8
Input Uncertainty (COLD SIDE) - Gaps Uncorr.	-28.6	-32.2	-35.1	-37.0	-37.7	-37.9	-37.5	-37.8	-39.4

Input Uncertainty (HOT):	tc02.1	tc02.2	tc02.3	tc02.4	tc02.5	tc02.6	tc02.7	tc02.8	tc02.9
External Heat Transfer Coefficients	5.1	3.8	3.8	3.9	4.1	4.3	5.0	4.9	5.4
Ambient Temperature	6.6	5.0	4.8	4.7	4.6	4.6	5.1	4.7	4.9
External Emissivity	1.9	2.4	2.5	2.5	2.5	2.5	2.4	2.4	2.4
Carbon Steel Emissivity	1.0	-0.2	-0.1	0.0	0.0	0.5	0.6	0.6	0.7
Aluminum Emissivity	0.0	-0.5	-0.4	-0.3	-0.3	0.1	0.1	0.1	0.1
Fuel Hydraulic Resistance	2.7	-0.5	-0.8	-0.6	-0.4	0.2	0.4	0.6	0.9
Total Decay Heat (u = 2%)	2.9	2.2	2.5	2.6	2.6	2.7	2.6	2.5	1.9
Fuel Thermal Conductivity	-1.6	1.6	2.7	2.6	2.7	2.7	3.1	2.5	-0.6
Thermal Gaps - Correlated	0.0	0.0	0.0	0.0	0.0	0.0	0.0	0.0	0.0
Input Uncertainty (HOT SIDE):	9.6	7.3	7.6	7.6	7.6	7.8	8.6	8.1	8.0

Compiled Results	tc02.1	tc02.2	tc02.3	tc02.4	tc02.5	tc02.6	tc02.7	tc02.8	tc02.9
Simulation Results:									
Experimental	423.7	443.4	463.8	467.3	467.4	464.6	454.4	440.0	405.9
Baseline CFD	437.2	456.5	485.7	496.2	498.8	497.6	489.9	479.7	449.9
Best Estimate	417.5	433.1	459.4	467.5	468.5	465.8	455.1	441.4	403.8
Comparison Error:									
Baseline - Experimental	13.4	13.1	21.9	29.0	31.4	33.0	35.4	39.7	44.0
Best Estimate - Experimental	-6.2	-10.3	-4.5	0.3	1.1	1.2	0.6	1.3	-2.1
Simulation Uncertainty:									
Negative (Gaps Correlated)	-45.0	-49.5	-55.6	-59.1	-60.7	-61.1	-61.4	-62.0	-62.9
Negative (Gaps Uncorrelated)	-30.4	-32.4	-35.4	-37.0	-37.8	-37.9	-37.5	-38.0	-39.5
Positive	14.1	8.1	8.9	7.6	7.7	8.0	8.9	9.3	8.7
Validation Uncertainty:									
Negative	-45.1	-49.5	-55.6	-59.2	-60.7	-61.2	-61.4	-62.0	-62.9
Positive	14.2	8.3	9.1	7.9	7.9	8.2	9.1	9.5	8.9
ISFSI Results:									
Baseline CFD	455.3	470.2	499.7	511.3	515.0	515.1	509.7	501.5	475.9
Best Estimate	433.8	447.7	474.4	483.8	486.3	485.6	479.0	469.3	439.0

Table A-6 Uncertainty Quantification Scorecard for Cell 6 Internal Temperatures

Validation Uncertainty Scorecard: Internal Temperatures, Cell 6 (K)

(95% Confidence Level)

Numerical Uncertainty:	tc06.1	tc06.2	tc06.3	tc06.4	tc06.5	tc06.6	tc06.7	tc06.8	tc06.9
Computer Roundoff	0.0	0.0	0.0	0.0	0.0	0.0	0.0	0.0	0.0
Iterative Convergence	0.7	0.3	0.2	0.1	0.1	0.1	0.1	0.1	0.1
Grid Convergence:	12.5	1.8	8.7	4.1	2.6	0.0	0.2	1.7	0.2
Total Numerical Uncertainty:	13.2	2.1	8.8	4.3	2.7	0.1	0.3	1.8	0.3

Experimental Uncertainty:	tc06.1	tc06.2	tc06.3	tc06.4	tc06.5	tc06.6	tc06.7	tc06.8	tc06.9
Total Experimental Uncertainty:	1.9	2.0	2.0	2.0	2.0	2.0	2.0	1.9	1.8

Input Uncertainty (COLD):	tc06.1	tc06.2	tc06.3	tc06.4	tc06.5	tc06.6	tc06.7	tc06.8	tc06.9
External Heat Transfer Coefficients	-4.0	-3.7	-3.5	-3.6	-3.7	-3.8	-4.0	-4.2	-4.6
Ambient Temperature	-5.0	-5.0	-5.0	-4.9	-4.9	-5.0	-5.0	-5.1	-5.3
External Emissivity	-2.3	-2.2	-2.2	-2.3	-2.3	-1.6	-2.2	-1.5	-1.5
Carbon Steel Emissivity	0.5	0.1	0.0	-0.1	-0.1	0.5	0.4	0.4	0.3
Aluminum Emissivity	0.1	-0.1	-0.2	-0.2	-0.2	0.5	0.5	0.5	0.4
Fuel Hydraulic Resistance	-0.6	1.2	0.3	-0.3	-0.6	-0.3	-0.9	-1.5	-2.1
Total Decay Heat (u = 2%)	-2.6	-2.8	-3.3	-3.5	-3.6	-2.8	-3.4	-2.6	-2.1
Fuel Thermal Conductivity	-0.2	-2.5	-3.6	-3.5	-3.5	-2.9	-3.5	-2.6	0.5
Thermal Gaps - Correlated	-45.4	-46.8	-52.2	-55.9	-57.4	-57.5	-58.3	-59.7	-63.6
Thermal Gaps - Uncorrelated	-27.2	-27.8	-30.6	-32.6	-33.3	-32.1	-33.3	-33.6	-35.4
Input Uncertainty (COLD SIDE) - Gaps Corr.	-45.9	-47.4	-52.8	-56.5	-58.0	-58.0	-58.9	-60.2	-64.1
Input Uncertainty (COLD SIDE) - Gaps Uncorr.	-28.1	-28.8	-31.7	-33.6	-34.3	-33.0	-34.3	-34.5	-36.3

Input Uncertainty (HOT):	tc06.1	tc06.2	tc06.3	tc06.4	tc06.5	tc06.6	tc06.7	tc06.8	tc06.9
External Heat Transfer Coefficients	4.5	4.2	4.2	4.4	4.6	5.5	5.1	6.0	6.5
Ambient Temperature	5.5	5.2	5.1	5.1	5.1	5.8	5.1	5.8	6.0
External Emissivity	2.1	2.3	2.5	2.5	2.5	2.5	2.4	2.4	2.3
Carbon Steel Emissivity	0.4	0.3	0.4	0.5	0.5	1.3	1.3	1.3	1.3
Aluminum Emissivity	-0.1	0.1	0.1	0.1	0.1	0.8	0.8	0.7	0.7
Fuel Hydraulic Resistance	-0.6	-0.8	-0.4	-0.1	0.0	0.9	1.1	1.3	1.5
Total Decay Heat (u = 2%)	2.9	2.2	2.5	2.6	3.4	4.1	3.9	3.7	3.2
Fuel Thermal Conductivity	0.1	2.8	3.4	3.2	3.2	4.0	3.2	3.6	0.4
Thermal Gaps - Correlated	0.0	0.0	0.0	0.0	0.0	0.0	0.0	0.0	0.0
Input Uncertainty (HOT SIDE):	8.0	7.9	8.2	8.3	8.7	10.3	9.4	10.3	9.9

Compiled Results	tc06.1	tc06.2	tc06.3	tc06.4	tc06.5	tc06.6	tc06.7	tc06.8	tc06.9
Simulation Results:									
Experimental	433.9	457.0	479.4	482.4	481.1	476.8	464.4	447.4	409.8
Baseline CFD	452.8	468.4	498.8	509.9	512.5	510.5	502.2	491.3	459.7
Best Estimate	431.2	445.7	473.4	482.2	483.1	479.2	467.2	452.0	410.8
Comparison Error:									
Baseline - Experimental	18.9	11.3	19.4	27.5	31.4	33.7	37.8	43.9	49.9
Best Estimate - Experimental	-2.7	-11.3	-6.0	-0.3	2.0	2.4	2.8	4.6	1.0
Simulation Uncertainty:									
Negative (Gaps Correlated)	-47.8	-47.5	-53.5	-56.6	-58.1	-58.0	-58.9	-60.3	-64.1
Negative (Gaps Uncorrelated)	-31.1	-28.9	-32.9	-33.9	-34.4	-33.0	-34.3	-34.5	-36.3
Positive	15.4	8.2	12.0	9.3	9.1	10.3	9.4	10.5	9.9
Validation Uncertainty:									
Negative	-47.8	-47.5	-53.6	-56.7	-58.1	-58.0	-59.0	-60.3	-64.1
Positive	15.6	8.4	12.2	9.5	9.3	10.5	9.6	10.7	10.1
ISFSI Results:									
Baseline CFD	465.2	480.9	512.9	525.5	529.3	529.4	523.4	514.3	486.2
Best Estimate	444.3	459.2	488.4	498.8	501.4	500.5	492.7	481.5	447.9

Table A-7 Uncertainty Quantification Scorecard for Cell 14 Internal Temperatures

Validation Uncertainty Scorecard: Internal Temperatures, Cell 14 (K)

(95% Confidence Level)

Numerical Uncertainty:	tc14.1	tc14.2	tc14.3	tc14.4	tc14.5	tc14.6	tc14.7	tc14.8	tc14.9
Computer Roundoff	0.0	0.0	0.0	0.0	0.0	0.0	0.0	0.0	0.0
Iterative Convergence	3.0	0.4	0.1	0.1	0.1	0.1	0.1	0.1	0.1
Grid Convergence:	3.1	1.8	5.9	4.2	2.7	2.0	1.3	4.2	1.1
Total Numerical Uncertainty:	6.1	2.2	6.0	4.3	2.8	2.1	1.4	4.3	1.2

Experimental Uncertainty:	tc14.1	tc14.2	tc14.3	tc14.4	tc14.5	tc14.6	tc14.7	tc14.8	tc14.9
Total Experimental Uncertainty:	1.9	2.0	2.1	2.1	2.1	2.1	2.0	2.0	1.8

Input Uncertainty (COLD):	tc14.1	tc14.2	tc14.3	tc14.4	tc14.5	tc14.6	tc14.7	tc14.8	tc14.9
External Heat Transfer Coefficients	-5.5	-3.7	-3.6	-3.6	-3.7	-3.8	-4.0	-4.1	-4.4
Ambient Temperature	-4.8	-4.8	-4.8	-4.9	-4.9	-4.9	-4.9	-5.0	-5.1
External Emissivity	-5.3	-2.4	-2.0	-2.0	-2.0	-2.0	-1.9	-1.9	-2.0
Carbon Steel Emissivity	1.9	0.3	-0.1	-0.1	0.0	-0.2	-0.2	-0.3	-0.3
Aluminum Emissivity	-2.1	-0.6	-0.2	-0.2	0.0	-0.2	-0.2	-0.2	-0.2
Fuel Hydraulic Resistance	-30.0	-3.4	0.0	-0.3	-0.4	-0.9	-1.4	-1.8	-2.2
Total Decay Heat (u = 2%)	-3.4	-3.1	-3.5	-3.7	-3.7	-3.7	-3.6	-3.4	-3.0
Fuel Thermal Conductivity	2.1	-2.0	-3.5	-3.4	-3.4	-3.4	-3.3	-3.1	-0.3
Thermal Gaps - Correlated	-49.2	-52.3	-57.5	-61.5	-63.4	-64.3	-65.8	-68.2	-74.8
Thermal Gaps - Uncorrelated	-28.8	-31.1	-33.8	-35.9	-36.6	-37.0	-36.9	-37.5	-39.7
Input Uncertainty (COLD SIDE) - Gaps Corr.	-58.5	-52.9	-58.1	-62.0	-63.9	-64.8	-66.3	-68.8	-75.2
Input Uncertainty (COLD SIDE) - Gaps Uncorr.	-42.8	-32.2	-34.8	-36.8	-37.5	-37.9	-37.9	-38.4	-40.5

Input Uncertainty (HOT):	tc14.1	tc14.2	tc14.3	tc14.4	tc14.5	tc14.6	tc14.7	tc14.8	tc14.9
External Heat Transfer Coefficients	4.5	4.1	4.3	4.5	4.7	4.9	5.2	5.4	5.7
Ambient Temperature	7.1	5.4	5.2	5.2	5.2	5.3	5.3	5.3	5.3
External Emissivity	1.3	2.2	2.5	2.6	2.5	2.5	2.4	2.3	2.3
Carbon Steel Emissivity	1.2	0.2	0.3	0.4	0.7	0.5	0.5	0.6	0.6
Aluminum Emissivity	-4.0	-0.3	0.2	0.2	0.3	0.1	0.1	0.1	0.1
Fuel Hydraulic Resistance	0.9	-0.3	-0.3	-0.1	0.3	0.2	0.4	0.6	0.7
Total Decay Heat (u = 2%)	-0.4	2.7	3.6	3.8	4.0	3.8	3.6	3.4	2.9
Fuel Thermal Conductivity	1.3	2.8	3.6	3.5	3.5	3.5	3.4	3.2	0.2
Thermal Gaps - Correlated	0.0	0.0	0.0	0.0	0.0	0.0	0.0	0.0	0.0
Input Uncertainty (HOT SIDE):	9.6	8.2	8.8	9.0	9.2	9.2	9.3	9.2	8.7

Compiled Results	tc14.1	tc14.2	tc14.3	tc14.4	tc14.5	tc14.6	tc14.7	tc14.8	tc14.9
Simulation Results:									
Experimental	451.5	474.8	498.5	502.4	500.4	493.8	478.8	459.4	417.0
Baseline CFD	466.7	484.2	516.7	529.3	532.4	531.0	522.2	510.9	478.9
Best Estimate	441.8	456.7	485.9	495.8	496.8	493.3	479.7	463.0	419.3
Comparison Error:									
Baseline - Experimental	15.3	9.4	18.1	26.9	32.0	37.2	43.4	51.5	61.9
Best Estimate - Experimental	-9.7	-18.1	-12.6	-6.6	-3.5	-0.5	1.0	3.6	2.4
Simulation Uncertainty:									
Negative (Gaps Correlated)	-58.8	-53.0	-58.4	-62.2	-63.9	-64.8	-66.3	-68.9	-75.2
Negative (Gaps Uncorrelated)	-43.2	-32.2	-35.3	-37.1	-37.7	-38.0	-37.9	-38.6	-40.6
Positive	11.4	8.5	10.7	10.0	9.6	9.5	9.4	10.2	8.7
Validation Uncertainty:									
Negative	-58.8	-53.0	-58.4	-62.2	-64.0	-64.9	-66.3	-68.9	-75.3
Positive	11.6	8.7	10.9	10.2	9.9	9.7	9.6	10.4	8.9
ISFSI Results:									
Baseline CFD	479.0	495.3	530.2	544.7	549.2	549.2	542.7	532.9	503.9
Best Estimate	453.7	469.3	500.8	512.6	515.6	514.3	505.2	492.7	457.1

Table A-8 Uncertainty Quantification Scorecard for Cell 19 Internal Temperatures

Validation Uncertainty Scorecard: Internal Temperatures, Cell 19 (K)

(95% Confidence Level)

Numerical Uncertainty:	tc19.1	tc19.2	tc19.3	tc19.4	tc19.5	tc19.6	tc19.7	tc19.8	tc19.9
Computer Roundoff	0.0	0.0	0.0	0.0	0.0	0.0	0.0	0.0	0.0
Iterative Convergence	3.0	0.5	0.1	0.1	0.1	0.1	0.1	0.1	0.1
Grid Convergence:	7.9	5.5	6.8	6.2	3.8	2.9	2.0	4.6	0.8
Total Numerical Uncertainty:	11.0	5.9	6.9	6.3	3.9	3.0	2.1	4.7	0.9

Experimental Uncertainty:	tc19.1	tc19.2	tc19.3	tc19.4	tc19.5	tc19.6	tc19.7	tc19.8	tc19.9
Total Experimental Uncertainty:	1.9	2.0	2.1	2.1	2.1	2.0	2.0	1.9	1.8

Input Uncertainty (COLD):	tc19.1	tc19.2	tc19.3	tc19.4	tc19.5	tc19.6	tc19.7	tc19.8	tc19.9
External Heat Transfer Coefficients	-4.0	-3.7	-3.6	-3.6	-3.7	-3.9	-4.0	-4.2	-4.5
Ambient Temperature	-4.8	-4.9	-4.9	-4.9	-5.0	-5.0	-5.0	-5.0	-5.1
External Emissivity	-2.5	-2.3	-2.2	-2.4	-2.3	-2.3	-2.3	-2.2	-2.3
Carbon Steel Emissivity	-0.5	0.0	0.0	-0.1	-0.2	-0.2	-0.2	-0.3	-0.3
Aluminum Emissivity	1.7	0.1	-0.1	-0.2	-0.2	-0.2	-0.2	-0.2	-0.2
Fuel Hydraulic Resistance	-37.3	-5.7	0.0	-0.4	-0.6	-0.9	-1.3	-1.7	-2.0
Total Decay Heat (u = 2%)	-2.8	-3.0	-3.5	-3.9	-4.0	-4.0	-3.8	-3.6	-3.3
Fuel Thermal Conductivity	-2.0	-2.4	-3.3	-3.4	-3.4	-3.4	-3.3	-3.1	-0.6
Thermal Gaps - Correlated	-48.9	-52.3	-57.3	-61.3	-63.2	-64.2	-65.8	-68.4	-75.2
Thermal Gaps - Uncorrelated	-28.1	-31.2	-34.1	-36.3	-37.1	-37.3	-37.2	-37.9	-40.4
Input Uncertainty (COLD SIDE) - Gaps Corr.	-62.0	-53.1	-57.8	-61.9	-63.8	-64.8	-66.4	-69.0	-75.6
Input Uncertainty (COLD SIDE) - Gaps Uncorr.	-47.3	-32.7	-35.0	-37.3	-38.1	-38.2	-38.2	-38.8	-41.2

Input Uncertainty (HOT):	tc19.1	tc19.2	tc19.3	tc19.4	tc19.5	tc19.6	tc19.7	tc19.8	tc19.9
External Heat Transfer Coefficients	5.5	4.2	4.2	4.3	4.5	4.7	5.0	5.2	5.5
Ambient Temperature	6.9	5.3	5.1	5.0	5.0	5.0	5.0	5.0	5.0
External Emissivity	3.7	2.7	2.6	2.6	2.6	2.5	2.4	2.3	2.3
Carbon Steel Emissivity	1.1	0.4	0.4	0.4	0.5	0.5	0.6	0.6	0.6
Aluminum Emissivity	1.8	0.6	0.3	0.2	0.1	0.1	0.1	0.1	0.0
Fuel Hydraulic Resistance	2.6	0.2	-0.1	-0.1	0.1	0.2	0.4	0.5	0.7
Total Decay Heat (u = 2%)	3.7	3.1	3.5	3.6	3.6	3.7	3.6	3.4	2.9
Fuel Thermal Conductivity	0.4	2.3	3.1	2.9	2.9	2.9	2.8	2.6	-0.2
Thermal Gaps - Correlated	0.0	0.0	0.0	0.0	0.0	0.0	0.0	0.0	0.0
Input Uncertainty (HOT SIDE):	10.8	8.3	8.5	8.4	8.6	8.7	8.8	8.8	8.3

Compiled Results	tc19.1	tc19.2	tc19.3	tc19.4	tc19.5	tc19.6	tc19.7	tc19.8	tc19.9
Simulation Results:									
Experimental	447.6	469.0	491.7	496.5	494.3	488.3	473.2	453.9	414.7
Baseline CFD	464.9	481.5	512.6	525.4	528.5	527.1	518.2	507.2	477.5
Best Estimate	439.8	453.9	482.3	492.3	493.3	489.7	475.9	459.2	417.6
Comparison Error:									
Baseline - Experimental	17.3	12.5	21.0	28.9	34.3	38.8	45.1	53.3	62.8
Best Estimate - Experimental	-7.8	-15.1	-9.4	-4.2	-0.9	1.4	2.8	5.3	3.0
Simulation Uncertainty:									
Negative (Gaps Correlated)	-62.9	-53.5	-58.2	-62.2	-63.9	-64.8	-66.4	-69.1	-75.6
Negative (Gaps Uncorrelated)	-48.6	-33.2	-35.7	-37.8	-38.3	-38.4	-38.3	-39.1	-41.2
Positive	15.4	10.2	11.0	10.6	9.4	9.2	9.0	9.9	8.4
Validation Uncertainty:									
Negative	-63.0	-53.5	-58.3	-62.3	-63.9	-64.9	-66.4	-69.2	-75.6
Positive	15.5	10.4	11.1	10.8	9.6	9.5	9.3	10.1	8.6
ISFSI Results:									
Baseline CFD	477.3	492.8	526.4	541.0	545.6	545.5	538.8	529.2	502.5
Best Estimate	452.5	467.0	497.4	509.3	512.3	511.0	501.7	489.3	455.7

Table A-9 Uncertainty Quantification Scorecard for Cell 24 Internal Temperatures

Validation Uncertainty Scorecard: Internal Temperatures, Cell 24 (K)

(95% Confidence Level)

Numerical Uncertainty:	tc24.1	tc24.2	tc24.3	tc24.4	tc24.5	tc24.6	tc24.7	tc24.8	tc24.9
Computer Roundoff	0.0	0.0	0.0	0.0	0.0	0.0	0.0	0.0	0.0
Iterative Convergence	1.5	0.4	0.2	0.2	0.1	0.1	0.1	0.1	0.1
Grid Convergence:	11.8	2.2	7.1	3.9	7.5	6.2	5.3	11.7	0.2
Total Numerical Uncertainty:	13.3	2.6	7.3	4.0	7.6	6.4	5.4	11.8	0.3

Experimental Uncertainty:	tc24.1	tc24.2	tc24.3	tc24.4	tc24.5	tc24.6	tc24.7	tc24.8	tc24.9
Total Experimental Uncertainty:	1.9	1.9	2.0	2.0	2.0	2.0	2.0	1.9	1.8

Input Uncertainty (COLD):	tc24.1	tc24.2	tc24.3	tc24.4	tc24.5	tc24.6	tc24.7	tc24.8	tc24.9
External Heat Transfer Coefficients	-4.8	-4.0	-3.6	-3.6	-3.7	-3.9	-4.1	-4.3	-4.7
Ambient Temperature	-6.0	-5.2	-4.9	-5.0	-5.0	-5.0	-5.1	-5.1	-5.3
External Emissivity	-5.7	-2.5	-2.3	-2.3	-3.9	-2.2	-2.2	-2.1	-2.1
Carbon Steel Emissivity	-2.9	1.4	1.4	1.5	-0.2	-0.2	-0.3	-0.3	-0.4
Aluminum Emissivity	-3.8	1.1	1.4	1.4	-0.2	-0.2	-0.2	-0.2	-0.2
Fuel Hydraulic Resistance	-16.0	-0.1	1.3	1.2	-0.6	-0.8	-1.4	-1.9	-2.5
Total Decay Heat (u = 2%)	-6.1	-2.9	-3.1	-3.3	-5.0	-3.4	-3.3	-3.1	-2.7
Fuel Thermal Conductivity	-0.8	-1.9	-3.3	-3.2	-4.8	-3.3	-3.2	-3.0	-0.1
Thermal Gaps - Correlated	-45.4	-45.1	-50.8	-54.4	-57.5	-58.2	-58.8	-59.7	-62.4
Thermal Gaps - Uncorrelated	-29.9	-27.4	-30.4	-32.3	-36.1	-36.3	-36.0	-36.1	-37.6
Input Uncertainty (COLD SIDE) - Gaps Corr.	-49.7	-45.8	-51.4	-55.0	-58.4	-58.8	-59.4	-60.3	-63.0
Input Uncertainty (COLD SIDE) - Gaps Uncorr.	-36.1	-28.6	-31.5	-33.4	-37.5	-37.2	-37.0	-37.1	-38.5

Input Uncertainty (HOT):	tc24.1	tc24.2	tc24.3	tc24.4	tc24.5	tc24.6	tc24.7	tc24.8	tc24.9
External Heat Transfer Coefficients	2.2	4.2	4.3	4.5	3.0	4.8	5.1	5.4	5.9
Ambient Temperature	3.4	5.2	5.0	5.1	3.6	5.2	5.2	5.2	5.4
External Emissivity	2.4	2.6	2.7	2.7	2.6	2.6	2.4	2.4	2.3
Carbon Steel Emissivity	-2.5	1.7	1.9	2.1	0.5	0.6	0.6	0.6	0.7
Aluminum Emissivity	-2.1	1.9	1.8	1.8	0.1	0.1	0.0	0.0	0.0
Fuel Hydraulic Resistance	-1.5	1.3	1.4	1.6	0.1	0.2	0.4	0.6	0.9
Total Decay Heat (u = 2%)	0.2	4.3	4.6	4.9	3.3	3.3	3.2	3.0	2.5
Fuel Thermal Conductivity	-1.8	2.5	3.1	3.0	1.4	3.0	3.0	2.8	-0.2
Thermal Gaps - Correlated	0.0	0.0	0.0	0.0	0.0	0.0	0.0	0.0	0.0
Input Uncertainty (HOT SIDE):	6.2	9.2	9.5	9.8	6.5	8.8	8.9	9.0	8.8

Compiled Results	tc24.1	tc24.2	tc24.3	tc24.4	tc24.5	tc24.6	tc24.7	tc24.8	tc24.9
Simulation Results:									
Experimental	428.6	450.8	474.9	480.4	478.8	474.5	462.3	444.8	408.5
Baseline CFD	445.5	459.9	490.0	501.1	505.3	504.0	495.9	485.2	454.9
Best Estimate	424.7	438.1	465.4	474.2	476.2	473.3	461.6	446.9	407.7
Comparison Error:									
Baseline - Experimental	16.9	9.0	15.1	20.8	26.5	29.6	33.6	40.4	46.4
Best Estimate - Experimental	-3.9	-12.7	-9.5	-6.2	-2.6	-1.2	-0.6	2.1	-0.8
Simulation Uncertainty:									
Negative (Gaps Correlated)	-51.4	-45.9	-52.0	-55.1	-58.9	-59.1	-59.6	-61.4	-63.0
Negative (Gaps Uncorrelated)	-38.4	-28.7	-32.4	-33.7	-38.3	-37.7	-37.4	-39.0	-38.5
Positive	14.7	9.6	12.0	10.6	10.0	10.8	10.4	14.8	8.8
Validation Uncertainty:									
Negative	-51.4	-46.0	-52.0	-55.2	-58.9	-59.1	-59.6	-61.5	-63.0
Positive	14.8	9.7	12.1	10.8	10.2	11.0	10.6	15.0	9.0
ISFSI Results:									
Baseline CFD	458.8	473.7	504.6	516.8	520.6	520.7	515.0	506.3	479.8
Best Estimate	438.4	452.6	480.7	490.9	493.5	492.7	485.4	474.8	443.4

Table A-10 Uncertainty Quantification Scorecard for Cell 28 Internal Temperatures

Validation Uncertainty Scorecard: Internal Temperatures, Cell 28 (K)

(95% Confidence Level)

Numerical Uncertainty:	tc28.1	tc28.2	tc28.3	tc28.4	tc28.5	tc28.6	tc28.7	tc28.8	tc28.9
Computer Roundoff	0.0	0.0	0.0	0.0	0.0	0.0	0.0	0.0	0.0
Iterative Convergence	1.1	0.3	0.2	0.1	0.1	0.1	0.1	0.1	0.1
Grid Convergence:	2.2	3.2	2.5	0.3	1.8	2.8	3.0	3.2	6.3
Total Numerical Uncertainty:	3.3	3.5	2.7	0.5	2.0	2.9	3.1	3.2	6.4

Experimental Uncertainty:	tc28.1	tc28.2	tc28.3	tc28.4	tc28.5	tc28.6	tc28.7	tc28.8	tc28.9
Total Experimental Uncertainty:	1.8	1.9	1.9	1.9	1.9	1.9	1.9	1.9	1.8

Input Uncertainty (COLD):	tc28.1	tc28.2	tc28.3	tc28.4	tc28.5	tc28.6	tc28.7	tc28.8	tc28.9
External Heat Transfer Coefficients	-4.8	-4.1	-3.7	-3.7	-3.8	-3.9	-4.2	-4.4	-4.9
Ambient Temperature	-5.3	-5.2	-5.0	-5.0	-5.1	-5.1	-5.2	-5.3	-5.6
External Emissivity	-4.5	-2.4	-1.0	-0.9	-0.9	-2.3	-2.2	-2.2	-2.2
Carbon Steel Emissivity	-2.2	-0.2	-0.2	-0.1	-0.1	-0.2	-0.2	-0.3	-0.4
Aluminum Emissivity	-2.9	-0.5	-0.3	-0.2	-0.2	-0.2	-0.2	-0.2	-0.2
Fuel Hydraulic Resistance	-6.9	-1.3	-0.5	-0.5	-0.6	-0.9	-1.4	-2.1	-2.8
Total Decay Heat (u = 2%)	-4.5	-2.5	-1.4	-1.5	-1.6	-2.9	-2.8	-2.7	-2.2
Fuel Thermal Conductivity	-2.0	-2.2	-1.9	-1.8	-1.8	-3.2	-3.1	-2.8	0.1
Thermal Gaps - Correlated	-32.7	-33.8	-39.1	-42.0	-43.1	-43.6	-43.8	-43.8	-43.7
Thermal Gaps - Uncorrelated	-23.8	-21.0	-24.0	-25.3	-25.7	-27.4	-25.6	-25.6	-26.1
Input Uncertainty (COLD SIDE) - Gaps Corr.	-35.1	-34.7	-39.7	-42.5	-43.7	-44.4	-44.5	-44.6	-44.5
Input Uncertainty (COLD SIDE) - Gaps Uncorr.	-26.9	-22.5	-24.9	-26.2	-26.6	-28.6	-26.9	-27.0	-27.4

Input Uncertainty (HOT):	tc28.1	tc28.2	tc28.3	tc28.4	tc28.5	tc28.6	tc28.7	tc28.8	tc28.9
External Heat Transfer Coefficients	3.9	4.4	5.6	5.9	6.1	4.9	5.2	5.6	6.3
Ambient Temperature	2.7	5.0	6.5	6.7	6.7	5.3	5.3	5.4	5.7
External Emissivity	2.9	2.8	2.9	2.8	2.8	2.7	2.5	2.4	2.4
Carbon Steel Emissivity	-1.6	0.4	0.5	0.5	0.5	0.5	0.5	0.6	0.6
Aluminum Emissivity	-0.8	0.4	0.2	0.1	0.1	0.1	0.1	0.1	0.0
Fuel Hydraulic Resistance	-0.4	0.1	0.0	0.1	0.2	0.2	0.4	0.7	1.0
Total Decay Heat (u = 2%)	-0.9	2.0	2.6	2.8	2.9	2.8	2.7	2.6	2.1
Fuel Thermal Conductivity	-3.4	2.2	4.4	4.3	4.3	3.0	2.9	2.7	-0.3
Thermal Gaps - Correlated	0.0	0.0	0.0	0.0	0.0	0.0	0.0	0.0	0.0
Input Uncertainty (HOT SIDE):	6.8	7.9	10.4	10.6	10.8	8.7	8.9	9.0	9.1

Compiled Results	tc28.1	tc28.2	tc28.3	tc28.4	tc28.5	tc28.6	tc28.7	tc28.8	tc28.9
Simulation Results:									
Experimental	404.0	424.9	446.6	451.3	450.7	447.4	437.6	424.3	394.7
Baseline CFD	420.5	434.1	460.7	469.9	472.1	471.0	463.8	454.3	426.3
Best Estimate	411.0	423.4	448.0	455.7	456.6	454.2	444.4	432.0	397.6
Comparison Error:									
Baseline - Experimental	16.5	9.2	14.1	18.7	21.4	23.5	26.2	30.0	31.5
Best Estimate - Experimental	7.0	-1.5	1.5	4.4	5.9	6.7	6.8	7.7	2.9
Simulation Uncertainty:									
Negative (Gaps Correlated)	-35.2	-34.9	-39.8	-42.5	-43.7	-44.5	-44.6	-44.7	-45.0
Negative (Gaps Uncorrelated)	-27.1	-22.7	-25.1	-26.2	-26.7	-28.7	-27.1	-27.2	-28.2
Positive	7.6	8.6	10.7	10.7	10.9	9.2	9.4	9.6	11.2
Validation Uncertainty:									
Negative	-35.3	-35.0	-39.8	-42.5	-43.8	-44.5	-44.7	-44.8	-45.0
Positive	7.8	8.8	10.9	10.8	11.1	9.4	9.6	9.8	11.3
ISFSI Results:									
Baseline CFD	437.7	450.7	476.1	485.8	488.8	489.0	484.5	477.5	454.5
Best Estimate	425.7	438.8	463.5	472.1	474.4	473.9	468.1	459.5	432.0

Table A-11 Uncertainty Quantification Scorecard for Cell 31 Internal Temperatures

Validation Uncertainty Scorecard: Internal Temperatures, Cell 31 (K)

(95% Confidence Level)

Numerical Uncertainty:	tc31.1	tc31.2	tc31.3	tc31.4	tc31.5	tc31.6	tc31.7	tc31.8	tc31.9
Computer Roundoff	0.0	0.0	0.0	0.0	0.0	0.0	0.0	0.0	0.0
Iterative Convergence	2.5	0.4	0.2	0.2	0.1	0.1	0.1	0.1	0.1
Grid Convergence:	6.5	3.9	4.2	2.0	0.6	0.3	0.6	5.8	5.3
Total Numerical Uncertainty:	9.0	4.3	4.4	2.2	0.8	0.4	0.7	5.9	5.4

Experimental Uncertainty:	tc31.1	tc31.2	tc31.3	tc31.4	tc31.5	tc31.6	tc31.7	tc31.8	tc31.9
Total Experimental Uncertainty:	1.9	1.9	2.0	2.0	2.0	2.0	1.9	1.9	1.8

Input Uncertainty (COLD):	tc31.1	tc31.2	tc31.3	tc31.4	tc31.5	tc31.6	tc31.7	tc31.8	tc31.9
External Heat Transfer Coefficients	-5.8	-3.9	-3.5	-3.6	-3.8	-3.9	-4.1	-4.3	-4.7
Ambient Temperature	-5.8	-5.1	-4.8	-4.9	-5.0	-5.0	-5.1	-5.1	-5.4
External Emissivity	-3.3	-2.2	-2.3	-1.7	-2.2	-1.7	-1.7	-1.6	-1.6
Carbon Steel Emissivity	-0.5	-0.6	-0.6	-0.2	-0.2	-0.2	-0.3	-0.3	-0.4
Aluminum Emissivity	1.4	-0.5	-0.7	-0.2	-0.3	-0.3	-0.3	-0.3	-0.2
Fuel Hydraulic Resistance	-0.8	-0.9	-0.8	-0.4	-0.6	-0.8	-1.3	-1.9	-2.6
Total Decay Heat (u = 2%)	-3.4	-2.6	-3.1	-2.8	-3.4	-2.9	-2.7	-2.5	-2.0
Fuel Thermal Conductivity	2.7	-1.6	-3.3	-2.8	-3.3	-2.8	-2.7	-2.5	0.4
Thermal Gaps - Correlated	-44.1	-48.8	-54.7	-58.0	-59.6	-60.2	-60.4	-60.8	-61.7
Thermal Gaps - Uncorrelated	-28.6	-31.2	-34.0	-35.1	-35.8	-35.9	-35.7	-35.8	-37.3
Input Uncertainty (COLD SIDE) - Gaps Corr.	-45.2	-49.4	-55.2	-58.5	-60.1	-60.7	-60.9	-61.3	-62.2
Input Uncertainty (COLD SIDE) - Gaps Uncorr.	-30.3	-32.1	-35.0	-35.9	-36.7	-36.7	-36.5	-36.7	-38.2

Input Uncertainty (HOT):	tc31.1	tc31.2	tc31.3	tc31.4	tc31.5	tc31.6	tc31.7	tc31.8	tc31.9
External Heat Transfer Coefficients	2.8	4.0	4.2	4.9	4.6	5.2	5.5	5.8	6.5
Ambient Temperature	3.6	5.0	5.0	5.6	5.1	5.6	5.6	5.7	6.0
External Emissivity	3.3	3.0	3.0	2.8	2.7	2.6	2.4	2.3	2.3
Carbon Steel Emissivity	-1.1	-0.5	-0.2	0.4	0.5	0.5	0.6	0.6	0.6
Aluminum Emissivity	0.5	-0.2	-0.3	0.2	0.1	0.1	0.0	0.0	0.0
Fuel Hydraulic Resistance	2.4	-0.2	-0.5	0.0	0.1	0.2	0.4	0.6	0.9
Total Decay Heat (u = 2%)	0.9	1.8	2.4	3.2	3.3	3.2	3.1	2.9	2.4
Fuel Thermal Conductivity	0.2	2.5	3.1	3.5	3.0	3.5	3.5	3.2	0.4
Thermal Gaps - Correlated	0.0	0.0	0.0	0.0	0.0	0.0	0.0	0.0	0.0
Input Uncertainty (HOT SIDE):	6.3	7.7	8.2	9.3	8.6	9.4	9.5	9.6	9.5

Compiled Results	tc31.1	tc31.2	tc31.3	tc31.4	tc31.5	tc31.6	tc31.7	tc31.8	tc31.9
Simulation Results:									
Experimental	423.9	444.7	467.4	472.7	471.2	467.0	455.0	438.1	405.0
Baseline CFD	437.4	455.3	484.0	494.1	496.6	495.4	487.7	477.6	448.5
Best Estimate	418.1	431.9	457.7	465.6	466.6	463.9	453.1	439.5	402.8
Comparison Error:									
Baseline - Experimental	13.5	10.6	16.6	21.4	25.5	28.4	32.7	39.5	43.5
Best Estimate - Experimental	-5.7	-12.7	-9.7	-7.1	-4.6	-3.1	-1.9	1.4	-2.2
Simulation Uncertainty:									
Negative (Gaps Correlated)	-46.1	-49.5	-55.4	-58.5	-60.1	-60.7	-60.9	-61.6	-62.4
Negative (Gaps Uncorrelated)	-31.6	-32.4	-35.2	-35.9	-36.7	-36.7	-36.5	-37.2	-38.6
Positive	11.0	8.9	9.3	9.5	8.6	9.4	9.5	11.2	10.9
Validation Uncertainty:									
Negative	-46.2	-49.6	-55.4	-58.6	-60.2	-60.7	-61.0	-61.6	-62.5
Positive	11.2	9.1	9.5	9.7	8.9	9.6	9.7	11.4	11.1
ISFSI Results:									
Baseline CFD	454.8	469.0	498.1	509.7	513.4	513.9	508.5	500.4	475.5
Best Estimate	432.8	446.4	472.7	482.2	484.7	484.3	477.6	468.0	438.4

NRC FORM 335
(12-2010)
NRCMD 3.7

U.S. NUCLEAR REGULATORY COMMISSION

BIBLIOGRAPHIC DATA SHEET

(See instructions on the reverse)

1. REPORT NUMBER
(Assigned by NRC, Add Vol., Supp., Rev., and Addendum Numbers, if any.)
NUREG/CR-7260

2. TITLE AND SUBTITLE
CFD Validation of Vertical Dry Cask Storage System

3. DATE REPORT PUBLISHED

MONTH	YEAR
May	2019

4. FIN OR GRANT NUMBER

5. AUTHOR(S)
Alden Research Labratory: Kimball Hall
NRC TM: Ghani Zigh; Jorge Solis
NRC PM: Don Algama

6. TYPE OF REPORT
Technical

7. PERIOD COVERED (Inclusive Dates)

8. PERFORMING ORGANIZATION - NAME AND ADDRESS (If NRC, provide Division, Office or Region, U. S. Nuclear Regulatory Commission, and mailing address; if contractor, provide name and mailing address.)
Alden Research Laboratory, Inc.
Holden, MA 01541

9. SPONSORING ORGANIZATION - NAME AND ADDRESS (If NRC, type "Same as above", if contractor, provide NRC Division, Office or Region, U. S. Nuclear Regulatory Commission, and mailing address.)
Division of Systems Analysis
Office of Nuclear Regulatory Research
U.S. Nuclear Regulatory Commission
Washington, DC 20555-0001

10. SUPPLEMENTARY NOTES

11. ABSTRACT (200 words or less)
This report discusses validation and uncertainty quantification of a CFD model using experimental data. Uncertainty quantification follows the procedures outlined in ASME V&V20-2009. Sources of uncertainty that were examined in the analysis include iterative uncertainty, spatial discretization, and uncertainty due to approximately twenty input parameters. Input parameters investigated include environmental conditions, material properties, decay heat, and the spacing of the many small gaps in the installation. The uncertainty in gap size was found to be the principal source of uncertainty in this particular installation. The effect of the multiple fluid gap dependence and correlation on the uncertainty quantification was evaluated and discussed. As a result, the uncertainty quantification due to the fluid gaps was determined to be dependent due to the heat path dependence, and as such, a correlated error estimation was used.

12. KEY WORDS/DESCRIPTORS (List words or phrases that will assist researchers in locating the report.)
CFD; ASME; Dry Storage;

13. AVAILABILITY STATEMENT
unlimited

14. SECURITY CLASSIFICATION
(This Page)
unclassified
(This Report)
unclassified

15. NUMBER OF PAGES

16. PRICE

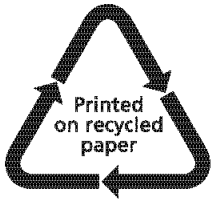

Federal Recycling Program

UNITED STATES
NUCLEAR REGULATORY COMMISSION
WASHINGTON, DC 20555-0001

OFFICIAL BUSINESS